COMPARISON OF THREE LINAC-BASED STEREOTACTIC RADIOSURGERY TECHNIQUES

by

Silvana C. Oliveira
Medical Physics Unit
McGill University, Montréal
June 2003

A Thesis submitted to the
Faculty of Graduate Studies and Research
in partial fulfillment of the
requirements for the degree of
Master of Science
in
Medical Physics

ABSTRACT

In this thesis, physical and biological aspects of three linear-accelerator-based stereotactic radiosurgery techniques, namely the dynamic rotation, static conformal beam, and intensity-modulated beam, are compared. Comparisons are carried out using simulated targets which include spheres, hemispheres and a C-shaped target wrapped around a critical structure, inserted within modified slabs of an Alderson Rando anthropomorphic phantom. The phantom is CT-scanned with a stereotactic frame, and the images are transferred to the treatment planning systems. The best possible treatment plans are generated for each simulated target and for each of the three techniques. Treatment plans are compared using both physical (homogeneity and conformity indices) and biological parameters (integral biologically effective dose, tumour control probability and normal tissue complication probability). Possible correlation between physical and biological parameters is investigated for the three techniques. Finally, some experiments are performed to explain the lack of correlation obtained when multiple isocenters are employed in the dynamic rotation technique for the treatment of irregular targets.

RÉSUMÉ

Lors de cette thèse, les aspects biologiques et physiques des trois techniques de radiochirurgie stéréotaxique par accélérateur linéaire sont comparées : la rotation dynamique, le faisceau statique conforme et le faisceau à intensité modulée. L'étude comporte à simuler des cibles en forme de sphère, d'hémisphère et en forme de C entourant une structure critique, celles-ci étant insérées à l'intérieur de couches modifiées du fantôme anthropomorphique Alderson-Rando. Le fantôme est ensuite examiné par tomographie axiale, utilisant un support stéréotaxique, et les images sont alors transférées au système de planification de traitement. Les plans de traitement optimums y sont générés pour chaque cible simulée ainsi que chaque technique utilisée. Ces plans sont comparés à l'usage de paramètres physiques (indices de conformité et d'homogénéité) et biologiques (dose effective totale, probabilité de contrôle tumoral, probabilité de complications). Les corrélations possibles entre ces deux types de paramètres sont étudiées pour les trois techniques. Finalement, des expériences sont accomplies afin d'expliquer le manque de corrélation obtenu lorsque plusieurs isocentres sont utilisés, avec la technique de rotation dynamique, pour le traitement de cibles à forme irrégulière.

ACKNOWLEDGEMENTS

The research for this thesis was done in the Departments of Medical Physics and Radiation Oncology of the Montreal General Hospital under the auspices of McGill University, Montreal, Canada.

I wish to deeply thank my supervisor, Horacio Patrocinio, for his encouragement, support, and patience throughout the completion of this work, and also for proposing this project, that I enjoyed so much to do. I wish to thank Dr. Ervin Podgorsak for his wisdom and encouragement throughout the whole course and principally, for having given me the opportunity to study in this renowned University, because this was the dream of my life. I would like to acknowledge the financial support received from the Medical Physics Department, without which it would be impossible for me to accomplish this goal.

I wish to thank the staff and students of the Medical Physics Department, and especially my colleagues for their friendship, help, discussions, and support during these past two years. In particular, I wish to thank Dr. Slobodan Devic, William Parker, François Deblois, Margery Knewstubb, Wamied Abdel-Rahman, Dr. Sergio Faria, Dr. Luis Souhami, Svetlana Denissova, Nada Tomic, Lalith Kumaraswamy, Conrad Yuen, and Edwin Sham, for their friendship, help and useful discussions that in some way contributed to this project. Many thanks are also due to Robin Van Gils who promptly made the modifications in the Rando phantom that enabled me to perform my comparative study, to Emily Heath, who helped me to perform the commissioning of the micro-multileaf collimator for use with the CORVUS treatment planning system, and also to Hugo Bouchard who gently translated my abstract to French.

I would like to thank my very beloved parents, sisters, my niece, and my nephew for their unconditional love and support. Overall I wish to thank God for giving me the strength and courage to overcome all the difficulties and complete this course.

TABLE OF CONTENTS

CHAPTER 1

INTRODUCTION TO STEREOTACTIC RADIOSURGERY

In this introductory chapter the general aspects of stereotactic radiosurgery are presented, beginning with a historical perspective that emphasizes the important facts related to the history of stereotactic radiosurgery. The clinical relevance of the method is then discussed. Finally, the physical aspects of the method are presented; specifically, the issues discussed are those related to ancillary equipment for stereotactic radiosurgery, such as stereotactic frames, imaging modalities, as well as treatment planning systems.

1.1 DEFINITION

Stereotactic radiosurgery has become a well-accepted technique for delivery of relatively high doses of radiation, with a rapid dose fall-off outside the target volume, implying a dose concentration such that the dose can be delivered in one single fraction. The technique is employed for the treatment of small, stereotactically localized intracranial lesions, ranging from primary and metastatic malignancies to benign tumours, inoperable arteriovenous malformations (AVMs), pain disorders, and other functional neurologic conditions. Recently, the use of stereotactic radiosurgery has been expanded to treatment of extracranial lesions.

1.2 HISTORICAL DEVELOPMENT

Stereotactic radiosurgery was first described by Lars Leksell of the Karolinska Institute in Stockholm (Sweden) in 1951.[1] The first implementation was a treatment with a large number of collimated stationary orthovoltage X-ray beams, converging upon a common focus.[2]

Unfortunately, due to the large entrance dose and low tissue penetration produced by the orthovoltage X-ray beams, secondary lesions could possibly develop, making it obvious that higher beam energies had to be used.

By mid 1950s, Leksell, in collaboration with the radiobiologist Borge Larsson from the Gustaf Werner Institute at the University of Uppsala (Sweden), started to use a proton beam from a synchrocyclotron for radiosurgery. Initial studies with patients as well as a series of animal experiments were performed with the proton beam, and the idea of a more effective radiosurgical approach proved to be feasible. However, the procedures associated with proton irradiation sessions were very cumbersome and expensive.

Following the pioneering initial experience with proton beams by Leksell and Larsson, stereotactic radiosurgery with protons and heavy charged particles is today performed in several specialized institutions around the world, with good clinical results, particularly for patients with large and peripherally-located lesions.[3,4] The small number of institutions performing radiosurgery with charged particles is explained by the very high costs involved with the installation and operation of cyclotrons.

In 1968, Leksell and Larsson developed the first Gamma Knife unit, using a design wherein 179 collimated cobalt-60 beams delivered radiation to a common focus.[5] The instrument was subsequently modified evolving into the commercially available Leksell Gamma Knife, which contains 201 collimated cobalt-60 sources (activity: 1.11 TBq each source) located in a hemisphere, also convergent upon a common focal point.

Though it has emerged as one of the most elegant innovations in radiosurgery, and the fact that its clinical applications continue to grow, data from April 2001 reports that only 150 Gamma Knife units are installed at leading neurosurgical institutions worldwide.[6] This relatively small number of units is due to the high acquisition and maintenance costs involved and also the fact that a Gamma Knife is a dedicated radiosurgery unit that cannot be used for any other purpose than radiosurgery alone.

In 1974, Larsson *et al.*[7] proposed the use of isocentric linear accelerators (linacs) as viable radiation sources for radiosurgery and, in the late 1980s, several techniques using modified linacs were introduced as a means of performing stereotactic radiosurgery. In 1984, Betti and Derechinsky[8] in Buenos Aires (Argentina) developed the multiple non-coplanar converging arcs radiosurgical technique. Soon thereafter, the technique developed by Betti and Derechinsky was introduced clinically by several other groups. Colombo *et al.*[9,10] in Vicenza (Italy) introduced the converging arcs technique for treatment with a 4 MV linac using five to ten non-coplanar arcs. Hartmann *et al.*[11] in Heidelberg (Germany) used up to eleven 140° arcs. Lutz *et al.*[12] in Boston (U.S.A.) also developed this technique for a 6 MV linac using a series of four non-coplanar arcs: a transverse arc of 260° followed by three vertex arcs of 100° each. In 1986, Podgorsak *et al.*[13] in Montreal (Canada) developed the dynamic stereotactic rotation technique on a 10 MV linac whose main characteristic is the simultaneous and continuous gantry and couch rotation during treatment. Since then, hundreds of centers have implemented linac-based stereotactic radiosurgery techniques, mostly of the multiple non-coplanar converging arcs type.

All these techniques use circular collimators and various arrangements of non-coplanar convergent arcs to focus the radiation on the target and minimize irradiation to healthy tissues outside the target volume. Conformity to irregularly-shaped targets may be obtained by optimizing the collimator size, arc weight as well as the angle of incidence and, principally, by the use of multiple isocenter placements distributed over the target volume.

While stereotactic radiosurgery has been successfully employed in the accurate delivery of radiation to intracranial targets, the delivery mechanism, namely a large dose delivered through circularly-shaped apertures, has remained largely unchanged for several decades. It is only recently that the implementation of a micro-multileaf collimator (μ-MLC) system has provided the capability of a better conformity of the beams to irregularly-shaped targets while excluding normal structures, with the additional advantage of a single isocenter approach, resulting in a more homogeneous dose within

the target volume. Also, dynamic leaf motion, possible with the μ-MLC, enabled the implementation of intensity-modulated stereotactic radiosurgery (IMRS), further improving dose distributions for irregularly-shaped targets and minimizing the dose to critical structures.

Recently, Accuray Inc. (Santa Clara, CA) introduced a robotic arm linac-based system, known as the "Cyberknife".[14] This system represents a radically different approach to linac-based radiosurgery, with the use of a non-invasive image-guided target localization instead of the conventional frame-based stereotaxy. It also replaces the conventional isocentric linac design with a miniature 6 MV linac mounted on an industrial robotic manipulator. The system is currently designed to deliver multiple static beams; however, dynamic beam delivery may also be available in the future.

1.3 CLINICAL INDICATIONS FOR STEREOTACTIC RADIOSURGERY

Many diseases, basically belonging to one of the following four categories: functional disorders, vascular lesions, benign tumours and malignant tumours, have been treated with stereotactic radiosurgery.[15] In the following, a brief description of each of these categories is given.

1.3.1 Functional Disorders

Treatment of functional disorders was the first application of stereotaxy, and stereotactic radiosurgery offers minimally invasive and effective treatment options for many functional disorders such as intractable pain, seizures, Parkinson's disease, trigeminal neuralgia and epilepsy.

1.3.2 Vascular Lesions

Stereotactic radiosurgery is largely used in the treatment of intracranial vascular lesions including, in a majority of cases, arteriovenous malformations (AVMs). An AVM is a

conglomeration of blood vessels that are prone to bleed resulting in headaches and neurological damage that can cause death. The objective of the treatment of an AVM is obliteration, which means that no further blood will flow through the AVM, providing a general protection to the patient from possible future hemorrhages associated with the lesion. Surgery is the most common treatment for AVMs, however, surgical procedures are often difficult or impossible to perform because of the particular location of the AVM, and other treatment techniques such as embolization or radiosurgery may be used.

The success of stereotactic radiosurgery in treatment of AVMs is due to the following factors:

- The non-cancerous nature of these lesions makes them amenable to a non-fractionated treatment;
- In contrast to tumours, the dose needed to effect a cure in the case of AVMs is within a range that is usually well-tolerated by the surrounding normal tissues;
- AVMs are often well circumscribed and non-infiltrative, particularly the smaller ones that are natural candidates for radiosurgery, with some studies reporting high rates (up to 90%) of obliteration in these cases.[16-19]

Less frequently, other vascular lesions such as radiologically occult cavernous angiomas are also treated using stereotactic radiosurgery.

1.3.3 Benign Tumours

Benign tumours successfully treated with radiosurgery include acoustic neuromas, meningiomas and pituitary adenomas. For acoustic neuromas, radiosurgery offers sparing of the facial motor and sensory nerves when compared to surgical resection. For meningiomas, that are difficult to remove because of location near the skull base or the cavernous sinus, or for those that are recurrent after surgery and conventional irradiation, radiosurgery is particularly useful. For pituitary adenomas, radiosurgery can spare the optic nerve and chiasm as well as the hypothalamus.

1.3.4 Malignant Tumours (primary and metastatic lesions)

The malignant tumours most often treated with radiosurgery include the hemangioblastomas, chordomas, chondrosarcomas, ependymomas, schwanomas, low grade astrocytomas, craniopharyngiomas, gliomas and brain metastases.

Because primary brain tumours often have extensions into the normal brain, surgical resection is sometimes not possible. For this reason, the standard radiation treatment is often delivered by larger fields, with stereotactic radiosurgery given focally to the tumour as a boost, in order to increase the dose, with minimal risk to the surrounding normal tissues.

Brain metastases are particularly ideal targets, being usually spherical and displacing normal brain, rather than infiltrating into it. For these cases, success rate is high with a majority of metastases undergoing cessation of growth or shrinkage in size after treatment.[20-24]

In general, literature suggests that radiosurgery can be a safe and efficient method for the management of many difficult brain lesions, while it avoids the loss in quality of life, morbidity, and convalescence associated to other more invasive methods.[25-27] The rationale for stereotactic radiosurgery lies in its ability to deliver a well-localized distribution of dose in order to achieve sterilization of the lesion in a single fraction. However, for certain applications as in the case of malignant tumours, based on well-known radiobiological principles,[28] the effectiveness of the treatment could be further improved by using multiple fractions, rather than single session treatment. The technique is then referred to as stereotactic radiotherapy (SRT), rather than stereotactic radiosurgery.

The most important biological rationale for fractionating a treatment is that the repair of radiation damage for late responding normal tissues is greater than that for most tumours. Additionally, fractionation leads to a better reoxygenation of hypoxic tumour cells

between fractions, making these cells more radiosensitive, consequently, improving the therapeutic ratio.[29] However, the reason for employing a single-fraction treatment for malignant tumours is that the focused dose distribution, characteristic of stereotactic radiosurgery, provides sufficient sparing of normal tissues, and so there is no justification for extending the overall treatment time to reduce normal tissue sequellae. The advantage of using a single fraction treatment in these cases would then compensate for the loss of the radiobiological advantage of fractionation. Stereotactic radiotherapy is thus a treatment modality that combines the radiobiological advantage of fractionation with the stereotactic method of dose localization and delivery.

1.4 PHYSICAL ASPECTS OF STEREOTACTIC RADIOSURGERY

1.4.1 Stereotactic Frames

To achieve the highly focused doses of radiation to the target volume, characteristic of stereotactic radiosurgery and stereotactic radiotherapy, requires an accurate localization of this target volume as well as an accurate alignment of the prescribed dose distribution with this localized target. For stereotactic radiosurgery of intracranial lesions, these requirements are usually satisfied by the use of a stereotactic frame. Stereotactic frames were originally designed for the accurate placement of surgical instruments into predetermined locations within the brain during neurosurgery.[30-32]

In radiosurgery, a stereotactic frame is used for target localization, treatment setup, and patient immobilization during treatment. First, the frame is rigidly attached to the patient's skull with a set of pins. For the localization procedure, a localizing box with N-shaped localization rods as fiducial markers is attached to the frame during computed tomography (CT) or magnetic resonance (MR) imaging, whereas for angiography, a localizing box containing small radiopaque beads is used. These localization rods or radiopaque beads create markers on the diagnostic images. With the positions of these markers on an image, a coordinate transformation matrix between the image coordinate system and the frame coordinate system can be determined, allowing the determination of

the coordinates of the target and of other critical organs within the brain. Figure 1.1 shows a stereotactic frame with a localizing box containing N-shaped localizing rods used during CT or MR imaging. The frame system in Figure 1.1 was built in the Medical Physics department of the Montreal General Hospital.

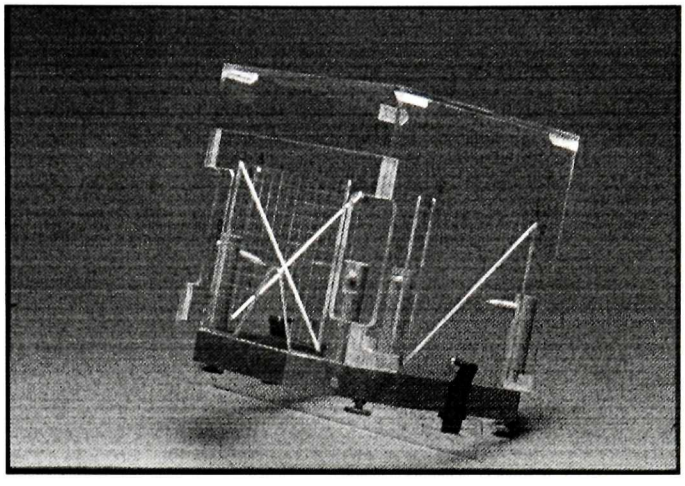

Figure 1.1 – Stereotactic frame with localizing box containing N-shaped localizing rods used during CT or MR imaging. The frame was built by the mechanical group of the Medical Physics Department of the Montreal General Hospital.

Subsequent to the target localization, the stereotactic frame with a target localizing box attached to it indicating the required isocenter position is used for patient setup on the treatment machine. Once the isocenter is precisely placed in the planned position, the box is removed from the frame so that it does not interfere with the dose delivery.

1.4.2 Imaging Techniques for Stereotactic Radiosurgery

Diagnostic imaging techniques, such as the computerized tomography (CT) scan, magnetic resonance imaging (MRI) and digital subtraction angiography (DSA), used in conjunction with compatible stereotactic frames and localizing boxes, are employed to outline the shape and location of the lesion and critical structures, as well as to determine the patient surface contours prior to the radiosurgical procedure. Figure 1.2 shows examples of diagnostic images, (a) CT, (b) MR, and (c) DSA, of patients with various brain lesions.

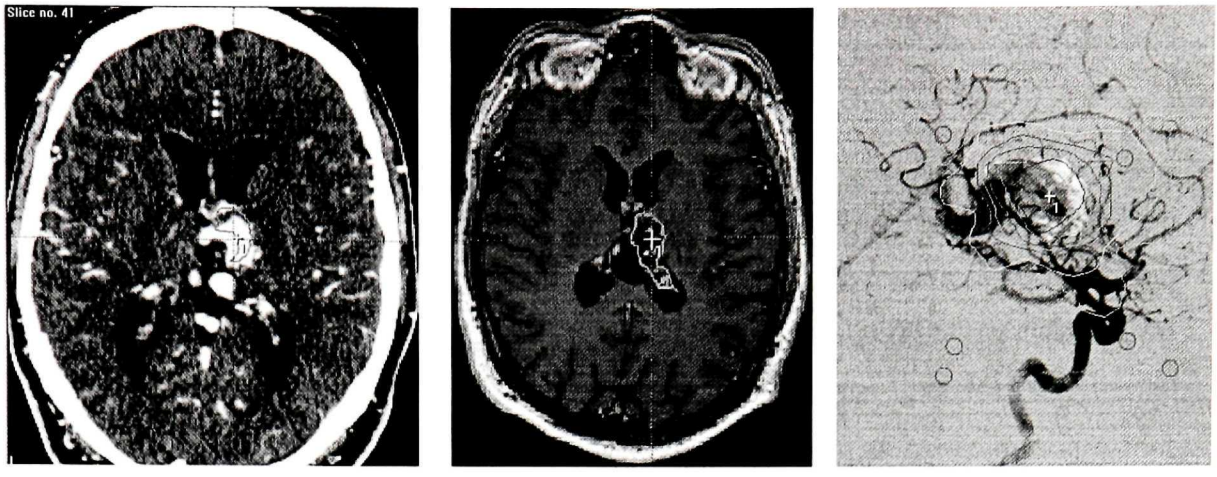

(a) CT (b) MR (c) DSA

Figure 1.2 – Diagnostic images of patients with various brain lesions.

The CT scan is the technique by which image data for treatment planning is typically obtained, as it provides superior and not geometrically-distorted images of calcified tumours and the skull. However, the most common problem in CT imaging is that, as the principle of image acquisition is based on differences in the structures' attenuation coefficients at orthovoltage X-ray energies, the technique does not provide a good contrast between normal brain and the tumour.

MRI is capable of resolving tissues 1 mm in diameter and, compared to CT, MR images can provide a better definition between normal brain and tumour, and can depict better the swelling associated with these tumours. However, the difficulty in this technique stems from the fact that inhomogeneities in the magnetic field and eddy currents produced within the patient can distort the images and produce warping or displacements in the image, relative to the stereotactic frame coordinate system.[33] A precaution that can be taken to minimize this effect is to place the volume of interest in the center of the main magnetic field, as displacements of 20 cm or more from this point can produce gross distortions in the MR image.

By combining the characteristic advantages of CT and MRI in an image fusion process, an accurate localization to within ±1 mm, and delineation of the lesion, internal structures, as well as the patient surface contours is possible.[34]

DSA, in clinical practice, is a technique for visualization of blood vessels in the human body. In conventional X-ray projection images, blood vessels are hardly visible due to the very low contrast between the vessels and the surrounding tissue. In DSA, this contrast is enhanced by the injection of a radiopaque contrast medium (an iodinated solution) into the vessels to be subtracted. The process consists of producing an image by subtracting a radiograph without the contrast medium from a radiograph taken after contrast medium has been administered into the vessels. The result of this subtraction process is the visualization of vessels filled with the contrast medium free from overlying structures.

The major cause of image quality degradation in DSA is due to possible patient motion between the initial image and the image obtained with the contrast injected. However, when this technique is employed in radiosurgery, this problem is eliminated by the immobilization provided by the use of the stereotactic frame.

Given these characteristics, in radiosurgery applications, DSA is commonly used for the definition of the coordinates of vascular lesions, such as the AVMs. The localization procedure is performed with orthogonal image pairs acquired with a stereotactic frame in conjunction with a localizing box containing metallic beads as fiducial markers. These images provide a localization accuracy to within ±1 mm for all three stereotactic coordinates.

1.4.3 Treatment Planning Systems for Stereotactic Radiosurgery

The ideal radiosurgical treatment plan achieves a high and relatively homogeneous target dose while simultaneously delivering the lowest possible dose to healthy intracranial critical structures. Such a dose distribution is obtained, in linac-based radiosurgery, either by aiming at the target with radiation beams from a large number of non-coplanar

directions, or by using multiple non-coplanar arcs, transforming treatment planning in radiosurgery into a complex three-dimensional problem. In addition, since the treatment is given in a single fraction, a high dose is generally prescribed to the target, imposing stringent requirements related to the dosimetric and positional accuracy in dose delivery. For these reasons, treatment planning is a very demanding task, regarded as a key component of a radiosurgical procedure.

In the early days of stereotactic radiosurgery, treatment planning was very rudimentary, with almost all treatments being given with a single isocenter. This single isocenter approach resulted in the irradiation of a relatively large volume of normal tissues surrounding the target, due to the poor agreement between the spherical isodose surfaces produced by the single isocenter plans and the generally non-spherical target volumes.

The development of linac-based radiosurgery techniques in the 1980s imposed the requirement for 3-D radiosurgery treatment planning systems, resulting in significant advances in treatment planning. A general requirement for a treatment planning system to be used in radiosurgery is that it must be capable of calculating three-dimensional dose distributions based on the patient's anatomical data, as well as superimposing this dose distribution onto CT, MR or DSA images. With the development of these systems, issues regarding target localization, prescribed tumour dose, homogeneity of dose inside the target volume, as well as the dose received by normal structures surrounding the target could be more precisely and accurately taken into account.

The institutions involved in the development of these linac-based techniques had to develop their own treatment planning systems, as 3-D radiosurgery treatment planning systems were not commercially available.[11,35,36] Today, many radiosurgical treatment planning systems are commercially available, offering more options for the planning process. These options include the use of non-coplanar beams, support for shaped beams and for intensity-modulated beams to produce conformal dose distributions, with the latter using a different philosophy of treatment planning, called inverse treatment planning.

Inverse treatment planning is a process by which the optimum intensity distribution is determined by the treatment planning system by minimizing (or maximizing) an objective function that is used to describe the clinical goals of a treatment. The objective function can be expressed in terms of biological indices, or in terms of dose and dose/volume requirements, the latter referring to maximum limits in the dose which may be given to some fractional volume of a critical structure, or equivalently, minimum dose limits to a fraction of the target volume.

A description of the three radiosurgical techniques evaluated in our study, as well as the characteristics of the treatment planning system used for each technique are presented in Chapter 2.

1.4.4 Treatment Plan Evaluation Tools

The introduction of 3-D treatment planning systems enabled a much greater number of possible treatment plans, and the quantitative evaluation of such plans became virtually impossible without some special evaluation tools.

To facilitate the evaluation of three-dimensional radiosurgical treatment plans a number of tools, both qualitative and quantitative, have been developed and incorporated into 3-D radiosurgery treatment planning systems. Among the qualitative tools there are the beam's eye view (BEV) as well as visual inspection by the planner, of the isodose lines superimposed on selected transverse, sagittal or coronal images through the target or critical structures. These planar dose distribution displays are used for the evaluation and side-by-side comparison of plans.

Quantitative plan evaluation tools are those capable of condensing the 3-D information into numerical indices that may be correlated to the clinical consequences of a plan. The quantitative evaluation tools provided by treatment planning systems include: (i) the degree of dose coverage of the target volume, (ii) the volume of normal tissue

encompassed by specific isodose surfaces, (iii) conformity and homogeneity indices, and (iv) dose-volume histograms (DVHs).

Specifically, a DVH[37] graphically summarizes the 3-D dose distribution data into a single curve for each outlined anatomical structure, and is considered a powerful tool for plan evaluation, not only because it provides important quantitative information regarding the dose distribution, but also because it can be used as a basis for further calculations of biological indices such as the tumour control probability (*TCP*), the normal tissue complication probability (*NTCP*), and the integral biologically effective dose (*IBED*).

In Chapter 3, the physical and biological parameters used to evaluate and compare the three radiosurgery techniques used in our study are described. Specifically, a full description of the *TCP* and *NTCP* models used, as well as the methodology employed for the application of these models to radiosurgery are given.

1.4.5 Definition of Volumes

Concerning the target volume, as recommended in the ICRU report 50,[38] three volumes can be determined for treatment planning. These are the gross tumour volume (GTV), the clinical target volume (CTV), and the planning target volume (PTV).

The GTV constitutes the palpable or visible extent of the malignant tumour. Usually, a margin has to be added around the GTV to include sub-clinical disease spread. The GTV plus this added margin constitutes the CTV. Due to probable changes in the spatial relationship between the CTV and the therapy beam(s) during treatment, an additional margin must be added to the CTV, constituting the PTV. The GTV and CTV are then clinical concepts, whereas the PTV is a geometrical concept defined for treatment planning purposes.

In radiosurgery, due to the immobilization provided by the use of the stereotactic frame, no margin needs to be added around the CTV, and the PTV and the CTV are then the

same. However, for some techniques, such as the static conformal beam, a small margin, around 1 mm, to account for beam penumbra, is usually added.

1.5 PURPOSE OF THE THESIS

Studies have been carried out extensively comparing different stereotactic radiosurgery modalities and techniques, including the Leksell Gamma Knife, linac-based stereotactic radiosurgery techniques, and radiosurgery with protons and heavy charged particles.[39-52] Several parameters, both physical and biological, have been used in these studies to evaluate and compare different treatment plans.

Physical parameters such as the *PITV* (planning isodose volume to target volume ratio) conformity index as well as the *MDPD* (maximum dose to the prescription dose ratio) homogeneity index, proposed by the Radiation Therapy Oncology Group (RTOG),[53] have been used extensively in the evaluation of radiosurgery treatment plans, even for non-protocol patients. Biological indices, such as several models proposed for tumour control probability (*TCP*) and normal tissue complication probability (*NTCP*), have also been used.[48]

The purpose of the present work is to compare three different linac-based radiosurgery techniques, namely the dynamic rotation, static conformal beam, and intensity- modulated beam, for different shapes and sizes of targets, since a comparative study between these three techniques has not yet been performed.[39-52] The endpoints used for this comparison are: (i) the physical parameters *PITV* and *MDPD*, (ii) the volume of a given structure encompassed by specific isodose levels, and (iii) the biological indices *TCP*, *NTCP*, and integral biologically effective dose (*IBED*).

However, unlike previous studies, the present work also attempts to establish a possible correlation between the various parameters, particularly, the possible correlation between the physical parameters and the biological indices *TCP*, *NTCP* and *IBED*.

The importance of establishing a correlation between physical and biological parameters is that, traditionally, treatment plans in routine radiosurgery have been evaluated and ranked only by the physical parameters; however, the extent to which these physical parameters actually reflect the biological consequences of a given dose distribution is still unknown.

To achieve these goals, a phantom (Alderson Rando phantom) was modified in order to allow insertion of different shapes of targets to be evaluated by the three techniques.

The methods and materials used to perform the comparisons are presented in Chapter 4. Chapter 5 presents the results and discussion obtained from this study. Finally, conclusions and suggestions for future work are presented in Chapter 6.

REFERENCES

1 L. Leksell, "The stereotaxis method and radiosurgery of the brain," Acta Chir. Scand. **102**, 316-319 (1951).

2 L. D. Lunsford, *Stereotactic Radiosurgery Update* (Elsevier, New York, 1992).

3 F. J. Vernimmen, J. K. Harris, J. A. Wilson, R. Melvill, B. J. Smit, and J. P. Slabbert, "Stereotactic proton beam therapy of skull base meningiomas," Int. J. Radiat. Oncol., Biol., Phys. **49**, 99-105 (2001).

4 R. P. Levy, R. W. Schulte, J. D. Slater, D. W. Miller, and J. M. Slater, "Stereotactic radiosurgery – the role of charged particles," Acta Oncol. **38**, 165-169 (1999).

5 L. Leksell, "Cerebral radiosurgery I. Gamma thalamotomy in two cases of intractable pain," Acta Chir. Scand. **134**, 585-595 (1968).

6 "Gamma Knife Surgery: An Emerging Standard of Care. A Report on the Exponential Growth of Gamma knife Surgery in the Last Five Years" (Elekta, 2001).

7 B. Larsson, K. Liden, and B. Sorby, "Irradiation of small structures through intact skull," Acta Radiol. Ther. Phys. Biol. **13**, 513-534 (1974).

8 O. O. Betti and V. E. Derechinsky, "Hyperselective encephalic irradiation with linear accelerator," Acta Neurochir. Suppl. (Wien) **33**, 385-390 (1984).

9 F. Colombo, A. Benedetti, F. Pozza, A. Zanardo, R. C. Avanzo, G. Chierego, and C. Machetti, "Stereotactic radiosurgery utilizing a linear accelerator," Appl. Neurophysiol. **48**, 133-145 (1985).

10 F. Colombo, A. Benedetti, F. Pozza, R. C. Avanzo, C. Marchetti, G. Chierego, and A. Zenerdo, "External stereotactic irradiation by linear accelerator," Neurosur. **16**, 154-159 (1985).

11 G. H. Hartmann, W. Schlegel, V. Sturm, B. Kober, O. Pastyr, and W. J. Lorenz, "Cerebral radiation surgery using moving field irradiation at a linac facility," Int. J. Radiat. Oncol., Biol., Phys. **11**, 1185-1192 (1985).

12 W. Lutz, K. R. Winston, and N. Maleki, "A system for stereotactic radiosurgery with a linear accelerator," Int. J. Radiat. Oncol., Biol., Phys. **14**, 373-381 (1988).

13 E. B. Podgorsak, A. Olivier, M. Pla, P. Y. Lefebvre, and J. Hazle, "Dynamic stereotactic radiosurgery," Int. J. Radiat. Oncol., Biol., Phys. **14**, 115-125 (1988).

14 J. R. Adler and R.S. Cox, "Preliminary clinical experience with the Cyberknife: Image-guided stereotactic radiosurgery," in *Radiosurgery*, edited by D. Kondziolka (Karger, Pittsburgh, PA, 1995), pp. 317-326.

15 M. H. Phillips, *Physical Aspects of Stereotactic Radiosurgery* (Plenum Medical Book Company, New York, 1993).

16 M. Shin, S. Kawamoto, H. Kurita, M. Tago, T. Sasaki, A. Morita, K. Ueki, and T. Kirino, "Retrospective analysis of a 10-year experience of stereotactic radiosurgery for arteriovenous malformations in children and adolescents," J. Neurosurg. **97**, 779-784 (2002).

17 J. C. Flickinger, D. Kondziolka, A. H. Maitz, and L. D. Lunsford, "An analysis of the dose-response for arteriovenous malformation radiosurgery and other factors affecting obliteration," Radiother. Oncol. **63**, 347-354 (2002).

18 H. Aoyama, H. Shirato, T. Nishioka, K. Kagi, R. Onimaru, K. Suzuki, S. Ushikoshi, K. Houkin, S. Kuroda, H. Abe, and K. Miyasaka, "Treatment outcome of single or hypofractionated single-isocenter stereotactic irradiation (STI) using a linear accelerator for intracranial arteriovenous malformation," Radiother. Oncol. **59**, 323-328 (2001).

19 J. H. Chang, J. W. Chang, Y. G. Park, and S. S. Chung, "Factors related to complete occlusion of arteriovenous malformations after gamma knife radiosurgery," J. Neurosurg. **93**, 96-101 (2000).

[20] P. D. Brown, C. A. Brown, B. F. Pollock, D. A. Gorman, and R. L. Foote, "Stereotactic radiosurgery for patients with "radioresistant" brain metastases," Neurosurgery **51**, 656-665 (2002).

[21] P. Y. Wen and J. S. Loeffler, "Brain metastases," Curr. Treat. Options Oncol. **1**, 447-458 (2000).

[22] A. Schoeggl, K. Kitz, M. Reddy, and C. Zauner, "Stereotactic radiosurgery for brain metastases from colorectal cancer," Int. J. Colorectal Dis. **17**, 150-155 (2002).

[23] B. Wowra, M. Siebels, A. Muacevic, F. W. Kreth, A. Mack, and A. Hofstetler, "Repeated gamma knife surgery for multiple brain metastases from renal cell carcinoma," J. Neurosurg. **97**, 785-793 (2002).

[24] A. Zabel, S. Milker-Zabel, C. Thilmann, I. Zuna, B. Rhein, M. Wannenmacher, and J. Debus, "Treatment of brain metastases in patients with non-small cell lung cancer (NSCLC) by stereotactic linac-based radiosurgery: prognostic factors," Lung Cancer **37**, 87-94 (2002).

[25] A. T. Villavicencio, P. M. Black, D. C. Shrieve, M. P. Fallon, E. Alexander, and J. S. Loeffler, "Linac radiosurgery for skull base meningiomas," Acta Neurochir. (Wien) **143**, 1141-1152 (2001).

[26] C. Dunoyer, J. Ragheb, T. Resnick, L. Alvarez, P. Jayakar, N. Altman, A. Wolf, and M. Duchowny, "The use of stereotactic radiosurgery to treat intractable childhood partial epilepsy," Epilepsia **43**, 292-300 (2002).

[27] P. M. Black, "Solitary brain metastases. Radiation, resection, or radiosurgery?" Chest **103**(Supll.4), 367S-369S (1993).

[28] H. Withers, "The 4 R's of Radiotherapy," in *Advances in radiation biology Vol.15*, edited by J. Lett and H. Adler (Academic Press, New York, 1975), pp. 241-271.

29 Y. Lo, C.C. Ling, and D. A. Larson, "The effect of setup uncertainties on the radiobiological advantage of fractionation in stereotactic radiotherapy," Int. J. Radiat. Oncol., Biol., Phys. **34**, 1113-1119 (1996).

30 R. L. Galloway and R. J. Maciunas, "Stereotactic neurosurgery," Biomedical Engineering **18**, 181-205 (1990).

31 R. J. Maciunas, R. L. Galloway, and J. W. Latimer, "The application accuracy of stereotactic frames," Neurosurgery **35**, 682-694 (1994).

32 R. J. Maciunas, R. L. Galloway, J. W. Latimer, C. Cobb, E. Zaccharias, A. Moore, and V. R. Mandava, "An independent application accuracy evaluation of stereotactic frame systems," Stereotact. Funct. Neurosurg. **58**, 103-107 (1992).

33 F. J. Prott, U. Haverkamp, H. Eich, A. Resch, O. Micke, A. R. Fischedick, N. Willich, and R. Potter, "Effect of distortions and asymmetry in MR images on radiotherapeutic treatment planning," Int. J. Cancer **90**, 46-50 (2000).

34 T. M. Peters, J. A. Clark, A. Olivier, E. P. Marchand, G. Mawko, M. Diemeregard, L. W. Muresan, and R. Ethier, "Integrated stereotaxic imaging with CT, MRI and DSA," Radiol. **161**, 821-826 (1986).

35 H. M. Kooy, L. A. Medzi, J. S. Loefler, E. Alexander, C. W. Cheng, E. G. Mannarino, E. J. Holupka, and R. L. Siddon, "Treatment planning for stereotactic radiosurgery of intracranial lesions," Int. J. Radiat. Oncol., Biol., Phys. **21**, 44-45 (1991).

36 B. G. Pike, E. B. Podgorsak, T. M. Peters, and C. Pla, "Dose distributions in dynamic stereotactic radiosurgery," Med. Phys. **14**, 780-789 (1987).

37 R. E. Drzymala, R. Mohan, L. Brewster, J. Chu, M. Goitein, W. Harms, and M. Urie, "Dose-volume histograms," Int. J. Radiat. Oncol., Biol., Phys. **21**, 71-78 (1991).

38 ICRU Report 50, *Prescribing, Recording and Reporting Photon Beam Therapy* (ICRU, Bethesda, MD, 1993).

39 L. J. Verhey, V. Smith, and C. F. Serago, "Comparison of radiosurgery treatment modalities based on physical dose distributions," Int. J. Radiat. Oncol., Biol., Phys. **40**, 497-505 (1998).

40 V. Smith, L. Verhey, and C. F. Serago, "Comparison of radiosurgery treatment modalities based on complication and control probabilities," Int. J. Radiat. Oncol., Biol., Phys. **40**, 507-513 (1998).

41 A. S. Shiu, H. M. Kooy, J. R. Ewton, S. S. Tung, J. Wong, K. Antes, and M. H. Maor, "Comparison of miniature multileaf collimation (M-MLC) with circular collimation for stereotactic treatment," Int. J. Radiat. Oncol., Biol., Phys. **37**, 679-688 (1997).

42 S. Y. Woo, W. H. Grant, D. Bellezza, R. Grossman, P. Gildenberg, S. Carpenter, M. Carol, and E. B. Butler, "A comparison of intensity modulated conformal therapy with a conventional external beam stereotactic radiosurgery system for the treatment of single and multiple intracranial lesions," Int. J. Radiat. Oncol., Biol., Phys. **35**, 593-597 (1996).

43 C. Yu, G. Luxton, G. Jozsef, M. L. J. Apuzzo, and Z. Petrovich, "Dosimetric comparison of three photon radiosurgery techniques for an elongated ellipsoid target," Int. J. Radiat. Oncol., Biol., Phys. **45**, 817-826 (1999).

44 E. B. Podgorsak, G. B. Pike, A. Olivier, M. Pla, and L. Souhami, "Radiosurgery with high energy photon beams: a comparison among techniques," Int. J. Radiat. Oncol., Biol., Phys. **16**, 857-865 (1989).

45 R. M. Cardinale, S. H. Benedict, Q. Wu, R. D. Zwicker, H. E. Gaballa, and R. Mohan, "A comparison of three stereotactic radiotherapy techniques; arcs vs. noncoplanar fixed fields vs. intensity modulation," Int. J. Radiat. Oncol., Biol., Phys. **42**, 431-436 (1998).

46 T. D. Solberg, K. L. Boedeker, R. Fogg, M. T. Selch, and A. A. F. DeSalles, "Dynamic arc radiosurgery field shaping: a comparison with static field conformal and noncoplanar circular arcs," Int. J. Radiat. Oncol., Biol., Phys. **49**, 1481-1491 (2001).

47 R. J. Hamilton, F. T. Kuchnir, P. Sweeney, S. J. Rubin, M. Dujovny, C. A. Pelizzari, and G. T. Y. Chen, "Comparison of static conformal field with multiple noncoplanar arc techniques for stereotactic radiosurgery or stereotactic radiotherapy," Int. J. Radiat. Oncol., Biol., Phys. **33**, 1221-1228 (1995).

48 F. Colombo, P. Francescon, S. Cora, A. Testolin, and G. Chierego, "Evaluation of linear accelerator radiosurgical techniques using biophysical parameters (NTCP and TCP)," Int. J. Radiat. Oncol., Biol., Phys. **31**, 617-628 (1995).

49 L. Ma, P. Xia, L. J. Verhey, and A. L. Boyer, "A dosimetric comparison of fan-beam intensity modulated radiotherapy with gamma knife stereotactic radiosurgery for treating intermediate intracranial lesions," Int. J. Radiat. Oncol., Biol., Phys. **45**, 1325-1330 (1999).

50 V. S. Khoo, M. Oldham, E. J. Adams, J. L. Bedford, S. Webb, and M. Brada, "Comparison of intensity-modulated tomotherapy with stereotactically guided conformal radiotherapy for brain tumors," Int. J. Radiat. Oncol., Biol., Phys. **45**, 415-425 (1999).

51 H. D. Kubo, C. T. E. Pappas, and R. B. Wilder, "A comparison of arc-based and static mini-multileaf collimator-based radiosurgery treatment plans," Radiother. Oncol. **45**, 89-93 (1997).

52 B. G. Clark, J. L. Robar, and A. M. Nichol, "Analysis of treatment parameters for conformal shaped field stereotactic irradiation: comparison with non-coplanar arcs," Phys. Med. Biol. **46**, 3089-3101 (2001).

53 E. Shaw, R. Kline, M. Gillin, L. Souhami, A. Hirschfeld, R. Dinapoli, and L. Martin, "Radiation therapy oncology group: radiosurgery quality assurance guidelines," Int. J. Radiat. Oncol., Biol., Phys. **27**, 1231-1239 (1993).

CHAPTER 2

STEREOTACTIC RADIOSURGERY TECHNIQUES

In this chapter the general aspects of the three radiosurgical techniques evaluated in this study are described. For each technique, the characteristics of the treatment planning system used are also presented. Considerations about the treatment planning process, dose calculation algorithm, and output information provided by the treatment planning system are discussed for each technique.

2.1 INTRODUCTION

In radiosurgery a high dose is delivered in a single fraction; thus a radiosurgery technique should ideally concentrate this dose inside the target volume while providing a steep and isotropic dose fall-off outside the target. By using an almost 2π distribution (beam entry points located in the upper hemisphere of the skull), an approximately isotropic dose distribution outside the target can be obtained with the additional advantage of avoiding the use of parallel-opposed beams that degrade the steepness of the dose fall-off outside the target.

As mentioned in Section 1.2, many linac-based techniques have been developed that use different approaches to spread, as much as possible, the beam entry points over the upper hemisphere of the skull; however, only the three techniques used in this study are described in the following sections.

2.2 DYNAMIC ROTATION

The dynamic rotation technique was developed in 1986 by Podgorsak *et al.* at McGill University[1] using a 10 MV linear accelerator [Varian, Clinac-18 (Varian Medical Systems, Palo Alto, CA)] with two types of commercially available stereotactic

couch-mounted frames (OBT frame, Tipal Instruments, Montreal and Leksell frame, Elekta Instruments, Stockholm). In this technique, the patient is treated in the supine position with the couch-mounted frame used for target localisation, patient setup and immobilization during treatment (as described in Section 1.4.1). The technique is based on a continuous and simultaneous rotation of the gantry and couch during treatment; the gantry rotates 300°, from 30° to 330°, and the couch 150°, from 75° to -75°. Thus, the couch's angular speed corresponds to one half of the gantry's angular speed. Figure 2.1 shows several successive positions of the gantry and couch during a complete dynamic rotation procedure. The continuous motion of gantry and couch during a complete rotation results in a peculiar trace on the patient's head (similar to a baseball seam) that is shown in Figure 2.2.

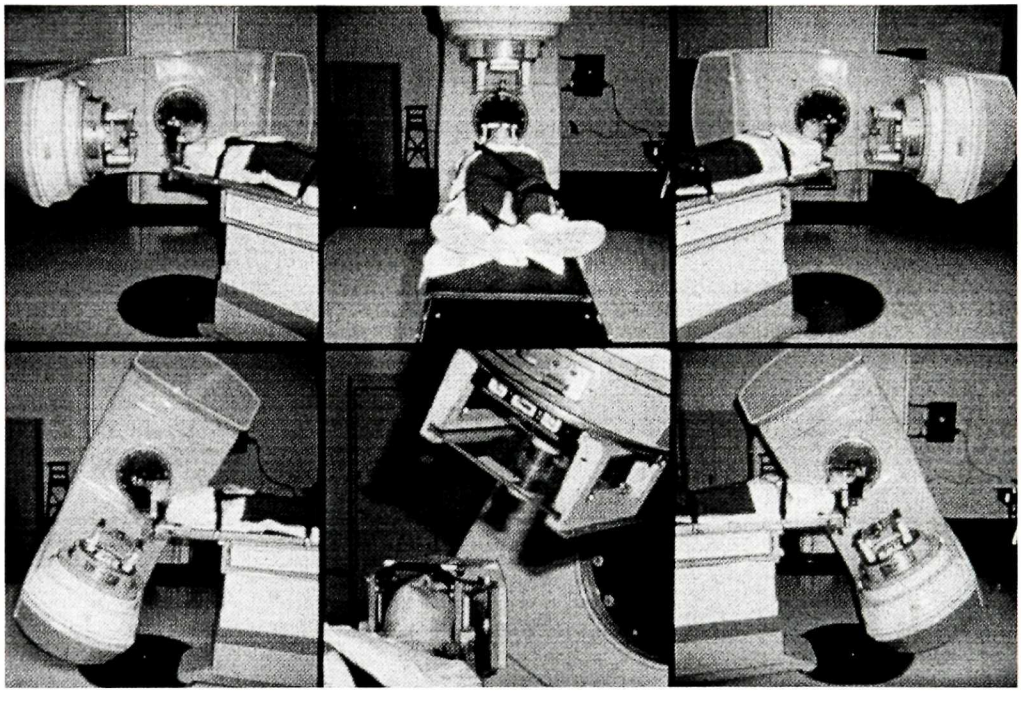

Figure 2.1 – Several successive positions of the gantry and couch during a dynamic rotation procedure, starting with the gantry and couch, respectively, at 30° and 75° (lower left), and finishing at 300° and -75°, respectively (lower right). (Courtesy of the Medical Physics Department of the Montreal General Hospital).

Figure 2.2 – Beam entry trace on the patient's head obtained during a complete dynamic rotation, with point T representing the isocenter.

The technique uses circular collimators with diameters ranging from 0.5 to 4.0 cm, which provide spherical dose distributions. For targets that deviate from a spherical geometry, multiple isocenters must be used in order to achieve a dose distribution that conforms to the target volume. The reasoning for the use of multiple isocenters is that each isocenter represents a small spherically symmetric dose distribution and, by packing several of these dose distributions within the target, a tight dose conformity to the surface of the target can be achieved. For example, an elliptical dose distribution may be achieved using two isocenters. Likewise, triangular distributions may be achieved with three isocenters and rectangular distributions with four.

In addition to the adaptations that must be made in a standard linac in order to make it useful for radiosurgery, such as: (i) the use of additional collimation to achieve the small, well defined circular fields, (ii) the attachment of a bracket to the head of the treatment couch to fasten the stereotactic frame to the couch and immobilize the patient during treatment, and (iii) the use of a brake to immobilize lateral and longitudinal couch motions in order to avoid shifting of the isocenter during treatment, the dynamic rotation technique also incorporates a remotely controlled couch rotation to enable the simultaneous couch and gantry rotation, and a couch angular position readout on the machine console. In the current study, treatment planning for the dynamic rotation technique was performed using the SimuPlan treatment planning system developed at

McGill University.[2] The system had been previously commissioned for use of the 10 MV beam from the Clinac 18 linear accelerator and the circular collimators.

2.2.1 The Treatment Planning System

Treatment planning for the dynamic rotation technique was performed using the stereotactic radiosurgery/radiotherapy module of the SimuPlan – The Montreal Treatment Planning System – developed at McGill University.[2] The steps required to produce a treatment plan using this system are: (i) acquisition of patient images, (ii) CT localization and external contour, (iii) outlining of structures, (iv) selection of number, collimator size and position of isocenters, (v) calculation of dose distributions, (vi) calculation of DVHs, (vii) selection of prescription dose and prescription isosurface.

CT localization is performed prior to treatment planning in order to define the coordinates of the target and of any critical organ within the brain in the stereotactic frame coordinate system. Treatment planning begins with the placement of isocenters. Isocenters can be placed at any position on any slice (previously localized in fiducial space) defined by the user, or automatically at the geometrical center of the tumour volume with a suggested field size that appropriately covers the tumour. When more than one isocenter is used, the user must define the best position and field size for each isocenter.

Dose distributions in the radiosurgery module of the SimuPlan system are calculated with the Clarkson dose algorithm.[3,4] In this algorithm, dose distributions are calculated from measurements of tissue-maximum ratios (*TMR*) (converted to percentage depth dose (*PDD*) values) and profiles (Off-Axis ratios - *OAR*) at several depths. Measured relative dose factors (*RDF*) data are used to account for the dependence of the beam output on field size. Using these measured data, the dose in a point of interest Q within the head is given by the following equation:[5]

$$D_Q(d,A_Q)=P\left(d,A_i\frac{f_i-d_i+d}{f_i+d},f_i\right)\left(\frac{f_i+d}{f_i+d_{\max}}\right)^2\left(\frac{f_i}{f_i-d_i+d}\right)^2 OAR(d,r_Q), \qquad (2.1)$$

where d is the depth of the point of interest Q within the head; f_i is the source-axis distance; $d_{\max}$ and d_i are the depth of maximum dose and the isocenter depth, respectively; A_Q and A_i are the field diameters at point Q and at isocenter, respectively; r_Q is the distance from the central axis to point Q at depth d, and P refers to the percentage depth dose, obtained from measurements of *TMR*.

The system assumes the target volume, brain tissues and the skull to be homogeneous, of unit density, and the fields are generally considered to be small enough that corrections for variations in surface contour or obliquity of the beam are not accounted for.

The system calculates DVHs, differential and cumulative, for all outlined structures. Cumulative DVHs for the target and normal tissue are presented simultaneously and combined, enabling the verification of the quality of a treatment plan by the analysis of tumour coverage by a selected isosurface and also, the amount of normal tissue encompassed by this isosurface.

Treatment plans are evaluated by DVHs and by isodose lines superimposed on image sections of the patient. Also, the DVH information, in the form of tables, can be printed, helping in the further calculation of biological indices like *IBED*, *TCP* and *NTCP*. Figure 2.3 shows an image obtained from the SimuPlan treatment planning system, which displays information provided by the system concerning the treatment plan, such as: (i) axial image sections of the patient, (ii) the coordinates and cone size of the isocenter, (iii) a 3-D perspective of the dose distribution, and (iv) the isodose lines superimposed on a selected axial image of the patient.

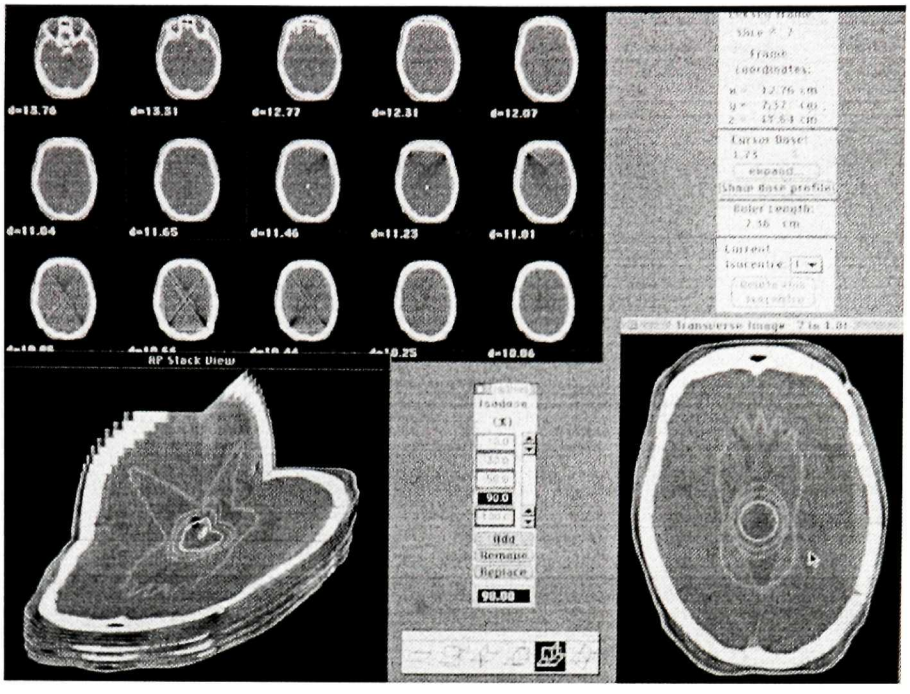

Figures 2.3 – Image obtained from the SimuPlan treatment planning system, displaying information provided by the system concerning the treatment plan, such as: (i) axial image sections of the patient, (ii) the coordinates and cone size of the isocenter, (iii) a 3-D perspective of the dose distribution, and (iv) the isodose lines superimposed on a selected axial image of the patient.

2.3 STATIC CONFORMAL BEAM TECHNIQUE

The static conformal beam technique uses non-coplanar uniform static fields with apertures conforming to the beam's eye view projections of the target volume. Typically five to six beams are used. The shaping of the fields is carried out using a micro-multileaf collimator (μ-MLC). Figure 2.4 shows a three-dimensional view of a radiosurgical treatment plan consisting of several static conformal beams shaped by a μ-MLC.

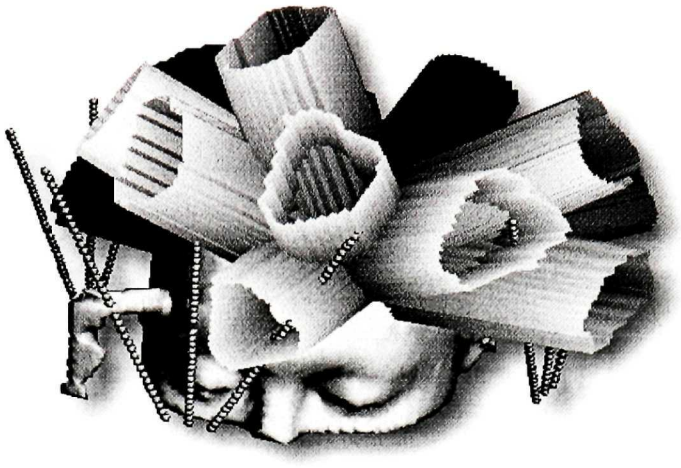

Figure 2.4 – Three-dimensional view of a radiosurgical treatment plan consisting of several uniform static conformal beams (Courtesy of BrainLAB Inc., AG, Germany).

In this study, field shapes were defined by the micro-multileaf collimator BrainLAB m3 (BrainLAB, AG, Germany). The BrainLAB m3 μ-MLC is an add-on collimator that is attached to the linac head by a latch mechanism, with the power for its functioning drawn from the linac head. Field shaping is done by 26 leaf pairs, which move perpendicularly to the beam central axis (i.e., unfocused). The BrainLAB m3 has variable leaf widths at isocenter. The finer 14 leaf pairs, 3 mm wide at isocenter, located in the center of the field area, allow improved shaping around smaller targets, of the size treated by radiosurgery. Intermediate and outer leaf pairs correspond to 6 leaf pairs each with, respectively, 4.5 and 5.5 mm projected leaf widths at isocenter. The maximum field area that can be defined at isocenter is only 9.8 cm x 9.8 cm, making this collimator unsuitable for the larger fields usually employed in conventional radiotherapy applications.

Compared to the dynamic rotation technique, the conformal beam technique uses the same patient positioning (supine) and the same Leksell-like frame (couch-mounted frame), however, with a different localizer box. In the current study, treatment planning was performed using the BrainSCAN treatment planning system (BrainLAB, AG, Germany)[6] that is a dedicated system used only for the static conformal beam technique. The BrainSCAN system had been previously commissioned locally for the use of 6 MV

beam from a Clinac 2300 linear accelerator (Varian Medical Systems, Palo Alto, CA) and the BrainLAB m3 μ-MLC.

2.3.1 The Treatment Planning System

Treatment planning for the conformal beam technique was performed using the conformal beam module of the BrainSCAN treatment planning system version 5.1.[6] The steps required to produce a treatment plan using this system are: (i) acquisition of patient images, (ii) CT localization, (iii) image fusion, (iv) outlining of structures, (v) addition of isocenters and beams, and (iv) dose calculations.

Treatment planning begins with the addition and optimization of isocenters and beams. For radiosurgery, usually a single isocenter is used, and this can be automatically positioned by the system at the center-of-mass of the currently defined planning target volume (PTV). Once an isocenter position has been defined, several beams can be added by the user, spaced as far as possible in three dimensions, to minimize the dose to healthy tissues. For each beam, a small margin, in the order of 1-2 mm, can be added to account for the penumbra, and also the collimator angle can be optimized in order to produce the smallest field area.

For dose calculations, the system uses a Clarkson dose algorithm[3,4] based upon three basic beam parameters: tissue maximum ratios (*TMR*), single beam profiles (off-axis ratios - *OAR*) and total scatter factors (S_t). These parameters, measured during commissioning for circular fields defined by the m3 μ-MLC using a scanning water tank, are entered in the system by the user in the form of tables. With these measured data, the system calculates interpolated *OAR* and *TMR* tables, and all dose calculations are performed based on these interpolations. However, some refinements were incorporated into the algorithm to deal with both the irregular shape of a conformal field and the irregularity of the skin surface.

To deal with the irregular shape of the conformal field, a modified Clarkson method is used for the calculation of the total scatter factor (S_t). The field shape is divided into multiple sectors with the beam central axis acting as the focal point (see Figure 2.5). The angle of each sector is determined so that the corners of the shape perimeter (AB in Figure 2.5) are 2 mm apart, i.e.; the angle θ is not fixed. This means that larger field areas are split into more sectors, improving calculation accuracy.

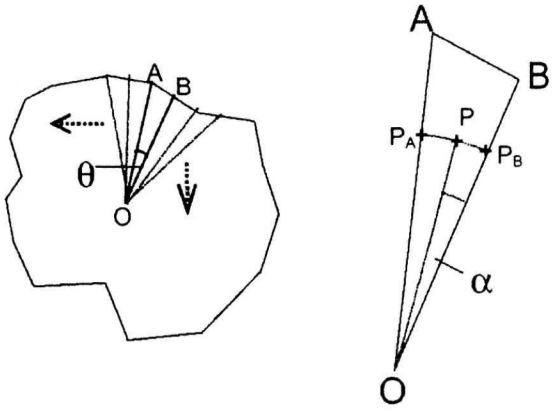

Figure 2.5 - Irregular field divided into sectors to illustrate the modified Clarkson method used by the BrainSCAN software, in the conformal beam radiotherapy module, to calculate the total scatter factor, S_t, for an irregular field shape. The angle θ is not fixed, while the perimeter AB, equal to 2 mm, is the same for all sectors.

To calculate the total scatter factor S_t for an irregular field, the mean radius $\overline{r_i}$ of each field sector i is calculated. These values are then used to determine corresponding values of $S_t(2\overline{r_i})$ for each sector by interpolation from tables of $S_t(c)$ measured for circular fields. $S_t(irreg)$ is then calculated as a sum of the individual $S_t(2\overline{r_i})$ values weighted to the area contribution of each sector to the total field area , i.e.:

$$S_t(irreg) = \sum_{i=1}^{N} S_t(2\overline{r_i}) \frac{\alpha_i}{2\pi}, \qquad (2.2)$$

where α_i = angle of the i_{th} sector.

To deal with the irregularity of skin surface, further refinements were introduced in the software for the calculation of the parameters *TMR* and *OAR*.[6]

Beam's eye view displays, isodose lines superimposed on image sections of the patient, and DVHs are used for treatment plan evaluation. Also, the DVH information, in the form of tables, can be printed, helping in the further calculation of biological indices like *IBED*, *TCP* and *NTCP*.

In the BrainSCAN software, DVHs are calculated with respect to a unique three-dimensional matrix of points centered on the PTV and encompassing all the other volumes defined for the patient. This three-dimensional matrix of points has a default resolution of 2 mm, which can be altered by the user from 0.5 mm until 16 mm, in 0.1 mm increments. This version of the software also incorporates an adaptive grid-size option for small objects which, when selected, the resolution is automatically adjusted depending on the volume of the organ for which the DVH is being calculated, with smaller grid sizes used for smaller volumes. Figure 2.6 shows an image obtained from the BrainSCAN treatment planning system, displaying information provided by the system concerning the treatment plan, such as: (i) 3-D views of the treatment plan, (ii) isodoses superimposed on selected coronal and sagittal image sections of the patient, and (iii) information about the isocenter (coordinates, etc), and of a selected beam (table, gantry, and collimator angles, etc).

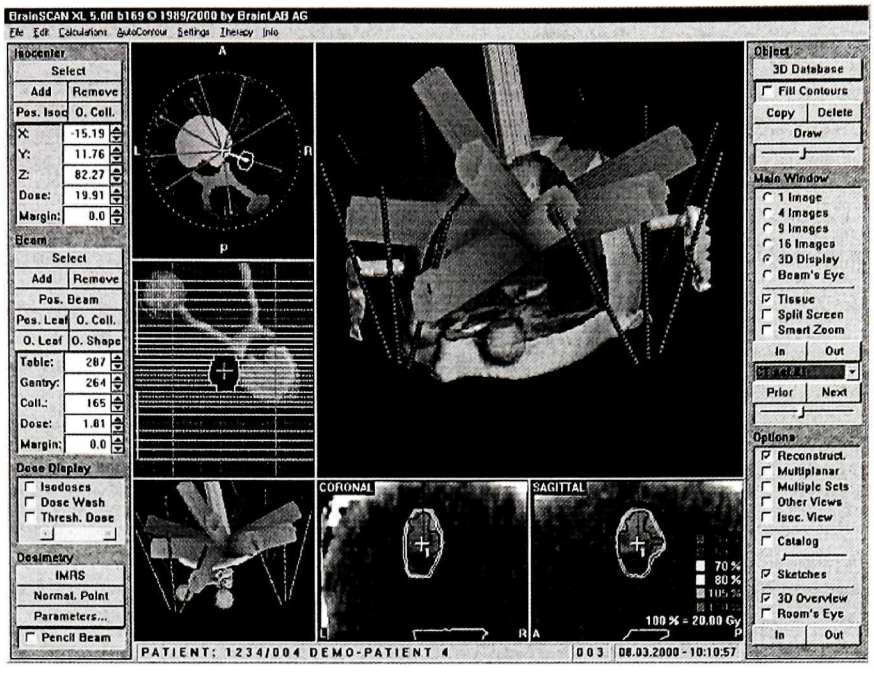

Figure 2.6 – Image obtained from the BrainSCAN treatment planning system, displaying information provided by the system concerning the treatment plan, such as: (i) 3-D views of the treatment plan, (ii) isodoses superimposed on selected coronal and sagittal image sections of the patient, and (iii) information about the isocenter (coordinates, etc), and of a selected beam (table, gantry, and collimator angles, etc). (Courtesy of BrainLAB Inc., AG, Germany).

2.4 INTENSITY-MODULATED RADIOSURGERY TECHNIQUE (IMRS)

The technology of computer-controlled multileaf collimators (MLCs) has opened the door to intensity-modulated radiosurgery (IMRS). Using this technique, the delivered dose can be tailored to fit inside the 3-D surface that encloses the target volume, while sparing nearby sensitive tissues, even in cases of targets that are adjacent to or wrapped around critical structures. The idea behind IMRS is that, when several beams are used to deliver a treatment so that the target volume is irradiated from multiple directions, the dose delivered by a field coming from one direction can be reduced within part of its aperture to spare a structure or to shape the dose distribution. The resulting dose inhomogeneity can be compensated for by increasing the intensity within portions of the beams coming from other directions.

The practical implementation of the IMRS consists of the following steps: definition of desired goals and prescription, beam optimization (to determine the intensity pattern to be

delivered from each beam in order to achieve the desired goals), and leaf motion calculation (to determine the sequences of apertures of the MLCs to create the intensity patterns).

For the definition of desired goals and prescription, cumulative DVHs (described in Section 3.3.1) are used as a means of imputing the desired clinical results; that is, the planner has to specify the minimum dose allowed to the target or to fractions of it, and the maximum dose allowed to fractions of each organ at risk, graphically, using cumulative DVHs.

Inverse planning solves the beam optimization problem by using an optimization (search) algorithm that tries to create a dose distribution in the patient that satisfies all prescribed parameters. Several optimization (search) algorithms have been developed for which, in general, different levels of priorities are assigned to each structure for the realisation of conflicting optimization goals should they occur, i.e., the importance of delivering the minimum dose to the target versus that of not exceeding the maximum dose to surrounding structures.[7-12] For the current study of the IMRS, the CORVUS treatment planning system was used (NOMOS Corporation, Sewickley, PA, USA).[13] The optimization algorithm used by CORVUS is based on simulated annealing criteria.[8]

The IMRS technique uses the same patient positioning (supine), the same couch-mounted Leksell-like frame, as well as the same ancillary equipment as the static conformal beam technique. The only difference is that, for the IMRS, a different treatment planning system, the CORVUS treatment planning system is used. For the current study, the CORVUS system was commissioned for the use of 6 MV beam from a Clinac 2300 (Varian Medical Systems, Palo Alto, CA) and the BrainLAB m3 μ-MLC. However, a limitation in the use of the CORVUS system for IMRS is that CORVUS does not support fiducial localization using the Leksell frame. Instead, an arbitrary origin must be defined by the planner, and several beams (also defined by the planner) are directed to a single isocenter, automatically placed at the center of the lesion. For the current study, not

having fiducial localization for the IMRS technique was not a problem, because the study was performed with phantoms, and treatment delivery was not considered.

2.4.1 The Treatment Planning System

Treatment planning for the intensity-modulated radiosurgery technique was performed using the CORVUS treatment planning system version 4.0.[13]

CORVUS is a dedicated treatment planning system, designed to perform IMRT. It is designed to support two intensity-modulation methods. In the current study, the MLC-based IMRT method was used with the intensity-modulation provided by the BrainLAB m3 μ-MLC. The dose delivery technique considered was the "step and shoot", in which a non-uniform field is decomposed into a number of uniform intensity subfields or segments of different beam shapes in such a way that, when the dose is delivered through these segments at a given gantry angle, the resulting dose distribution is equivalent to the planned non-uniform field.

The commissioning of the CORVUS system requires measurement of several data from the linac including leaf transmission, jaw transmission, output factors in air and in phantom for a number of field sizes as well as percent depth doses for these field sizes, diagonal profiles for a large field size, and also inplane and crossplane profiles for a few field sizes.

The steps required to produce a treatment plan using the CORVUS system are: (i) image registration, (ii) outlining of structures, (iii) dose prescription, and (iv) display results.

Strictly speaking, CORVUS is considered as a semi-automatic treatment planning system, because two degrees of freedom are not included in the optimization process. These are the gantry and treatment couch angles that must be defined by the user. In addition, the collimator angle can also be defined by the user, or the system can automatically determine a collimator angle based on minimizing the beam's eye view area.

Once all the parameters for a plan have been defined, the data are submitted to the dose engine for calculations. After completing the calculations, the results are displayed in the display results module. Several features are provided by CORVUS in this module that enable plan evaluation by the user. These include statistics and DVHs (predicted and obtained) for each outlined structure, isodose lines superimposed on axial, sagittal and coronal slices, digitally reconstructed radiographs (DRRs), etc. Also, the DVH information can be exported, helping in the further calculation of biological indices like *IBED*, *TCP* and *NTCP*. Once a plan has been approved, the planning system generates intensity maps, i.e., each beam is decomposed into segments, compatible to the specific modulating system used, that are subsequently transferred to the linac for treatment delivery. Figure 2.7 shows an image obtained from the CORVUS treatment planning system, displaying information provided by the system, concerning the treatment plan, such as: (i) cumulative DVHs, (ii) isodose lines superimposed on an axial image, and (iii) dose statistics.

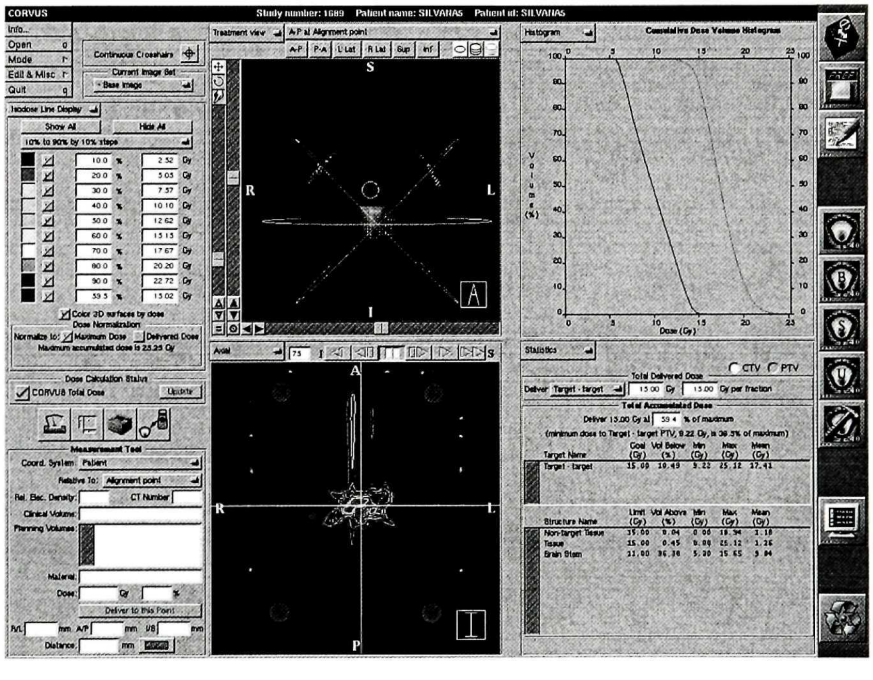

Figure 2.7 – Image obtained from the CORVUS treatment planning system, displaying information provided by the system, concerning the treatment plan, such as: (i) cumulative DVHs, (ii) isodose lines superimposed on an axial image, and (iii) dose statistics.

REFERENCES

1 E. B. Podgorsak, A. Olivier, M. Pla, P. Y. Lefebvre, and J. Hazle, "Dynamic stereotactic radiosurgery," Int. J. Radiat. Oncol., Biol., Phys. **14**, 115-125 (1988).

2 "SimuPlan treatment planning system manual – version for Apple Macintosh power PC computers" (SimuPlan Sociedad Limitada, 2000).

3 J. R. Clarkson, "A note on depth doses in field of irregular shapes," Br. J. Radiol. **14**, 265 (1941).

4 J. R. Cunningham, "Scatter-air-ratios," Phys. Med. Biol. **17**, 42-51 (1972).

5 B. Pike, E. B. Podgorsak, T. M. Peters, and C. Pla, "Dose distributions in dynamic stereotactic radiosurgery," Med. Phys. **14**, 780-789 (1987).

6 "BrainSCAN Software Guide Revision 1.0 – Version 5.1x" (BrainLAB, AG, Germany, 2001).

7 L. Xing and G. T. Y. Chen, "Iterative methods for inverse treatment planning," Phys. Med. Biol. **41**, 2107-2123 (1996).

8 S. Webb, "Optimization by simulated annealing of three-dimensional, conformal treatment planning for radiation fields defined by a multileaf collimator: II. Inclusion of two-dimensional modulation of the X-ray intensity," Phys. Med. Biol. **37**, 1689-1704 (1992).

9 A. B. Pugachev, A. L. Boyer, and L. Xing, "Beam orientation optimization in intensity-modulated radiation treatment planning," Med Phys. **27**, 1238-1245 (2000).

10 G. A. Ezzell, "Genetic and geometric optimization of three-dimensional radiation therapy treatment planning," Med Phys. **23**, 293-305 (1996).

11 J. Llacer, "Inverse radiation treatment planning using the Dynamically Penalized Likelihood method," Med Phys. **24**, 1751-1764 (1997).

12 S. M. Morrill, R. G. Lane, J. A. Wong, and I. I. Rosen, "Dose-volume considerations with linear programming optimization," Med Phys. **18**, 1201-1210 (1991).

13 "CORVUS inverse treatment planning system manual – version 4.0" (NOMOS Corporation, Sewickley, PA, USA).

CHAPTER 3

TOOLS FOR EVALUATION OF RADIOSURGICAL TREATMENT PLANS

In this chapter, the qualitative and quantitative plan evaluation tools used in our comparative study are described. Evaluation tools for 3-D treatment planning were briefly introduced in the introductory chapter in the section on treatment planning systems for stereotactic radiosurgery. Here they are discussed in detail.

3.1 INTRODUCTION

In conventional 2-D radiotherapy planning, treatment plans are evaluated by reviewing dose distributions on one or a few cross sections of the patient. A limited amount of quantitative information, such as the minimum tumour dose, the maximum tumour dose, and the maximum dose to normal structures outside the tumour can be extracted from such distributions. This relative ease in evaluating treatment plans cannot be maintained in the 3-D approach used in radiosurgery, and the reasons are as follows:

- The amount of data to be reviewed for a full 3-D evaluation is considerably greater, because 3-D dose distributions are voluminous, and the spatial relationship between the tumour volume and critical normal anatomy is complex;
- In radiosurgery, unconventional beam arrangements with non-coplanar fields are usually used with the dose distributions in these cases being quite different from those for traditional treatment plans. To evaluate such dose distributions and to draw conclusions about the possible biological consequences requires an extrapolation of clinical experience from traditional situations;
- The possibility of using non-coplanar beams that may be shaped and intensity-modulated to produce conformal dose distributions offers many more options in terms of different possible plans to explore in a 3-D approach.

For these reasons, discerning the differences, merits and shortcomings of one plan relative to another plan can be extremely difficult for non-coplanar 3-D beam configurations that are common to radiosurgery. Additional evaluation tools, both qualitative and quantitative, have been developed in order to assess the superiority of a given plan.

3.2 QUALITATIVE PLAN EVALUATION TOOLS

Qualitative plan evaluation tools include:

- ***Visual inspection of isodoses*** – Most treatment planning systems used to produce the dose distributions for radiosurgery treatments have the ability to display 2-D dose distributions superimposed on a series of transverse, sagittal or coronal images. These planar dose distribution displays can be used for the evaluation and side-by-side comparison of plans. However, comparing competing plans by displaying 2-D image sections side-by-side can be a difficult task because a plan may appear to be superior in one plane, but unacceptable in another. Different viewing modes for the irradiated volume, including the 3-D view of the isodose surfaces resulting from the treatment plan are also common.

- ***Beam's Eye View (BEV)*** – The BEV constitutes a display of the targets and critical structures as contoured on transverse images, and beam modifying devices, as they would appear if the observer's eye were placed at the source of radiation. The BEV display allows the planner to assess the extent of coverage of the target volume as well as sparing of surrounding normal tissues by a beam.

Although the qualitative tools are useful in the evaluation of different plans, in the 3-D approach there is no single plot or section that represents the entire plan. Moreover, there are about one to two orders of magnitude more data to review in a 3-D plan than in a 2-D plan. For these reasons, the condensation of data into a small number of quantities that may be correlated with clinical outcome is necessary.

3.3 QUANTITATIVE PLAN EVALUATION TOOLS

Quantitative plan evaluation tools include dose-volume histograms (DVHs),[1] conformity and homogeneity indices,[2] and biological indices such as the integral biologically effective dose (*IBED*),[3] tumour control probability (*TCP*) and normal tissue complication probability (*NTCP*).[4]

3.3.1 Dose-Volume Histograms (DVHs)

Dose-volume histograms are used to summarize graphically the dose distribution within a volume of interest in a given 3-D treatment plan.[1] They can be presented either in the differential (direct) or integral (cumulative) form. In a differential DVH, the absolute or relative volume in a specified dose interval is plotted against a set of equispaced dose intervals, whereas a cumulative DVH is a plot of the volume receiving a dose greater than or equal to a given dose, against that dose, over the expected dose range. Figure 3.1 shows examples of the two types of DVHs.

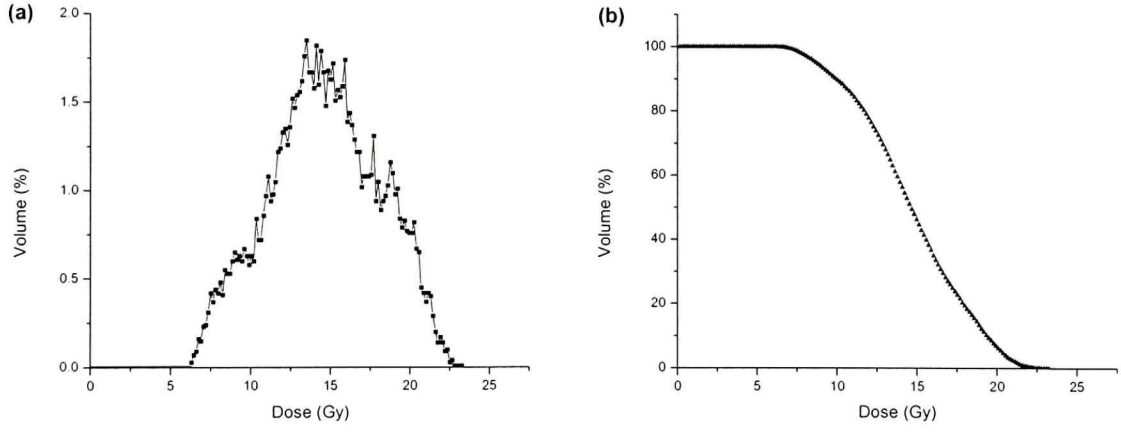

Figure 3.1 – Dose-volume histograms; (a): differential; (b): integral, in which relative volume is plotted against dose.

For the evaluation of a plan, DVHs provide useful information such as the existence and the magnitude of overexposed or underexposed regions. However, they have a major limitation in that the spatial distribution of dose is lost. For this reason, they must be

analyzed in conjunction with 3-D dose displays. In spite of this limitation, DVHs have proven to be a powerful tool in the evaluation and comparison of rival treatment plans. They can also be used as input data for the estimation of biological indices, such as the *IBED*, *TCP* and *NTCP* (discussed in Section 3.3.3).

3.3.2 Conformity and Homogeneity Indices

Conformity and homogeneity indices are used, respectively, to evaluate conformity of the prescription isodose surface to the target volume, and dose homogeneity inside the target volume.

- ***Conformity Index*** – A conformity index, as defined in the ICRU Report 62,[5] can be employed when the PTV is fully enclosed by the treated volume. It is defined as the quotient of the treated volume and the volume of the PTV.

The *PITV* ratio (planning isodose volume to the target volume ratio) is used as a conformity index for the evaluation of radiosurgical plans. Figure 3.2 illustrates how the *PITV* ratio is determined.

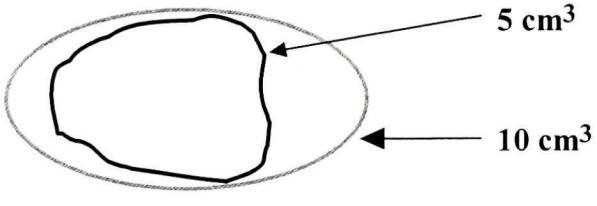

$$PITV = \frac{10\ cm^3}{5\ cm^3} = 2.0$$

Figure 3.2 – Scheme to illustrate how the *PITV* ratio is determined. The black and grey contours represent, respectively, the target and the prescription isodose line. In this case, 10 cm^3 is the volume enclosed by the prescription isodose and 5 cm^3 is the target volume. The *PITV* ratio is then $\left(\frac{10\ cm^3}{5\ cm^3}\right) = 2.0$.

In a randomized trial of radiosurgery of recurrent primary brain tumours and CNS metastases, the Radiation Therapy Oncology Group (RTOG) protocol 90-05, several guidelines were proposed that are now used in the evaluation of treatment plans even for non-protocol radiosurgical patients.[2, 6, 7] Based on these guidelines, a *PITV* ratio between

1.0 and 2.0 is considered per protocol. *PITV* ratios between 0.9 and 1.0 or between 2.0 and 2.5 are considered minor deviations, whereas *PITV* ratios less than 0.9 or greater than 2.5 are considered major deviations.

- ***Homogeneity Index*** – It is common practice in conventional radiation therapy to define the target absorbed dose at the center of the target volume and to allow hot and cold spots, keeping the dose in the target volume within –5% and +7% of the prescribed dose.[8] The clinical relevance of similar dose homogeneity within the target volume for stereotactic radiosurgery is not proven, and, in fact, in some techniques, improved dose conformity to irregular targets is commonly achieved by using multiple isocenters and prescribing to a lower isodose surface, resulting in large dose inhomogeneities within the target volume.

The homogeneity index *MDPD* (maximum dose to the prescription dose ratio) is defined as the ratio between the maximum dose (*MD*) inside the target, to the prescription dose (*PD*). Figure 3.3 shows a scheme illustrating how the *MDPD* index is calculated.

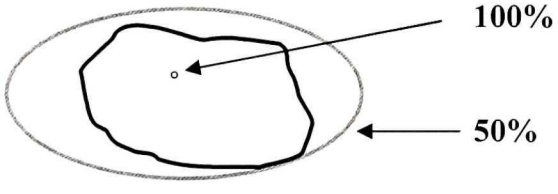

$$MDPD = \frac{100\%}{50\%} = 2.0$$

Figure 3.3 – Scheme to illustrate how the *MDPD* homogeneity index is calculated. The black and grey contours represent, respectively, the target and the prescription isodose line. In this case, 100% is the maximum dose given to the target and the dose is prescribed to the 50% isodose line, resulting in an *MDPD* of 2.0.

Based on the guidelines of the RTOG protocol 90-05,[2] for a case to be considered per protocol, the *MDPD* index must be less than or equal to 2.0. An *MDPD* greater than 2.0 but less than 2.5 is considered a minor deviation, whereas an *MDPD* greater than 2.5 is considered a major deviation.

3.3.3 Biological Indices

3.3.3.1 Integral Biologically Effective Dose (IBED)

The concept of biologically effective dose (*BED*) is based on the linear-quadratic (LQ) model of cell survival as a function of dose.[9] The cell surviving fraction s is defined as the ratio of the number of cells N which survive (retain reproductive capacity) a given dose to the number N_0 in the original, unexposed, sample, and it expresses the magnitude of the effect of a given dose of radiation.[10] Thus:

$$s = \frac{N}{N_o}. \tag{3.1}$$

In the LQ model, s can be described in terms of two mechanisms, one directly proportional to the total dose D, and the other proportional to the square of D, by the following relationship:

$$s = \exp-\left(\alpha D + \beta D^2\right), \tag{3.2}$$

where the two mechanisms of cell injury, for any dose D, are related by the coefficients α and β, which are constants and characteristic of the particular tissue irradiated. The ratio α/β has the dimensions of dose and represents the dose at which both mechanisms contribute equally to cell killing. Figure 3.4 shows a typical cell survival curve, illustrating the linear and quadratic mechanisms of cell killing for a low LET radiation as well as the ratio α/β.

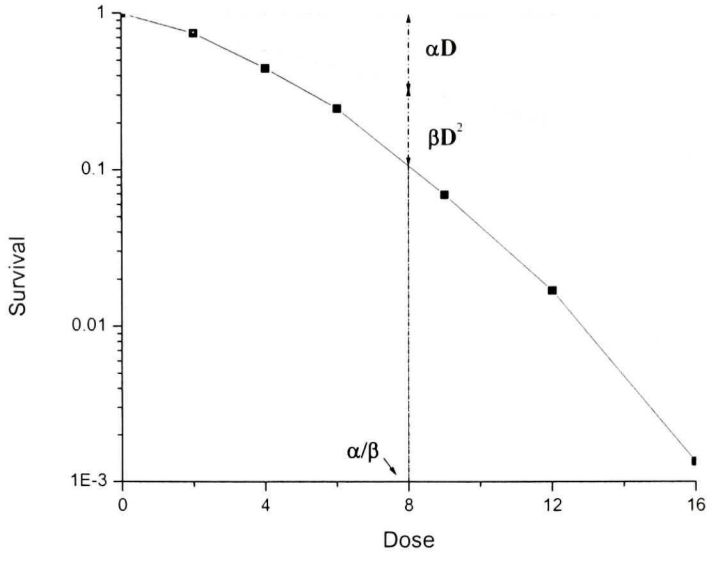

Figure 3.4 – Graph of a typical cell survival curve, illustrating both the linear and quadratic mechanisms that contribute to cell killing for a low LET radiation, and also, the ratio α/β that represents the dose for which the contribution of both effects is the same. The fraction of surviving cells (capable of dividing) is plotted on a logarithmic scale, against the radiation dose on a linear scale.

The biological effect E of the irradiation is determined from the survival and is defined as follows:

$$E = -\log(s) = \alpha D + \beta D^2, \tag{3.3}$$

or

$$\frac{E}{\alpha} = D\left(1 + \frac{D}{\alpha/\beta}\right). \tag{3.4}$$

The parameter E/α, referred to as the biologically effective dose (BED), can be used to compare different fractionation schemes.[11]

The equations presented so far are applied for a single fraction therapy, whereas, for fractionated therapy in which n fractions of dose per fraction d (with $n \cdot d = D$) are given separated by a time interval of at least 6 hours to allow sub-lethal damage repair, equation (3.4) can be modified to give:[10]

$$\left(E/\alpha\right)_n = nd\left(1+\frac{d}{\alpha/\beta}\right), \tag{3.5}$$

where the subscript n indicates that E/α is for a fractionated therapy.

Knowledge of the ratio α/β for the concerned tissues is a requirement for the application of the LQ model, and it has been shown that, for a wide range of acutely responding tissues, α/β is approximately 10 Gy and this value has been widely adopted.[9] It is believed that tumour response may be best described in this way, and so this value is also used for tumours.[9] The value for α/β of 3 Gy is often taken as applying to generalized late connective tissue damage, such as fibrosis, ulceration or necrosis, whereas values of 1.5 to 2 Gy are more appropriate to the spinal cord and brain.[9]

In hypofractionated stereotactic radiotherapy treatments, the LQ model has been applied using differential DVHs in the following way:[3, 12]

Each inhomogeneously irradiated outlined structure is divided into i dose bins of width 1%, in which the dose can be considered constant, with 100% being the value of the maximum dose delivered to the target volume and d_i the dose delivered to the i_{th} dose bin. The volume within each dose bin Δv_i expressed as a fraction of the total volume V of the structure, gives the partial volume $(\Delta v_i / V)$ for that dose bin.

An incremental *BED* (*ΔBED*) can be calculated for each dose bin using the equation:

$$\Delta BED = n \cdot d_i\left(1+\frac{d_i}{\alpha/\beta}\right)\frac{\Delta v_i}{V}. \tag{3.6}$$

The summation of the *ΔBED* values throughout the structure gives the integral *BED* (*IBED*), defined by the equation:

$$IBED = \sum_i n \cdot d_i \left(1 + \frac{d_i}{\alpha/\beta} \right) \frac{\Delta v_i}{V}. \qquad (3.7)$$

The *IBED* parameter has been introduced in a retrospective study to evaluate brain stem toxicity in hypofractionated stereotactic radiotherapy treatments.[3] The authors suggest that this parameter be used for comparison of dose-fractionation schedules rather than for absolute dose-response determination in the same way as it is recommended for the linear-quadratic model.

As most stereotactic treatment planning systems calculate DVHs for delineated structures, a routine for the calculation of *IBED*s can be implemented easily. In this study, *IBED*s for the targets as well as for the concerned normal tissues (brain and brain stem) were calculated, assuming α/β ratios of 10, 2 and 2.5 Gy respectively for tumour, brain, and brain stem. The calculated values were used to compare different linear accelerator stereotactic radiosurgery techniques and different radiosurgery treatment plans.

3.3.3.2 Tumour Control Probability (TCP)

The available clinical and laboratory data suggest that both tumours and normal tissues have a sigmoidal dose-response relationship (see Figure 3.6), and several mathematical models have been proposed for fitting these data.[4,13-22]

Tumour control probability is tumour specific and is dependent on tumour volume (the larger the tumour, the greater the dose needed to control it) as well as radiation dose.[23] Several *TCP* models have been proposed for fitting the available clinical and laboratory data.[13-16] While these models potentially provide a valuable quantitative biophysical measure of a 3-D dose distribution, their merit has not been proven yet due to the difficulty in precisely taking into account all variables that affect tumour control.[24] Moreover, there is a great deal of uncertainty in the values of the underlying model parameters.

In an attempt to reduce the complexity of *TCP* models, several authors[25-27] proposed the reduction of these models to simpler predictors of outcome; however, studies that actually confront these different predictors with clinical outcome data for individual patients are sparse.[28]

Three particularly common *TCP* models are the *probit* and *logit* empirical models[14,15] in which probit and logistic functions, respectively, are used to represent the sigmoidal dose-response relationships and the *Poisson* model[16] which assumes that cell kill is governed by Poisson statistics.

The equations giving the response probability for uniform irradiation of the total organ (partial volume $v = 1$) to dose D, $P(D, v = 1)$, for each of these models are given below:

Probit model:

$$P(D,1) = 0.5\left\{1 - Erf\left[\sqrt{\pi}\cdot\gamma_n\left(1 - \frac{D}{D_{50}}\right)\right]\right\} . \tag{3.8}$$

Logit model:

$$P(D,1) = \left\{1 + \left(\frac{D_{50}}{D}\right)^{4\gamma_n}\right\}^{-1} . \tag{3.9}$$

Poisson model:

$$P(D,1) = 2^{-e^{\left[e\cdot\gamma_n\left(1-\frac{D}{D_{50}}\right)\right]}} . \tag{3.10}$$

Each of the above functions is written in a standard format using only the parameters D_{50}, the dose that yields a 50% response, and γ_n, a dimensionless number equal to the maximum value of the normalized gradient γ of the dose-response curve $\left(\gamma = D \cdot \frac{dP}{dD}\right)$.

Of the three models, only the Poisson model is radiobiologically relevant,[17] since the probability for a cell to be hit by a given particle is extremely small, but the beam consists of a huge number of particles, so that the mean hit number is finite. The probit and logit empirical models are mathematically easier to use when analyzing a large amount of clinical data, but they have no biological basis and merely approximate the sigmoidal curve shape.

The effect of a homogeneous dose delivery to an entire tumour or organ at risk may be approximated by equations (3.8) through (3.10). However, in radiation therapy organs are not uniformly irradiated in their entire volume, rather, they receive a non-uniform dose distribution. The dose-volume response of the tissues needs then to be modeled, and the form this takes depends on basic assumptions about the architecture of the organ in terms of the arrangement of its functional sub-units (FSUs).[17]

For tumours, the classical approach is to assume a uniform and parallel structure so that the probability to control a fraction of the whole tumour volume, $v = V/V_{ref}$ of known response $P(1)$ for the reference volume $V_{ref}\,(v = 1)$ is given by:

$$P(v) = \left[P(1)\right]^{v}. \tag{3.11}$$

Particularly for the Poisson model, equation (3.10), the dose and volume dependent expression becomes:

$$P(D,v) = 2^{-e^{\left[e\cdot\gamma\left(1-\frac{D}{D_{50}}\right)+\ln v\right]}}. \tag{3.12}$$

Also, the assumption that the tumour is a tissue with a parallel architecture implies that all FSUs must be inactivated in order to destroy the tumour.[23] Thus, for predicting the *TCP* of a non-uniformly irradiated tumour, the tumour can be divided into voxels, or tumourlets, in which the dose can be assumed to be constant. The *TCP* of each tumourlet is computed using one of the proposed models, and the *TCP* for the whole tumour is the product of the response probabilities of the tumourlets, given by:

$$TCP = \prod_i \left[P(D_i, v_i) \right], \tag{3.13}$$

where $P(D_i, v_i)$ represents the response of the i^{th} tumourlet, with fractional volume v_i and irradiated to a dose D_i, and the functional form of $P(D, v)$ depends on the model that is being used.

The Poisson model for the calculation of *TCP* [equation (3.12)] has been used to compare different radiosurgery treatment modalities using differential DVHs.[23] Each dose bin in the differential DVH represents a small volume in which the dose can be assumed to be constant. Equation (3.12) is then applied to each dose bin and the *TCP* corresponding to the treatment plan is obtained by multiplying the responses for all dose bins.

However, as the input parameters for *TCP* calculations are based on a conventional 2 Gy per fraction radiation therapy schedule, the application of the model for radiosurgery requires that the single fraction doses in the original DVH be converted to equivalent 2 Gy per fraction doses before applying the model.[23,29] Single fraction doses ($D_{1-fraction}$) can be converted to equivalent 2 Gy per fraction doses (D_2) using the *BED* formalism, with the following expression:[29]

$$D_2 = D_{1-fraction} \frac{\left(\alpha/\beta + D_{1-fraction}\right)}{\left(\alpha/\beta + 2\right)}. \tag{3.14}$$

Once an equivalent 2 Gy per fraction DVH has been obtained, equation (3.12) is applied to each dose bin in this equivalent DVH, with D representing a homogeneous 2 Gy per fraction equivalent dose given to the dose bin, and v the fraction of the target volume represented by the referred dose bin. The *TCP* for the treatment plan is then calculated by multiplying the response probabilities for all dose bins in the equivalent DVH, as given by equation (3.13).

The application of equation (3.12) for a dose bin requires some considerations and assumptions regarding the parameters γ and D_{50}:

γ - As stated in the literature, an appropriate value of γ for an individual might be 8 and for a population might be between 1.5 and 4.[30] Making the assumption that the dose-response of all individuals is equal to that of the population, it has been suggested to assign γ a value of 3.[23]

D_{50} - There is evidence that D_{50} should increase with increasing tumour volume with an approximately log-linear relationship.[30] In order to derive an expression for D_{50}, a simple form of the dose-response relationship, based on the Poisson model can be used:[31]

$$P(D,1) = e^{-N_0 e^{\left(-D/D_0\right)}}, \tag{3.15}$$

where N_0 is the number of clonogens in the tumour and D_0 is the "effective mean lethal dose." Assuming that the clonogenic cell density is 10^7 cm^{-3} yields:[32]

$$N_0 = 10^7 \cdot V, \tag{3.16}$$

where V is the target volume in cm^3. Substituting in equation (3.15) for N_0 and $D = D_{50}$ [remembering that, by definition, $P(D_{50},1) = 0.5$], and rearranging yields:

$$D_{50} = D_0 \cdot \ln\left(10^7 \cdot \frac{V}{0.693}\right). \tag{3.17}$$

Equation (3.17), as previously suggested, shows a log-linear dependence of D_{50} on tumour volume V. Now, in order to calculate D_{50}, it is necessary to know the value for D_0. The latter can be chosen to yield a *TCP* of approximately 0.5 for a dose of 60 Gy delivered to 10^7 clonogens (equivalent to 1 cm^3 based on the assumed clonogenic cell density) using a conventional 2 Gy per fraction radiation therapy schedule.[33] A value of 3.7 Gy, yields D_{50} values of 52.5 Gy for a volume of 0.1 cm^3, 61 Gy for 1.0 cm^3 (approximately 60 Gy as stated above), and 69.5 Gy for 10 cm^3. These numbers can be considered representative of a "generic" tumour and have been applied in the literature for the ranking of treatment plans, as, for this purpose, the choice of tumour type is not as critical.[23]

It is important to note that in the literature[23,29,34] the *BED* formalism has been applied to convert single fraction DVHs into equivalent 2 Gy per fraction DVHs, without considering the effect of overall treatment time, or the effect of an altered fractionation on the oxygenation status of the tumour.

3.3.3.3 Normal Tissue Complication Probability (NTCP)

In recent years, several mathematical models for the calculation of *NTCP* have been presented in the literature.[17-22,4] These models have been applied in the optimization and evaluation of treatment plans, but the use of model estimates to guide clinical decisions still remains controversial due to the following reasons:

- Lack of reliable clinical input data (quality and quantity of data are not sufficient to draw definite conclusions);
- Normal tissues differ markedly from one another in their architecture. These differences result in different responses to radiation, that are not easily modeled;

- While tumour irradiation is more or less uniform for normal tissues, there is no incentive for uniform irradiation; indeed, it is often a goal of treatment to make normal tissue coverage highly non-uniform, since for many organs, when only a fraction of their volume is included in the high dose region, the tolerance is greatly increased.

The practical application of an *NTCP* model requires, initially, that the 3-D dose distribution in a normal structure be converted into a dose-volume histogram.[35] Next, a histogram reduction method has to be applied to this usually non-uniform irradiation, in such a way that the normal organ exposed to a non-uniform dose distribution (dose D_i in fractional volume v_i, $i = 1, 2...$) has the same *NTCP* as that corresponding to the reduced uniform irradiation (for which some clinical data exist).

This histogram reduction can be performed using: (i) interpolation[36] which reduces a cumulative DVH to an "equivalent" one in which a single effective dose is given to the whole, reference volume, V_{ref}, (ii) the effective volume method[19] that reduces a differential DVH yielding a one-step histogram with a uniform dose, given by the maximum organ dose, to the effective volume V_{eff}, which is equal to or less than the whole organ volume.

Figures 3.5 (a) and (b) show examples of DVH reduction using, respectively, linear interpolation and the effective volume method.

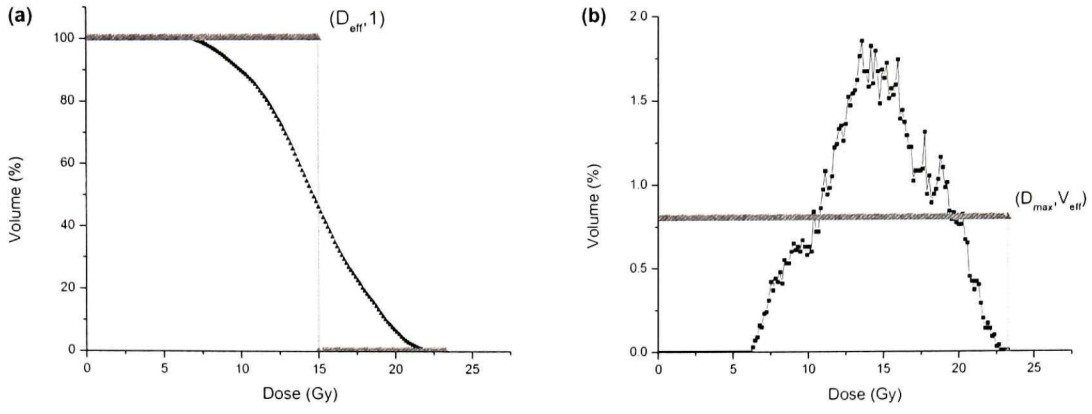

Figure 3.5 – (a) DVH reduction using linear interpolation; (b) DVH reduction using the effective volume method.

Following histogram reduction, one of the available *NTCP* models with the appropriate input parameters can be applied.

Existing *NTCP* models can be distinguished by their descriptions of the volume effect. Specifically, the empirical model proposed by Lyman[18] to fit clinical data[37,38] describes the tolerance doses and volume effects in terms of the following four parameters:

(i) $TD_{50}(1)$, the tolerance dose for whole-organ irradiation for which there is a 50% probability of complications occurring;

(ii) m, the steepness of the dose response curve;

(iii) V_{ref}, the reference volume; and

(iv) the parameter n, which represents the volume effect.

The following equations describe the model:

$$NTCP = \frac{1}{\sqrt{2\pi}} \int_{-\infty}^{t(D,v)} e^{\frac{-t'^2}{2}} dt' \tag{3.18}$$

$$v = V_{eff} / V_{ref} \tag{3.19}$$

$$t = (D - TD_{50}(v)) / (m \cdot TD_{50}(v)) \tag{3.20}$$

$$TD_{50}(1) = TD_{50}(v) \cdot v^{n} \tag{3.21}$$

The Lyman model cannot be fully understood without some considerations of the clinical data that the model has been proposed to fit.

Presently, a compilation of tolerance data by Emami *et al.*[37,38] for uniform irradiation of partial and whole organ represents the most complete set of clinical data, and most mathematical models have applied to this data. Emami *et al.* have compiled tolerance doses for many organs as a function of the whole and partial organ volumes, based on a conventional 2 Gy per fraction radiation therapy schedule. Particularly, they give information only for uniform irradiations of 1/3, 2/3 and 3/3 organ volume, and only for $NTCP$ = 0.05 and 0.50 (i.e., $TD_{5/5}$ and $TD_{50/5}$). The tolerance doses proposed by Emami for the endpoint necrosis of the brain and brain stem, which are the normal organs concerned in this study, are given in Table 3.1.

Table 3.1 - Tolerance doses for two *NTCP* levels ($TD_{5/5}$ and $TD_{50/5}$) tabulated for three volume categories (one-third, two-thirds, and whole organ) for the endpoint necrosis of the brain and brain stem. Values in parentheses correspond to predictions from the Lyman model (obtained by the fitting process). *From*: Tolerance of normal tissue to therapeutic irradiation. [IJROBP Vol. 21, 109-122 (1991)].

Organ	$TD_{5/5}(cGy)Volume$			$TD_{50/5}(cGy)Volume$			**Selected Endpoint**
	1/3	**2/3**	**3/3**	**1/3**	**2/3**	**3/3**	
Brain	6000 (6000)	5000 (5000)	4500 (4500)	7500 (7900)	6500 (6700)	6000 (6000)	Necrosis/Infarction
Brain Stem	6000 (6000)	5300 (5300)	5000 (5000)	—	—	6500 (6500)	Necrosis/Infarction

NTCP values for doses and volumes different from those presented in Table 3.1 and for the more realistic case of non-uniform irradiation can only be estimated by interpolation or extrapolation. This, in turn, requires the selection of a mathematical model that fits the existing data, allowing the prediction of the *NTCP* for other irradiation conditions.

For the Lyman model, the previously referred $TD_{50}(1)$, n and m parameters were obtained by fitting Emami's tolerance data to equation (3.18),[37] with the parameter V_{ref} being the whole organ volume. Table 3.2 lists the 4 parameters: V_{ref}, n, m, and $TD_{50}(1)$ for the endpoint necrosis for the brain and brain stem.

Table 3.2 – Four parameters of the Lyman model for the brain and brain stem for the endpoint necrosis/infarction considered by Emami *et al. From*: Fitting of normal tissue tolerance data to an analytic function. [IJROBP Vol. 21, 123-135 (1991)].

Organ	**Fit parameters**				**Endpoint**
	V_{ref}	n	m	$TD_{50}(1)(Gy)$	
Brain	Whole organ	0.25	0.15	60	Necrosis/Infarction
Brain Stem	Whole organ	0.16	0.14	65	Necrosis/Infarction

- ***Practical application of the Lyman model in radiosurgery treatment plans.***

Equations (3.18) through (3.21) can be applied for the calculation of the *NTCP* in radiosurgery, after performing some modifications in the original single fraction DVH of a radiosurgery plan. To calculate the *NTCP*, the integral in equation (3.18) has to be solved, but, before this integration can be performed, D and v, and the values of the four parameters have to be determined.

The first step consists in performing the histogram reduction, in order to obtain the values for D and v. However, as the input parameters in the Lyman model correspond to a conventional 2 Gy per fraction radiation therapy schedule, before performing the reduction, the single fraction doses in the original DVH must be converted to equivalent

2 Gy per fraction doses. Single fraction doses ($D_{1-fraction}$) can be converted to equivalent 2 Gy per fraction doses (D_2) using the *BED* formalism[23,29] in the same way as was done for tumours [equation (3.14)], but with different values for the ratio α/β.

In this case, no time correction factor is needed when equating the *BED*s because, for late-reacting tissues, no compensatory proliferation occurs during the weeks of radiotherapy.[9]

Equation (3.14) is applied to each dose bin in the original single fraction DVH, using a α/β ratio of 2 Gy for the brain[9] and 2.5 Gy for the brain stem[3], and histogram reduction is then performed in this resulting equivalent DVH (2 Gy per fraction).

In our study, the effective volume DVH reduction method was selected for use. Using the differential equivalent DVH, the value of the effective volume is calculated as:

$$V_{eff} = \sum V_i \left(D_i / D_{\max} \right)^{1/n}, \tag{3.22}$$

where V_i is a sub-volume irradiated to an equivalent 2 Gy per fraction dose D_i and $D_{\max}$ is the maximum dose in the equivalent histogram, with the summation being performed over all dose bins in the equivalent differential histogram. The choice of $D_{\max}$ as the dose for the single-step histogram assures that V_{eff} is always less than or equal to the whole organ volume.

Following histogram reduction using the effective volume method, DVHs which have the same mean dose but different dose uniformity will have different values for both $D_{\max}$ and V_{eff}.

In order to obtain the complication probability associated with this uniform irradiation to a partial organ volume, represented by the reduced histogram, the parameters V_{ref}, $TD_{50}(1)$, n and m must be known:

V_{ref} - For organs considered in this study (normal brain and brain stem) V_{ref} is equal to the whole organ volume.[37] The literature suggests that the best estimate for V_{ref} is that derived from CT data,[39] and, whenever the CT scans do not contain the entire volume of the organ, some arbitrary reference volume can be used.

$TD_{50}(1)$ - The parameter $TD_{50}(1)$ represents the tolerance dose for whole organ irradiation, based on a conventional fractionation schedule of 2 Gy per fraction, which leads to a complication probability of 50%. This data has been compiled by Emami *et al.* for several organs and different endpoints[37,38] (see Table 3.1 for data for the brain and brain stem).

n- Small values of n for normal tissues mean a high dependence of complication probability on dose, and, as n approaches zero, the complication probability correlates with the largest dose in the histogram. As n approaches unity, if the dose and volume of a histogram are modified so that their product that gives the integral dose is unaltered, then the complication probability should remain unaltered. Therefore, when n is equal to unity, the complication probability correlates with the integral dose.

The value of the parameter n can be determined using equation (3.21) with the doses $TD_{50}(1)$ and $TD_{50}(1/3)$.[37] In this case, $v = 1/3$, and $TD_{50}(1)$ and $TD_{50}(1/3)$ correspond, respectively, to the tolerance doses for uniform, whole and 1/3 organ irradiation predicted by the Lyman model (values in parentheses in Table 3.1), based on a conventional fractionation schedule of 2 Gy per fraction. Using these data in equation (3.21) we have:

$$TD_{50}(1) = TD_{50}(1/3) \cdot (1/3)^n ,$$

with

$$n = \frac{\ln\left(TD_{50}(1) / TD_{50}(1/3)\right)}{\ln(1/3)}. \tag{3.23}$$

m- The value of the parameter *m* can be determined using equations (3.18) and (3.20).[37] From equation (3.18), for a 5% complication probability (i.e., $NTCP = 0.05$), the variable *t* must have a value of -1.647. Substituting this value in equation (3.20), with *D* in this case equal to $TD_5(v)$, the parameter *m* can be calculated. Using these data in equation (3.20) and solving for *m*, we have:

$$m = \frac{1}{1.647} \cdot \left(1 - \frac{TD_5(1)}{TD_{50}(1)}\right), \tag{3.24}$$

where, in this case, $TD_5(1)$ and $TD_{50}(1)$ are, respectively, the tolerance doses for 5% and 50% complication probabilities for the whole organ irradiation, based on a conventional fractionation schedule of 2 Gy per fraction (values in parenthesis Table 3.1).

3.3.3.4 Probability of Uncomplicated Tumour Control (P_{utc})

The determination of *TCP* and *NTCP* in a treatment plan optimization process can be viewed as surrogate with the ultimate goal being to base clinical decisions on a balance between tumour control and normal tissue complication.[40] For this purpose, the probability of uncomplicated tumour control P_{utc} has been defined. Using both the *TCP* and the *NTCP*, the P_{utc} can be given by:

$$P_{utc} = TCP \cdot (1 - NTCP). \tag{3.25}$$

The parameter P_{utc} has been proposed because, as it quantifies the likelihood of treatment success in the context of both tumour control and normal tissue complications, it would provide a more realistic overall metric than either tumour control or normal tissue complication probability alone. However, its use has been criticized,[41] because it assumes that a certain fractional change in *TCP* can be balanced by a fractional change in *NTCP*, without regard to the very different nature of the consequences.

Figure 3.6 shows an example of the sigmoidal curves that represent *TCP* and *NTCP* as a function of dose, as well as a curve for the probability of uncomplicated tumour control. It can be seen from Figure 3.6 that, in this case, an optimum dose (B) can be chosen that will produce the maximum *TCP* with an acceptable incidence of complications. A lower dose (A) will result in a lower probability of tumour control, but without complications, and a higher dose (C) will result in a higher probability of tumour control, but with an unacceptable incidence of complications.

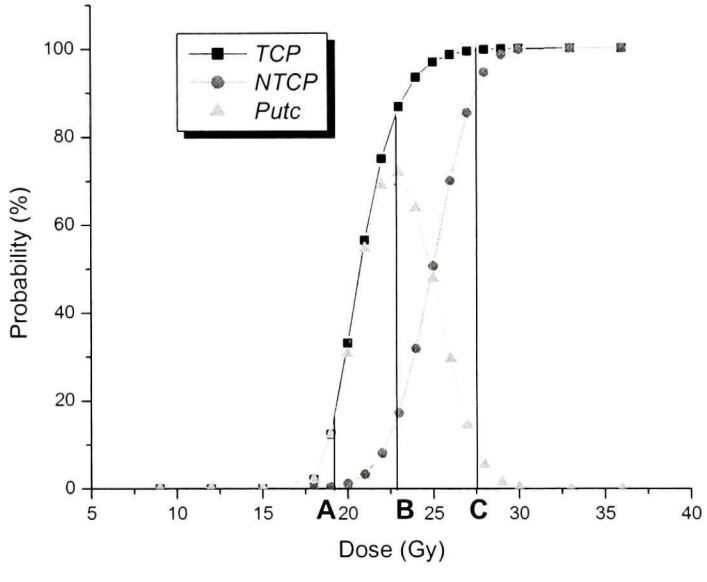

Figure 3.6 – Optimization of the uncomplicated tumour control (P_{utc}). *TCP* and *NTCP* are shown as a function of radiation dose. At dose A tumour control will be improbable, but complications will be negligible. At dose C, tumour control will be highly probable, but the complication rate will be excessive. The optimum dose B will result in the greatest probability of uncomplicated tumour control.

REFERENCES

1 R. E. Drzymala, R. Mohan, L. Brewster, J. Chu, M. Goitein, W. Harms, and M. Urie, "Dose-Volume Histograms," Int. J. Radiat. Oncol., Biol., Phys. **21**, 71-78 (1991).

2 E. Shaw, R. Kline, M. Gillin, L, Souhami, A. Hirschfeld, R. Dinapoli, and L. Martin, "Radiation Therapy Oncology Group: Radiosurgery Quality Assurance Guidelines," Int. J. Radiat. Oncol., Biol., Phys. **27**, 1231-1239 (1993).

3 B. G. Clark, L. Souhami, and C. Pla, "The integral biologically effective dose to predict brain stem toxicity of hypofractionated stereotactic radiotherapy," Int. J. Radiat. Oncol., Biol., Phys. **40**, 667-675 (1998).

4 G. J. Kutcher, "Quantitative plan evaluation: TCP/NTCP models," Front. Radiat. Ther. Oncol. **29**, 67-80 (1996).

5 ICRU Report 62, *Prescribing, Recording and Reporting Photon Beam Therapy (Supplement to ICRU Report 50)* (ICRU, Bethesda, MD, 1999).

6 E. Shaw, C. Scott, L. Souhami, R. Dinapoli, J. P. Bahary, R. Kline, M. Wharam, C. Schultz, P. Davey, J. Loeffler, J. D. Rowe, L. Marks, B. Fisher, and K. Shin, "Radiosurgery for the treatment of previously irradiated recurrent primary brain tumors and brain metastases: Initial report of Radiation Therapy Oncology Group protocol 90-05," Int. J. Radiat. Oncol., Biol., Phys. **34**, 647-654 (1996).

7 E. Shaw, C. Scott, L. Souhami, R. Dinapoli, R. Kline, J. Loeffler, and N. Farnan, "Single dose radiosurgical treatment of recurrent previously irradiated primary brain tumors and brain metastases: Final report of RTOG protocol 90-05," Int. J. Radiat. Oncol., Biol., Phys. **47**, 291-298 (2000).

8 ICRU Report 50, *Prescribing, Recording and Reporting Photon Beam Therapy* (ICRU, Bethesda, MD, 1993).

9 J. F. Fowler, "The linear quadratic formula and progress in fractionated radiotherapy – Review article," Br. J. Radiol. **62**, 679-694 (1989).

10 E. J. Hall, *Radiobiology for the Radiologist* (Lippincott Williams & Wilkins Publishers, 2000).

11 J. F. Fowler, "Intercomparisons of new and old schedules in fractionated radiotherapy," Semin. Radiat. Oncol. **2**, 67-72 (1992).

12 P. W. Hoban, L. C. Jones, and B. G. Clark, "Modeling late effects in hypofractionated stereotactic radiotherapy," Int. J. Radiat. Oncol., Biol., Phys. **43**, 199-210 (1999).

13 P. Okunieff, D. Morgan, A Niemierko, and H. D. Suit, "Radiation dose-response of human tumors," Int. J. Radiat. Oncol., Biol., Phys. **32**, 1227-1237 (1995).

14 M. Goitein and T. E. Schultheiss, "Strategies for treating possible tumor extension: Some theoretical considerations," Int. J. Radiat. Oncol., Biol., Phys. **11**, 1519-1528 (1985).

15 G. J. Kutcher, *et al.*, "Three-dimensional photon treatment planning for carcinoma of the nasopharynx," Int. J. Radiat. Oncol., Biol., Phys. **21**, 169-182 (1991).

16 T. R. Munro and C. W. Gilbert, "The relation between tumor lethal doses and the radiosensitivity of tumor cells," Br. J. Radiol. **34**, 246-251 (1961).

17 P. Källman, A. Ågreen, and A. Brahme, "Tumor and normal tissue responses to fractionated non-uniform dose delivery," Int. J. Radiat. Biol. **62**, 249-262 (1992).

18 J. T. Lyman, "Complication probability as assessed from dose-volume histograms," Radiat. Res. **104**, S13-S19 (1985).

19 G. J. Kutcher and C. Burman, "Calculation of complication probability factors for non-uniform normal tissue irradiation: The effective volume method," Int. J. Radiat. Oncol., Biol., Phys. **16**, 1623-1630 (1989).

20 A. Niemierko and M. Goitein, "Calculation of normal tissue complication probability and dose-volume histogram reduction schemes for tissues with a critical element structure," Radiother. Oncol. **20**, 166-176 (1991).

21 A. Niemierko and M. Goitein, "Modeling of normal tissue response to radiation: The critical volume model," Int. J. Radiat. Oncol., Biol., Phys. **25**, 135-145 (1993).

22 T. E. Schultheiss, C. G. Orton, and R. A. Peck, "Models in radiotherapy: Volume effects," Med. Phys. **10**, 410-415 (1983).

23 V. Smith, L. Verhey, and C. F. Serago, "Comparison of radiosurgery treatment modalities based on complication and control probabilities," Int. J. Radiat. Oncol., Biol., Phys. **40**, 507-513 (1998).

24 F. M. Khan and R. A. Potish, *Treatment Planning in Radiation Oncology* (Williams & Wilkins, 1998).

25 A. Niemierko, "Reporting and analyzing dose distributions: A concept of equivalent uniform dose," Med. Phys. **24**, 103-110 (1997).

26 A. Brahme, "Dosimetric precision requirements in radiation therapy," Acta Radiol. Oncol. **23**, 379-391 (1984).

27 J. Deasy, "Tumor Control Probability models for non-uniform dose distributions," In: *Volume and kinetics in tumor control and normal tissue complications* (Medical Physics Publishing, Madison, 1998).

28 A. Niemierko, "A concept of equivalent uniform dose (EUD)," In: *Volume and kinetics in tumor control and normal tissue complications* (Medical Physics Publishing, Madison, 1998).

29 B. Sanchez-Nieto and A. E. Nahum, "Bioplan: software for the biological evaluation of radiotherapy treatment plans," Med. Dosim. **25**, 71-76 (2000).

30 M. Goitein, "The probability of controlling an inhomogeneously irradiated tumor," In: *Evaluation of treatment planning for particle beam radiotherapy* (National Cancer Institute, Bethesda, 1986).

31 A. L. Boyer and T. E Schultheiss, "Effects of dosimetric and clinical uncertainty on complication-free local tumor control," Radiother. Oncol. **11**, 65-71 (1988).

32 S. Webb and A. E. Nahum, "A model for calculating tumor control probability in radiotherapy including the effects of inhomogeneous distributions of dose and clonogenic cell density," Phys. Med. Biol. **38**, 653-666 (1993).

33 G. K. Zagars, T. E. Schultheiss, and L. J. Peters, "Inter-tumor heterogeneity and radiation dose-control curves," Radiother. Oncol. **8**, 353-361 (1987).

34 J. E. Mignano, M. J. Engler, J. Tsai, and D. E. Wazer, "Comparison of radiobiologic modeling for one- and two-isocenter dose distributions applied to ellipsoidal radiosurgery targets," Int. J. Radiat. Oncol., Biol., Phys. **49**, 833-837 (2001).

35 V. Moiseenko, J. Battista, and J. V. Dyk, "Normal tissue complication probabilities: Dependence on choice of biological model and dose-volume histogram reduction scheme," Int. J. Radiat. Oncol., Biol., Phys. **46**, 983-993 (2000).

36 J. T. Lyman and A. B. Wolbarst, "Optimization of radiation therapy: 4. A dose volume reduction algorithm," Int. J. Radiat. Oncol., Biol., Phys. **13**, 103-109 (1987).

37 C. Burman, G. J. Kutcher, B. Emami, and M. Goitein, "Fitting of normal tissue tolerance data to an analytic function," Int. J. Radiat. Oncol., Biol., Phys. **21**, 123-135 (1991).

38 B. Emami, J. Lyman, A. Brown, L. Coia, M. Goitein, J. E. Munzenrida, B. Shank, L. J. Solin, and M. Wesson, "Tolerance of normal tissue to therapeutic irradiation," Int. J. Radiat. Oncol., Biol., Phys. **21**, 109-122 (1991).

39 G. J. Kutcher, C. Burman, L. Brewster, M. Goitein, and R. Mohan, "Histogram reduction method for calculating complication probabilities for three-dimensional treatment planning evaluations," Int. J. Radiat. Oncol., Biol., Phys. **21**, 137-146 (1991).

40 M. H. Phillips, *Physical Aspects of Stereotactic Radiosurgery* (Plenum Medical Book Company, New York, 1993).

41 R. Mohan and C. C. Ling, "When becometh less more?" Int. J. Radiat. Oncol., Biol., Phys. **33**, 235-237 (1995).

CHAPTER 4

METHODS AND MATERIALS

This chapter describes the experimental methods used to compare the dynamic rotation, static conformal beam, and intensity-modulated radiosurgery techniques. The chapter begins with a description of target shapes and sizes used in our comparative study, the reasons why these were chosen, and the implementation of these target shapes in different treatment planning systems. A description of the methods used for treatment planning and parameters that were altered in each technique in order to obtain the best possible plans is then given. A description of methods used to calculate the plan evaluation tools is also presented. Finally, a discussion of the methods used to evaluate possible correlation between physical and biological parameters is presented.

4.1 TARGETS TO BE EVALUATED FOR THE THREE RADIOSURGICAL TECHNIQUES

4.1.1 Choosing Sizes and Shapes

The comparative study was carried out for simulated targets placed at the center of the brain. The simulated targets included a small and a large sphere with 1.5 cm and 3.0 cm diameter, respectively, a small and a large hemisphere with 1.5 cm and 3.0 cm diameter, respectively, and a C-shaped target, with maximum dimension of 3.5 cm, wrapped around a critical structure.

Small and large spheres – Spherical targets were chosen to demonstrate the type of target shape that would likely be treated adequately by all three techniques.

Small and large hemispheres – Hemispherical targets were chosen because they have a sharp edge, imposing a challenge in terms of beam configuration for all three techniques.

For spherical and hemispherical targets, small and large sizes were chosen to determine the size dependence on the planning process and on the analysis of results.

C-shaped target – The C-shaped target was chosen, because it simulates a lesion with a critical structure enclosed by the target, and also because it presents a concave surface. In general, the shape of the high dose region using uniform intensity beams is convex, and, as such, it is not able to conform to concavities within the PTV. Figures 4.1 (a), (b), and (c), illustrate the shape of the spherical, hemispherical, and C-shaped targets, respectively.

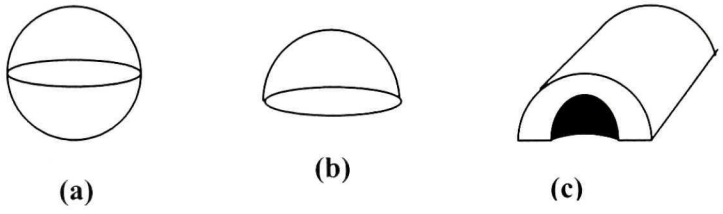

Figure 4.1 – Illustration of the spherical (a), hemispherical (b), and C-shaped (c) targets, evaluated in this study.

4.1.2 Modifications and Adaptations of the Alderson Rando Phantom

The practical implementation of these target shapes was done using a modified Alderson Rando anthropomorphic phantom (Alderson Rando® phantom, Radiology Support Devices Inc., Long Beach, CA, USA). The Rando phantom consists of a human skeleton embedded in rubber, moulded to form a sculpture of an average adult man, sliced in 2.54 cm thick transverse slabs. In order to have the exact same targets on different treatment planning systems, two slabs (third and fourth) from the head of the Rando phantom were replaced by specially machined Perspex slabs with the same thickness and approximately the same body contour as the original slabs. These slices were replaced in order to be possible to insert the different targets without damaging the original Rando phantom.

To insert the different targets, a square hole was made in the middle of the modified slabs. The target shapes consisted of two square Perspex plaques (see Figure 4.2), having the same dimensions as the holes in the slabs in such a way that these plaques could be inserted into the holes.

The different target shapes were simulated by machined holes made in these plaques. To simulate the small sphere, two plaques containing a 1 cm diameter hemispherical hole were inserted into the modified slices, with the hemispherical holes placed opposite to each other to form a sphere. The small hemisphere was simulated by inserting one of the above-mentioned plaques, together with a plain plaque. The same method was used for the large sphere and large hemisphere. The C-shaped target, wrapped around a critical structure, was simulated by a plaque containing a 3 cm diameter hemi-cylindrical hole (simulating the target) inserted opposite to a plaque containing a 1 cm diameter hemi-cylindrical Perspex insert attached to it (simulating the critical structure). Figure 4.2 shows the head of the Rando phantom with the modified slabs, and the plaques containing the holes machined to simulate the various target shapes.

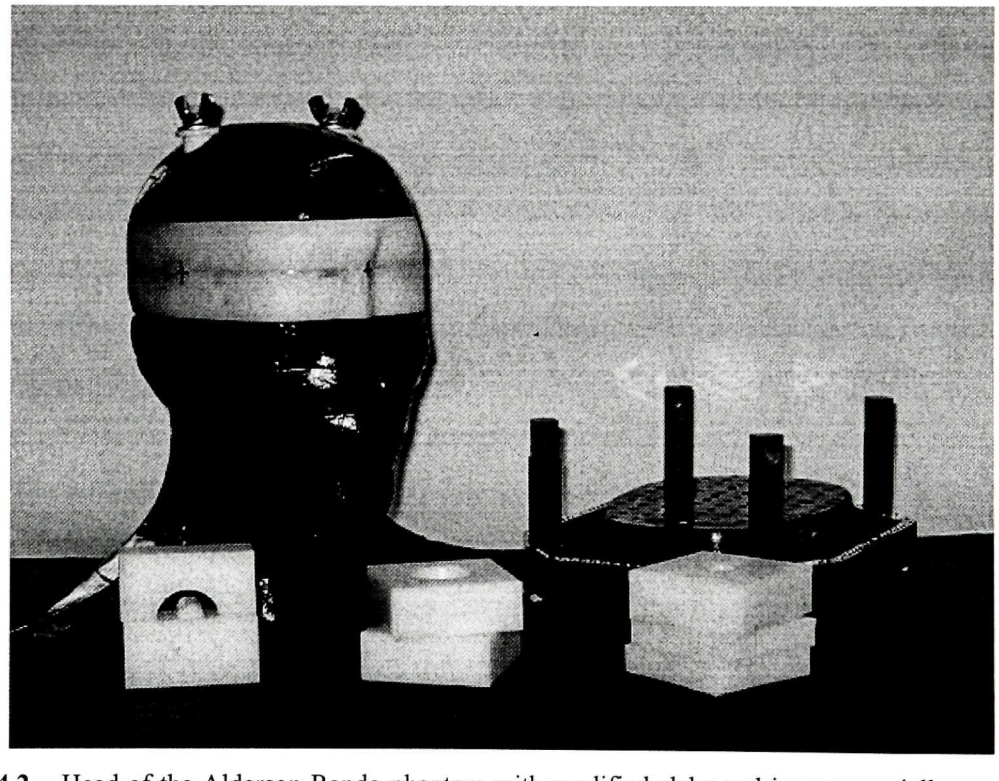

Figure 4.2 – Head of the Alderson Rando phantom with modified slabs and inserts specially machined to simulate the various target shapes used in this comparative study.

The idea behind this methodology, employed to simulate the target shapes, was that when the phantom with a given target was CT-scanned the region inside the hole, filled with air, would actually represent the target volume, and, as the CT image provides a very good contrast between air and Perspex, it would be easy to have the same target contours in different treatment planning systems. This was carried out to circumvent the problem that contoured volumes on one system cannot be transferred to another system.

4.1.3 Collection of Images for the Different Treatment Planning Systems

The Alderson Rando phantom, with the modified slabs, was then firmly fixed with pins to a Leksell stereotactic head frame, and a localizer box, containing CT-compatible N-shaped localization rods, was attached to the frame.

The phantom head was scanned on a Picker PQ-5000 CT scanner (Philips Medical Systems, Cleveland, OH, USA) with the five targets inserted, one at a time, into the modified slabs. Images were acquired with a slice thickness and slice increment of 2 mm from below the first modified slab to the top of the skull. The CT data for all targets was then transferred to the three different treatment planning systems. In each treatment planning system, images were localized relative to the stereotactic co-ordinate frame and contours were drawn on a slice-by-slices basis.

The veracity of this procedure, developed in order to have the same target dimensions in the different treatment planning systems, was checked by comparing the computed total target volumes on the three systems.

4.2 CREATING GOOD PLANS FOR EACH TECHNIQUE

Treatment planning of each target was performed for the three radiosurgery techniques. Since our objective was to compare the three techniques, plans for each target at each technique were generated. For each technique, the procedures performed in order to obtain optimal plans are described below.

4.2.1 Dynamic Rotation Technique

Treatment planning for the dynamic rotation technique was performed using the Stereotactic Radiosurgery/Radiotherapy module of the SimuPlan – The Montreal Treatment Planning System, as discussed in Section 2.2.1. Treatment planning for the two spherical targets was performed using a single isocenter, placed at the geometrical center of the target volume, with a cone diameter such that the maximum isodose surface completely encompassing the target volume was approximately 80 to 85% of the maximum dose. For the other three targets (two hemispherical and the C-shaped target), several plans were generated, varying the number of isocenters, with the number of isocenters chosen such that the dose distributions produced were compatible to the geometry of each target (see considerations about using multiple isocenters in Section 2.1.1). The objective of obtaining these plans was to verify the improvement in conformity (decrease in *PITV*) with increasing the number of isocenters.

In practice, the multiple isocenter plans were generated by first roughly placing the isocenters with appropriate collimator diameters. Then, by using the DVH analysis and 2-D displays of dose distributions, the position and collimator diameter of the isocenters were iteratively optimized on a trial and error basis. This optimization process continued until we had 50% as the highest isodose surface covering 100% of the target in order for the dose to be prescribed at this isodose (*MDPD* = 2.00), and also, until we obtained a reduced *PITV* whenever the number of isocenters was increased. These results, namely *PITV* vs. number of isocenters, were plotted for the two hemispherical and the C-shaped targets, and are presented in Chapter 5.

4.2.2 Static Conformal Beam Technique

Treatment planning for the static conformal beam technique was carried out using the Conformal beams module of the BrainSCAN version 5.1 treatment planning system (BrainLAB, AG, Germany), as discussed in Section 2.3.1. The static conformal beam technique uses non-coplanar uniform static fields, defined by the beam's eye view

projections of the target volume, and directed to a single isocenter. Using this technique, several plans were generated for each target. For the spherical targets, plans with 5 and 10 beams were generated, whereas for the hemispherical and C-shaped targets, plans with 5, 7, 9, 10 and 15 beams were generated.

To produce these plans, the treatment isocenter was first placed at the geometric center of the target. Then, the beams were entered, oriented in varied directions such as to minimize the overlap between the entrance and exit beam paths. A margin of around 1 mm was added to each beam in order to have approximately the 80% (of the maximum dose) isodose surface completely encompassing the target volume. This isodose surface was then normalized to 100% for the maximum dose to provide a direct indication of the homogeneity of dose inside the target. The collimator angle was always optimized in order to irradiate the smallest possible area for each beam. Plans were evaluated using DVHs and 2-D dose displays.

For the C-shaped target, beam orientations were chosen based on the geometric relationship between the target and the wrapped critical structure, and for each beam, whenever possible, the μ-MLC leaves were manually adjusted to minimize irradiation of the critical structure. Graphs of the *PITV* vs. number of beams were plotted for the two hemispherical and the C-shaped targets, and are presented in Chapter 5.

4.2.3 Intensity-Modulated Radiosurgery (IMRS) Technique

Treatment planning for the IMRS technique was performed using the CORVUS version 4.0 inverse treatment planning system (NOMOS Corporation, Sewickley, PA, USA), as discussed in Section 2.4.1. Treatment planning using the IMRS technique was performed using the same beam configurations (couch and gantry angles) as for the static conformal beam technique, with several plans with 5 and 10 beams generated for the spherical targets and plans with 5, 7, 9 and 10 beams generated for the hemispherical and the C-shaped targets.

For each beam configuration and each target the best plan in terms of lowest *PITV* and *MDPD* was generated. For the spherical and hemispherical targets, these optimal plans were generated by varying the prescription for normal tissue. In this case, the normal tissue was always considered as IMRS tissue type (terminology adopted by the CORVUS system, which means that a high degree of dose conformity to the target is sought in the optimization process) and the parameters: dose limit (Gy), volume of tissue above limit (%), and minimum and maximum doses (Gy) were varied in order to obtain the optimal plans. For the C-shaped target, again these parameters were varied but also, in this case, the prescription parameters for the critical structure (always allowed to be overexposed in order to adequately treat the tumour) were modified in order to obtain the optimal plans.

For all plans and all targets the prescription parameters for the target were not modified in the search for the best plans, with the target being considered of an IMRS type and a goal equal to the prescription dose (Gy), allowance of 0% of the target volume below goal, and with minimum and maximum doses, respectively, equal to the prescription and twice the prescription dose. Graphs of the *PITV* vs. number of beams for the IMRS technique were plotted for the two hemispherical and the C-shaped targets, and are presented in Chapter 5.

4.3 PRACTICAL IMPLEMENTATION OF THE PLAN EVALUATION TOOLS

In this section, the methods used to calculate all plan evaluation tools considered in our study are described. The following are general considerations applied in the treatment plan evaluations:

- The procedures described in the following were applied to all treatment plans, irrespective of the target shape or the technique;
- The information provided by the DVHs was the basis to calculate all evaluation tools;
- Doses were prescribed based on clinical practice in accordance with guidelines of the RTOG protocol 90-05[1] in which the maximum diameter of the lesion is taken into

account for prescription. The diameter ranges and respective prescription doses proposed by this protocol are:

- Diameter up to 20 mm → 24 Gy
- Diameter in the range 21 – 30 mm → 18 Gy
- Diameter in the range 31 – 40 mm → 15 Gy

Given these diameter ranges, 24 Gy was prescribed to the 1.5 cm diameter spherical and hemispherical targets, 18 Gy to the 3.0 cm diameter hemispherical target, and 15 Gy to the 3.0 cm diameter spherical and C-shaped targets.

- For all treatment plans, the dose was prescribed to the highest isodose surface that provided 100% target coverage. In this way, the prescription dose was always the minimum dose given to the target;
- Whenever the LQ model was used, it was assumed that the α/β ratio was 10 Gy for tumour tissue and 2 Gy for normal brain;
- The critical structure inside the C-shaped target was considered as brain stem, and an α/β ratio of 2.5 Gy and appropriate values for the parameters of the Lyman model were used in the calculation of the *IBED* and the *NTCP* for this structure.

4.3.1 Conformity (*PITV*) and Homogeneity (*MDPD*) Indices

The *PITV* was calculated by dividing the volume enclosed within the prescription isodose surface by the target volume. The *MDPD* was calculated by dividing the maximum dose inside the target volume by the prescription dose, which represented the minimum dose given to the target.

4.3.2 Integral Biologically Effective Dose (*IBED*)

*IBED*s were calculated from the differential DVHs. Calculations were performed using an EXCEL spreadsheet (Microsoft Corp., Redmond, WA, USA), with each row representing one dose bin of the DVH, for which the incremental *BED* (ΔBED) was calculated using equation (3.8) (see Section 3.3.3). The *IBED* was then obtained by summing the ΔBEDs over all dose bins in the histogram. *IBED*s were calculated for tumour, normal brain and

brain stem, with the whole volume, as determined by the treatment planning systems, used for the tumour and brain stem, and a reference volume of 1,500 cm^3 used for the brain. It is important to note that no correction factors due to radiobiological processes were used for the calculation of *IBED*s, since in our study, we were comparing different radiosurgery plans that implicitly have the same fractionation scheme, i.e., single-fraction. An example of an EXCEL spreadsheet used to calculate *IBED*s for tumour and normal brain for a plan generated for the 1.5 cm diameter hemispherical target using the static conformal beam technique is shown in Table A.1 in Appendix A.

4.3.3 Tumour Control Probability (*TCP*)

*TCP*s were calculated using the Poisson model, as described in Section 3.3.3, with the dose-volume response for tumours given by equation (3.12).

Equation (3.12) was applied for each dose bin in the 2 Gy per fraction equivalent differential DVH [obtained from the original DVH by applying equation (3.14)], and the *TCP* associated with the treatment plan was obtained by multiplying the probability for all dose bins, as given by equation (3.13). These calculations were performed using an EXCEL spreadsheet, with each row representing one dose bin for which equation (3.12) was applied. Table A.2 in Appendix A shows an example of an EXCEL spreadsheet used to calculate *TCP* for a plan generated for the 1.5 cm diameter hemispherical target using the static conformal beam technique.

4.3.4 Normal Tissue Complication Probability (*NTCP*)

*NTCP*s were calculated using the Lyman model, described in Section 3.3.3. For the practical implementation of the Lyman model, the following values were used for the parameters V_{ref}, $TD_{50}(1)$, m, and n [values obtained from fitting the input clinical data to equation (3.18) (see Table 3.2)]:

Normal brain:

V_{ref} - For normal brain an arbitrary volume of 1,500 cm^3 was used for V_{ref}.

$TD_{50}(1)$ = 60 Gy

m = 0.15

n = 0.25

Brain Stem:

V_{ref} - The value for V_{ref} in the case of the brain stem was considered as the whole organ volume, as given by the treatment planning systems.

$TD_{50}(1)$ = 65 Gy

m = 0.14

n = 0.16

Before performing the histogram reduction, as discussed in Section 3.3.3, the single-fraction DVH was converted to an equivalent 2 Gy per fraction DVH, using equation (3.14). Equation (3.14) was applied to each dose bin in the single-fraction DVH. Histogram reduction, using the effective volume method, was then performed in this resulting equivalent 2 Gy per fraction DVH. In order to perform the histogram reduction, an EXCEL spreadsheet was used, with each row corresponding to one dose bin in the equivalent DVH. For each dose bin in the equivalent DVH, a partial effective volume was calculated, and the effective volume V_{eff} was obtained by summing the results for all dose bins, as given by equation (3.22).

Once V_{eff} has been calculated, the partial volume v was obtained by dividing V_{eff} by V_{ref}, and the dose D used to calculate the *NTCP* was the maximum dose in the equivalent DVH. Using the calculated values for D and v as well as the parameters $TD_{50}(1)$, m and n, in equations (3.20) and (3.21), the parameter t, which gives the upper limit of the integral in equation (3.18) was calculated. Table A.3 in Appendix A shows an example of an EXCEL spreadsheet used to perform the histogram reduction (calculate V_{eff}) and to

calculate the parameter t in a plan generated for the 1.5 cm diameter hemispherical target using the static conformal beam technique.

To calculate the *NTCP* the integral in equation (3.18) was solved using the software ORIGIN (OriginLab® Corporation, Northampton, MA, USA). This was done by first making a graph of the function:

$$y = \frac{1}{\sqrt{2\pi}} \exp\left(\frac{-x^2}{2}\right), \tag{4.1}$$

and then integrating this function from -10 to the calculated value for t. The value of -10 was considered appropriate for the lower limit because, from equation (3.20), it represents the result for a dose D that is much lower than the tolerance dose $TD_{50}(v)$ and which is not clinically significant. Figure 4.3 shows the graph of the function used to calculate the *NTCP* using the software ORIGIN.

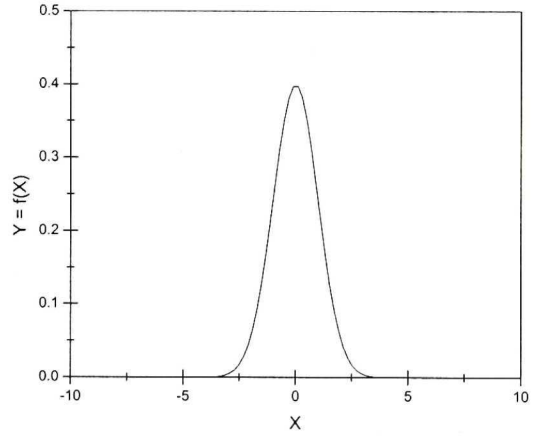

Figure 4.3 - Graph of the function used to calculate the *NTCP* using the software ORIGIN.

4.4 EVALUATION OF THE CORRELATION BETWEEN PHYSICAL AND BIOLOGICAL PARAMETERS

In this study, correlations between physical and biological parameters were investigated for all techniques. For this purpose, for each target and each technique, several plans were generated with decreasing the *PITV*, accompanied or not by a decrease in the *MDPD* and for each plan, all biological parameters were calculated. Correlations were evaluated by using the data from several plans generated for each target separately. In this way, the only variable would be the treatment plan (beam configuration) and not the target geometry, thereby avoiding biasing the results. Correlations were evaluated graphically by observing possible trends in the behaviour of a given parameter in relation to an increase or decrease in another parameter.

REFERENCES

1 E. Shaw, R. Kline, M. Gillin, L, Souhami, A. Hirschfeld, R. Dinapoli, and L. Martin, "Radiation Therapy Oncology Group: Radiosurgery Quality Assurance Guidelines," Int. J. Radiat. Oncol., Biol., Phys. **27**, 1231-1239 (1993).

CHAPTER 5

RESULTS AND DISCUSSION

This chapter presents results of our comparative study of the dynamic rotation, static conformal beam, and intensity-modulated radiosurgery techniques. The physical parameters associated with the best plan (in terms of physical parameters) obtained for various targets and each technique, are presented. Results of the evaluation of the correlation between physical and biological parameters are also presented for the three techniques. Experiments performed in order to explain the lack of correlation between physical and biological parameters when using the dynamic rotation technique are described. Results of the best plan (in terms of biological parameters) for each target and technique are also presented. Finally, a discussion of general aspects related to assumptions and methodologies used in this study is presented.

5.1 TARGETS EVALUATED BY THE THREE TECHNIQUES

The volumes of each simulated target, as calculated by the treatment planning systems used for the three techniques, were compared. The differences for the calculated target volumes were within 2.5% from the average value. This result assured that the same targets (within this uncertainty) were available on all treatment planning systems so that treatment planning could be initiated using the three techniques.

5.2 CREATING GOOD PLANS FOR EACH TECHNIQUE

5.2.1 Dynamic Rotation Technique

As mentioned in Section 4.2.1, with the dynamic rotation technique improvement in conformity (decrease in *PITV*) is achieved by increasing the number and optimizing the location of isocenters. Using this technique, several plans were generated for the 1.5 and 3.0 cm diameter hemispherical and C-shaped targets, with increasing the number of

isocenters and optimizing their locations. The results of these plans are shown in Figure 5.1, in which the *PITV* is plotted as a function of the number of isocenters for these three targets. Results for spherical targets are not shown in Figure 5.1 because spherical isodose distributions are obtained when using the dynamic rotation technique, so only one isocenter was used for these cases. Results for the spherical targets are shown in Appendix B.

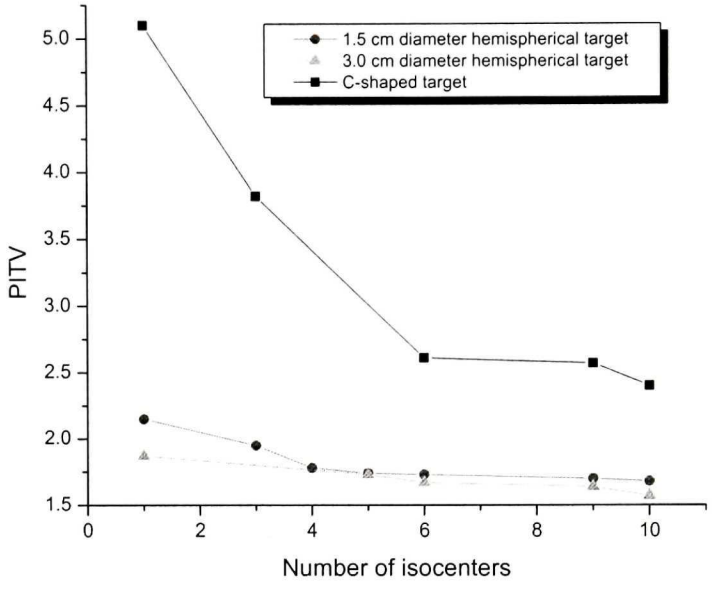

Figure 5.1 – Graph of the *PITV* vs. the number of isocenters for several plans obtained using the dynamic rotation technique for the hemispherical (1.5 and 3.0 cm diameter) and C-shaped targets.

The numbers of isocenters for each target were chosen taking into account the geometry of the target. During treatment planning, especially for the C-shaped target, it was observed that acceptable plans cannot be generated when a number of isocenters that is not compatible with the target geometry is used. It is thus imperative that when using the dynamic rotation technique, a clear 3-D view of the target is available in order to select the appropriate number and position of isocenters. However, for practical reasons, when treating patients with this technique, the number of isocenters should be kept to a minimum.

5.2.2 Static Conformal Beam Technique

For the static conformal beam technique, improvement in conformity (decrease in *PITV*) is achieved by increasing the number and optimizing the position of beams. Using this technique, several plans were generated for the 1.5 and 3.0 cm diameter hemispherical and C-shaped targets by increasing the number of beams and optimizing their positions. The results of these plans are shown in Figure 5.2 in which the *PITV* is plotted as a function of the number of beams for these three targets. Results for the spherical targets are shown in Appendix B.

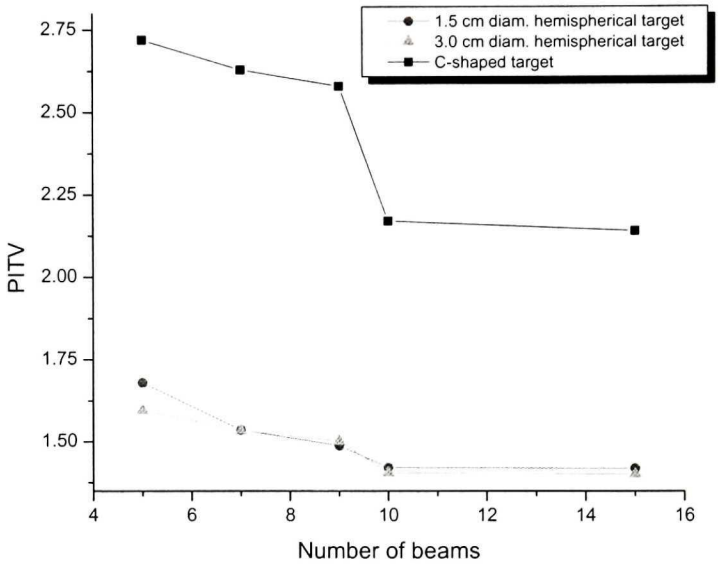

Figure 5.2 – Graph of the *PITV* vs. the number of beams for several plans obtained using the static conformal beam technique for the hemispherical (1.5 and 3.0 cm diameter) and C-shaped targets.

During treatment planning using the static conformal beam technique, especially in the case for the C-shaped target, it was noticed that by increasing the number of beams, better plans could be generated given that optimized directions were chosen that allowed the manual adjustment of the leaves of the micro-multileaf collimator in order to spare, as much as possible, the critical structure.

5.2.3 Intensity-Modulated Radiosurgery (IMRS) Technique

While improvement in conformity for the dynamic rotation and static conformal beam techniques is achieved, respectively, by increasing the number of isocenters and the number of beams, an analogous parameter for the IMRS technique is not easy to establish. This is because the IMRS technique is based on inverse treatment planning, in which parameters like beam margin and field size cannot be defined by the user. Moreover, the different beam weighting provided by the intensity-modulation reduces the importance of the choice of number and direction of beams, which are the only degrees of freedom defined by the user in the resulting dose distribution. To illustrate these considerations, Figure 5.3 shows a graph of the *PITV* as a function of the number of beams for the IMRS technique and the 1.5 and 3.0 cm diameter hemispherical and C-shaped targets. From Figure 5.3 it can be seen that the *PITV* does not necessarily decrease with increasing the number of beams. Results for the spherical targets are shown in Appendix B.

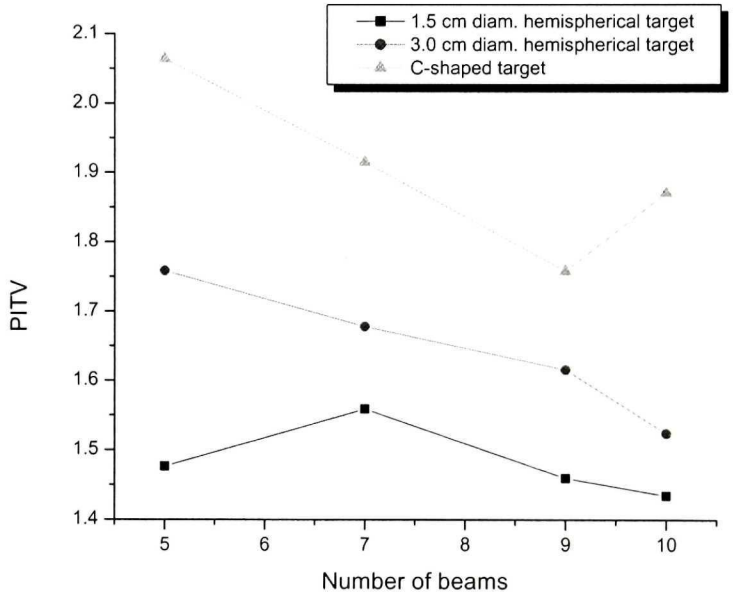

Figure 5.3 – Graph of the *PITV* vs. the number of beams for several plans obtained using the IMRS technique for the hemispherical (1.5 and 3.0 cm diameter) and C-shaped targets.

5.3 RESULTS FROM COMPARATIVE STUDY – PHYSICAL PARAMETERS

Tables 5.1 through 5.5 show the physical parameters (*PITV* and *MDPD*) and the complexity (number of isocenters for dynamic rotation, and number of beams for the static conformal beam and the IMRS techniques, as well as approximate time spent for treatment planning) to achieve the best plans, in terms of physical parameters, respectively, for the 1.5 cm diameter spherical, 3.0 cm diameter spherical, 1.5 cm diameter hemispherical, 3.0 cm diameter hemispherical, and C-shaped targets, for the dynamic rotation, static conformal beam, and IMRS techniques. These plans were considered the best, because no improvement was observed by either increasing the number of isocenters or number of beams, or the time spent for treatment planning.

Table 5.1 – Physical parameters (*PITV* and *MDPD*), and complexity (number of isocenters for dynamic rotation, and number of beams for the static conformal and the IMRS techniques, as well as approximate time spent for treatment planning), of the best plans, in terms of physical parameters, obtained for the 1.5 cm diameter spherical target for the dynamic rotation, static conformal beam, and IMRS techniques.

Technique / Parameter	Dynamic Rotation	Static Conformal	IMRS
PITV	1.46	1.43	1.37
MDPD	1.23	1.17	1.32
Complexity (#iso/beam;time(hr))	1 ; 0.5	10 ; 1.5	10 ; 2.0

From the results shown in Table 5.1, it can be seen that for the 1.5 cm diameter spherical target, the three techniques provided comparable plans in terms of physical parameters. The time required for treatment planning was longer for the static conformal beam and IMRS techniques.

Table 5.2 – Physical parameters (*PITV* and *MDPD*), and complexity (number of isocenters for dynamic rotation, and number of beams for the static conformal and the IMRS techniques, as well as approximate time spent for treatment planning), of the best plans, in terms of physical parameters, obtained for the 3.0 cm diameter spherical target for the dynamic rotation, static conformal beam, and IMRS techniques.

Technique / Parameter	Dynamic Rotation	Static Conformal	IMRS
PITV	1.30	1.37	1.35
MDPD	1.18	1.22	2.00
Complexity (#iso/beam;time(hr))	1 ; 0.5	10 ; 1.5	10 ; 2.0

From the results shown in Table 5.2, it can be seen that for the 3.0 cm diameter spherical target, the three techniques provided comparable plans in terms of physical parameters; however, with a higher degree of dose inhomogeneity (higher *MDPD*) for the IMRS technique. The time required for treatment planning was longer for the static conformal beam and IMRS techniques.

Table 5.3 – Physical parameters (*PITV* and *MDPD*), and complexity (number of isocenters for dynamic rotation, and number of beams for the static conformal and the IMRS techniques, as well as approximate time spent for treatment planning), of the best plans, in terms of physical parameters, obtained for the 1.5 cm diameter hemispherical target for the dynamic rotation, static conformal beam, and IMRS techniques.

Technique / Parameter	Dynamic Rotation	Static Conformal	IMRS
PITV	1.68	1.59	1.43
MDPD	2.00	1.21	1.40
Complexity (#iso/beam;time(hr))	10 ; 6.0	15 ; 2.0	10 ; 2.0

From the results shown in Table 5.3 it can be seen that for the 1.5 cm diameter hemispherical target, the static conformal beam and the IMRS techniques provided comparable plans in terms of physical parameters and complexity. While the plan generated using the dynamic rotation technique is acceptable in terms of physical parameters, the time required for treatment planning is longer when compared to the other two techniques. Also, concerning treatment delivery, considerably more time is required to deliver a plan with 10 isocenters when using the dynamic rotation technique than plans

with 15 and 10 beams when using the static conformal beam, and the IMRS techniques, respectively.

Table 5.4 – Physical parameters (*PITV* and *MDPD*), and complexity (number of isocenters for dynamic rotation, and number of beams for the static conformal and the IMRS techniques, as well as approximate time spent for treatment planning), of the best plans, in terms of physical parameters, obtained for the 3.0 cm diameter hemispherical target for the dynamic rotation, static conformal beam, and IMRS techniques.

Technique / Parameter	Dynamic Rotation	Static Conformal	IMRS
PITV	1.57	1.41	1.59
MDPD	2.00	1.19	2.00
Complexity (#iso/beam;time(hr))	10 ; 5.0	15 ; 2.0	10 ; 2.0

From the results shown in Table 5.4, it can be seen that for the 3.0 cm diameter hemispherical target, the best plan in terms of physical parameters was generated using the static conformal beam technique. The plans generated using the dynamic rotation and the IMRS techniques are comparable in terms of physical parameters. The approximate time spent for treatment planning was the same for the static conformal beam and the IMRS techniques, and longer for the dynamic rotation technique. Concerning treatment delivery, considerably more time is required to deliver the plan generated using the dynamic rotation technique, than the plans generated using the static conformal beam and the IMRS techniques.

Table 5.5 – Physical parameters (*PITV* and *MDPD*), and complexity (number of isocenters for dynamic rotation, and number of beams for the static conformal and the IMRS techniques, as well as approximate time spent for treatment planning), of the best plans, in terms of physical parameters, obtained for the C-shaped target for the dynamic rotation, static conformal beam, and IMRS techniques.

Technique / Parameter	Dynamic Rotation	Static Conformal	IMRS
PITV	2.40	2.14	1.76
MDPD	2.00	1.45	1.89
Complexity (#iso/beam;time(hr))	10 ; 7.0	15 ; 3.0	10 ; 3.0

From the results shown in Table 5.5, it can be seen that for the C-shaped target, the best plan in terms of physical parameters was generated using the IMRS technique. The plans generated using the dynamic rotation and static conformal beam techniques are comparable in terms of *PITV*. The approximate time spent for treatment planning was the same for the static conformal beam and the IMRS techniques, and longer for the dynamic rotation technique. Concerning treatment delivery, considerably more time is required to deliver the plan generated using the dynamic rotation technique, than the plans generated using the static conformal beam and the IMRS techniques.

The plans shown in Tables 5.1 through 5.5 were selected from many plans generated for each target with each technique. The selection parameter for these plans was the *PITV*, i.e., these plans were the ones that provided the lowest values of the *PITV*. The *PITV* was chosen as a selection parameter because in clinical practice, treatment plans are manually optimized based on minimizing the *PITV*.

5.4 RESULTS FOR BIOLOGICAL AND TECHNICAL PARAMETERS

As was seen in Figures 5.1 and 5.2, an increase in the number of isocenters and beams, respectively, in the dynamic rotation, and the static conformal beam techniques, is accompanied by a decrease in the *PITV*. However, as treatment outcome may possibly be reflected better by biological instead of physical parameters, the biological parameters associated with the plans (*TCP*, *NTCP* and *IBED*) were calculated and plotted as a function of number of isocenters for the dynamic rotation technique, and number of beams for the static conformal beam technique. In addition, biological parameters were plotted as a function of number of beams for the IMRS technique, in order to see if the same behaviour that was observed for physical parameters was also observed for biological parameters.

Figures 5.4 through 5.7 show, respectively, graphs of *TCP*, *NTCP*, *IBED*(tumour), and *IBED*(brain) as a function of the number of isocenters for the 1.5 and 3.0 cm diameter

hemispherical targets as well as the C-shaped target, for the same plans as plotted in Figure 5.1 for the dynamic rotation technique.

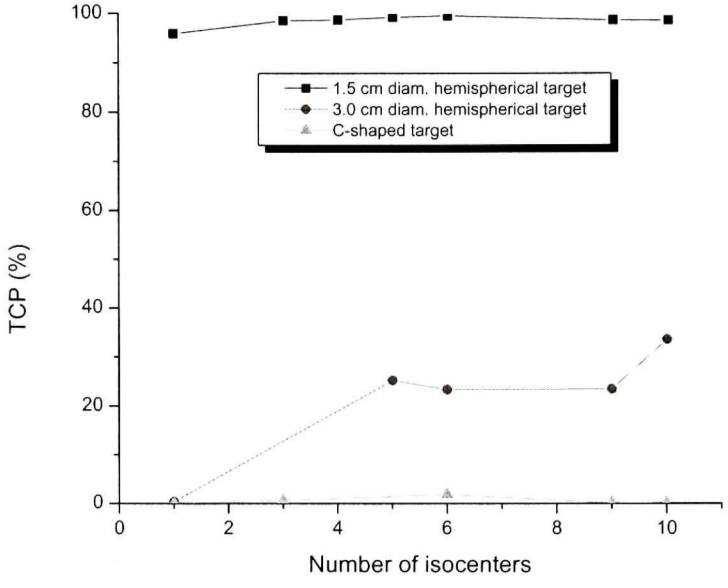

Figure 5.4 – Graphs of the *TCP* vs. the number of isocenters for several plans obtained for the hemispherical (1.5 and 3.0 cm diameter) and C-shaped targets using the dynamic rotation technique.

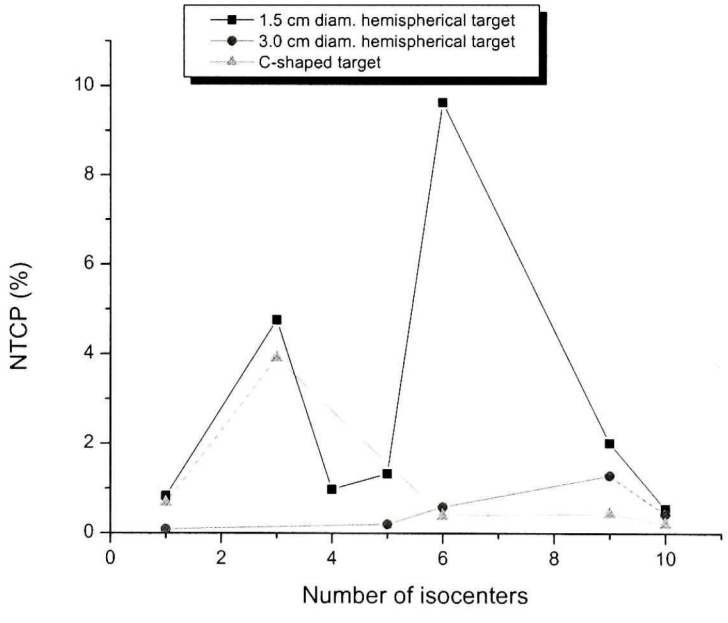

Figure 5.5 – Graphs of the *NTCP* vs. the number of isocenters for several plans obtained for the hemispherical (1.5 and 3.0 cm diameter) and C-shaped targets using the dynamic rotation technique.

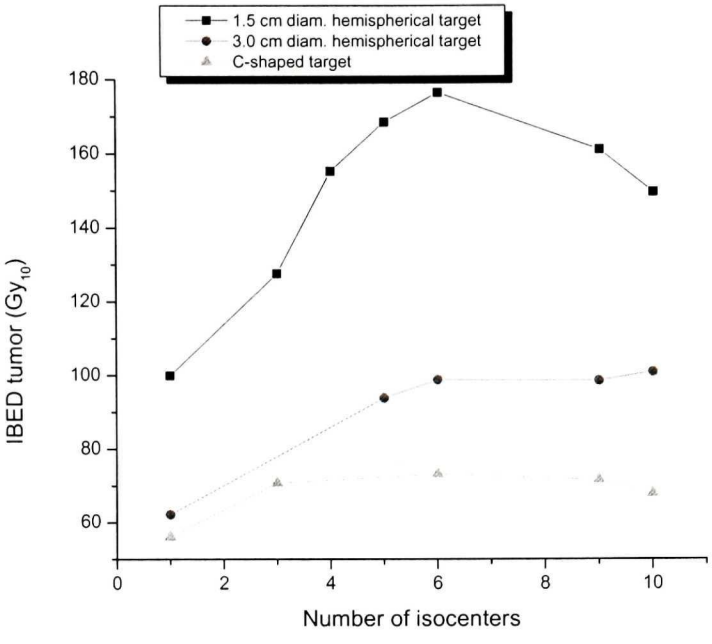

Figure 5.6 – Graphs of *IBED*(tumour) vs. the number of isocenters for several plans obtained for the hemispherical (1.5 and 3.0 cm diameter) and C-shaped targets using the dynamic rotation technique.

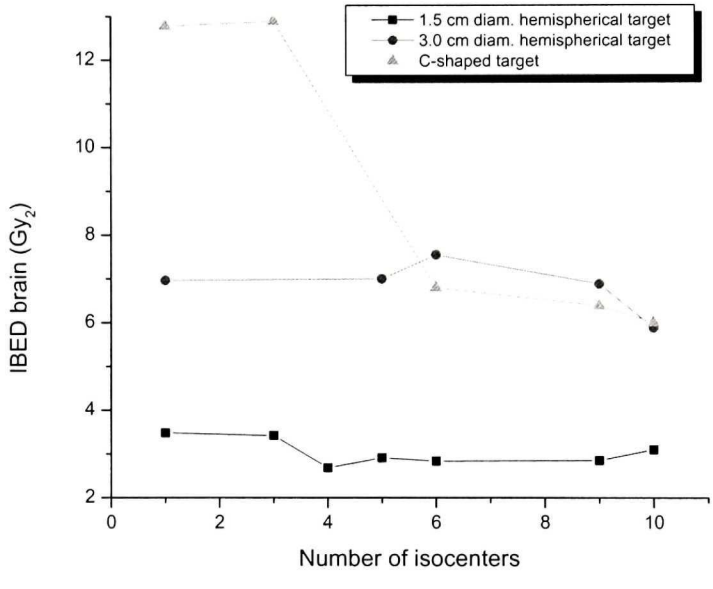

Figure 5.7 – Graphs of *IBED*(brain) vs. the number of isocenters for several plans obtained for the hemispherical (1.5 and 3.0 cm diameter) and C-shaped targets using the dynamic rotation technique.

Figures 5.8 through 5.11 show, respectively, graphs of *TCP*, *NTCP*, *IBED*(tumour), and *IBED*(brain) as a function of the number of beams for the 1.5 and 3.0 cm diameter

hemispherical targets as well as the C-shaped target, for the same plans as plotted in Figure 5.2 for the static conformal beam technique.

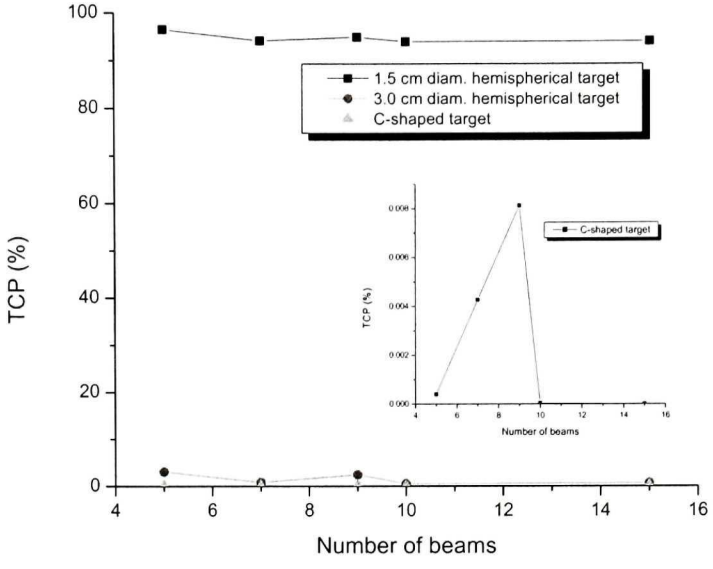

Figure 5.8 – Graphs of the *TCP* vs. the number of beams for several plans obtained for the hemispherical (1.5 and 3.0 cm diameter) and C-shaped targets using the static conformal beam technique. The insert shows the results for the C-shaped target in a smaller scale.

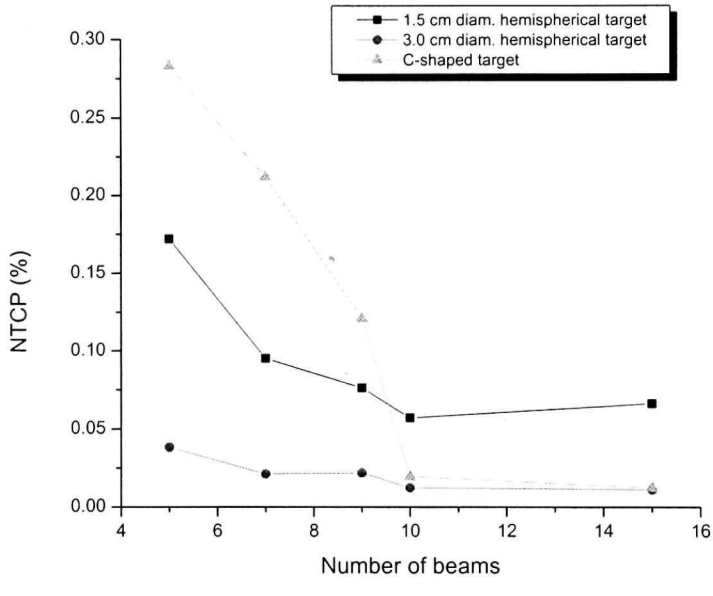

Figure 5.9 – Graphs of the *NTCP* vs. the number of beams for several plans obtained for the hemispherical (1.5 and 3.0 cm diameter) and C-shaped targets using the static conformal beam technique.

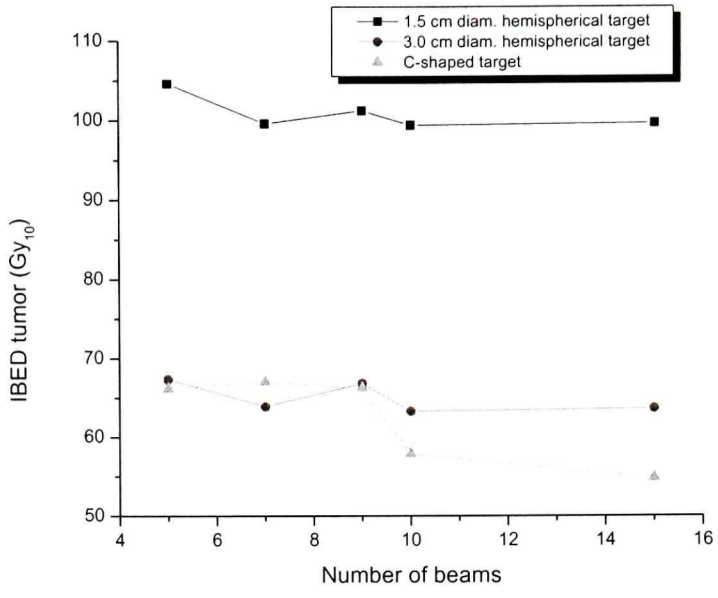

Figure 5.10 – Graphs of *IBED*(tumour) vs. the number of beams for several plans obtained for the hemispherical (1.5 and 3.0 cm diameter) and C-shaped targets using the static conformal beam technique.

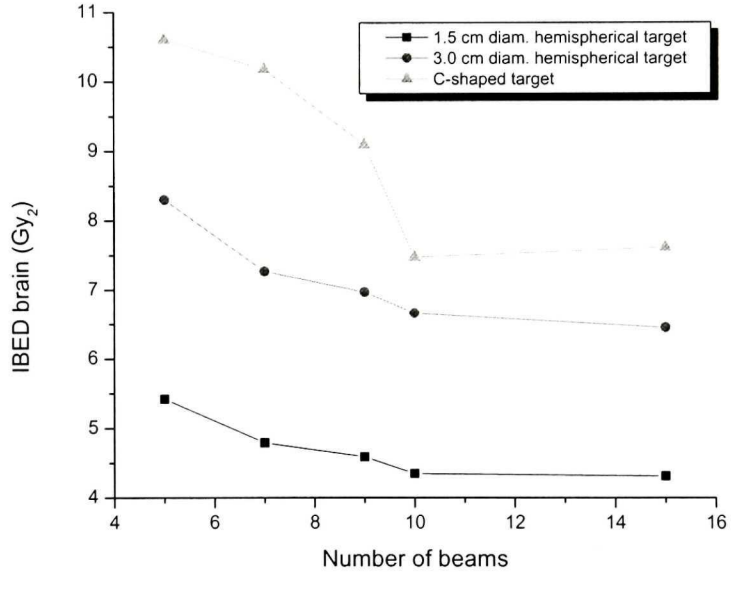

Figure 5.11 – Graphs of *IBED*(brain) vs. the number of beams for several plans obtained for the hemispherical (1.5 and 3.0 cm diameter) and C-shaped targets using the static conformal beam technique.

Figures 5.12 through 5.15 show, respectively, graphs of *TCP*, *NTCP*, *IBED*(tumour), and *IBED*(brain) as a function of number of beams for the 1.5 and 3.0 cm diameter hemispherical targets as well as the C-shaped target, for the same plans as plotted in Figure 5.3 for the IMRS technique.

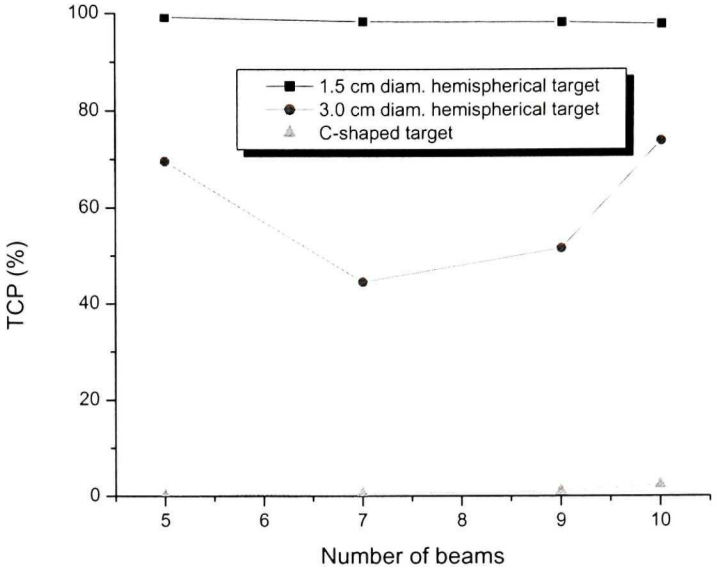

Figure 5.12 – Graphs of the *TCP* vs. the number of beams for several plans obtained for the hemispherical (1.5 and 3.0 cm diameter) and C-shaped targets using the IMRS technique.

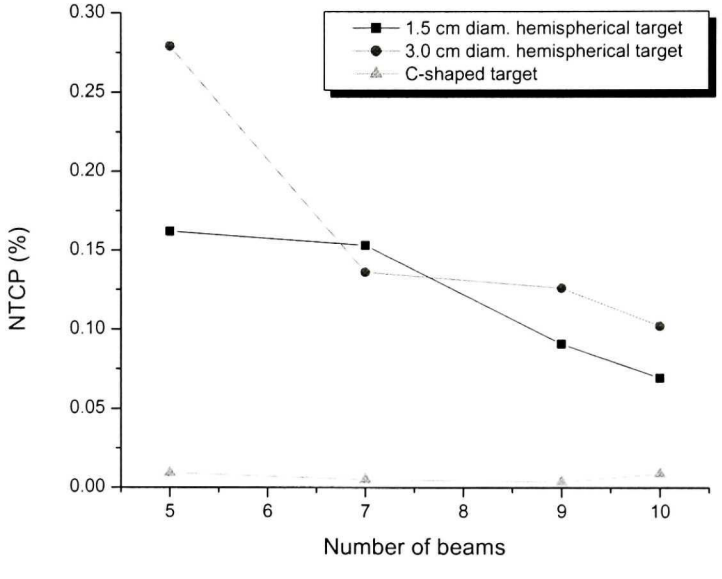

Figure 5.13 – Graphs of the *NTCP* vs. the number of beams for several plans obtained for the hemispherical (1.5 and 3.0 cm diameter) and C-shaped targets using the IMRS technique.

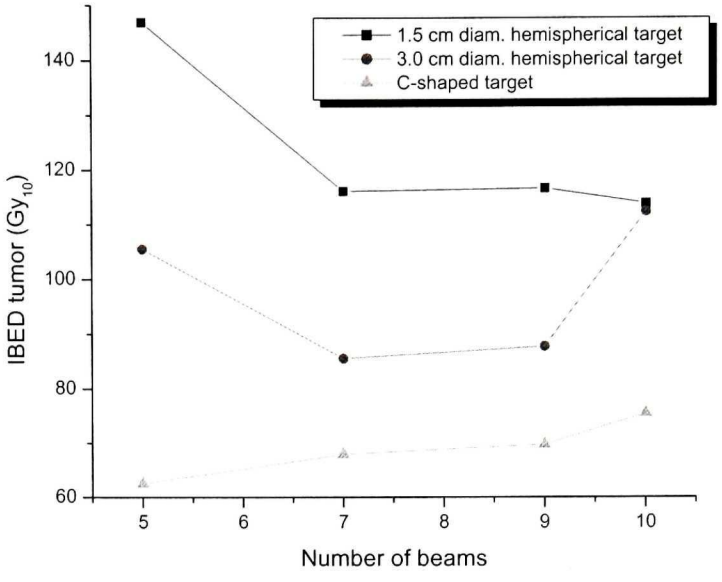

Figure 5.14 – Graphs of *IBED*(tumour) vs. the number of beams for several plans obtained for the hemispherical (1.5 and 3.0 cm diameter) and C-shaped targets using the IMRS technique.

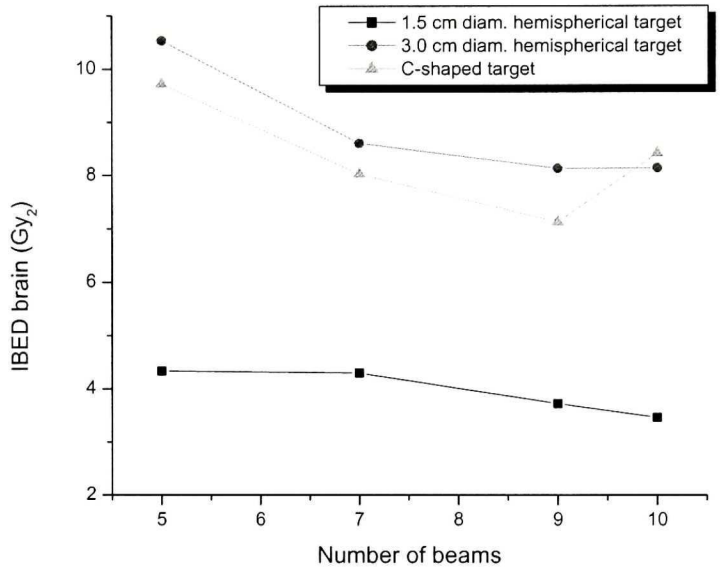

Figure 5.15 – Graphs of *IBED*(brain) vs. the number of beams for several plans obtained for the hemispherical (1.5 and 3.0 cm diameter) and C-shaped targets using the IMRS technique.

By analyzing and comparing the results shown in Figures 5.4 through 5.15, the following observations can be made:

Biological parameters vs. number of isocenters or beams – Concerning the dynamic rotation technique, in general, a trend in the behaviour of biological parameters as a function of the number of isocenters was not observed for any of the targets evaluated. For the static conformal beam technique, in general, *NTCP* and *IBED*(brain) decreased with increasing the number of beams, and a trend in the behaviour of *TCP* and *IBED*(tumour) as a function of the number of beams was not observed. For the IMRS technique, in general, the same behaviour as was observed for the *PITV* as a function of number of beams was also observed for *NTCP* and *IBED*(brain), and not for *TCP* and *IBED*(tumour) as a function of number of beams.

TCP and NTCP values - Calculated values of the *TCP* were very low for the 3.0 cm diameter hemispherical (see Figure 5.8) and C-shaped targets (see Figures 5.4, 5.8, and 5.12). The *TCP* model used is dependent on dose and volume, the bigger the volume, the higher the dose necessary to achieve tumour control (as expressed by the parameter D_{50}) (see Section 3.3.3). On the other hand, side-effects become more frequent with an increase of the irradiated volume and the larger the tumour volume the larger is the amount of normal tissue irradiated. Consequently, the prescribed dose has to be reduced for larger targets to limit complications. In clinical practice, this means that lower doses are administered to larger volumes, leading to a lesser probability of achieving a curative effect. Doses of 15 Gy were prescribed to the C-shaped and 3.0 cm diameter spherical targets, 18 Gy to the 3.0 cm diameter hemispherical target and 24 Gy to the 1.5 cm diameter spherical and 1.5 cm diameter hemispherical targets. As the prescribed doses were reduced for the largest targets when, based on the *TCP* model, they should in fact increase, the calculated *TCP* values were very low in these cases.

For the largest targets the calculated *NTCP* were also very low in some cases (see Figures 5.5, 5.9 and 5.13) suggesting that in these cases the prescribed dose could be increased in an attempt to improve the *TCP*, while still keeping the *NTCP* at an acceptable level. However, in the present work, doses were prescribed based on the guidelines of a dose escalation study which determined the highest acutely tolerable doses for single fraction radiosurgery as a function of the maximum diameter of the lesion.[1]

Given this consideration, the extremely low values, especially for the *NTCP*, calculated for the largest targets are not compatible to what was observed in clinical practice. This discrepancy between our theoretical results and the clinical findings reflects the simplicity of the *TCP* and *NTCP* models used and the limited amount of input clinical data for these models.

Considering the *TCP* and *NTCP* models used, for each target a dose could have been prescribed, located in the linear portion of the *TCP* curve, based on maximizing the P_{utc} parameter (defined in Section 3.3.3.4) (see Figure 5.16). For the largest targets, this dose would be higher than the doses used in clinical practice. However, as the intention was to rank the treatment plans, the absolute values calculated for the *TCP* were not considered as important, although it can be argued that if we had used higher doses for the largest targets located outside the saturation region of the *TCP* curve, better correlation between physical and biological parameters for these targets may have been found.

Comparison between the TCP and IBED(tumour) and between the NTCP and IBED(brain) - For some targets and techniques, the behaviour of the *TCP* and *IBED*(tumour) as a function of the number of isocenters or beams was not the same. See, for example, data for the C-shaped target in Figures 5.8 (insert) and 5.10, for the static conformal beam technique, and also, data for the 1.5 cm diameter hemispherical target in Figures 5.4 and 5.6, for the dynamic rotation technique. In these cases, the calculated values of the *TCP* were very low (~0%) and high (~100%), respectively. Considering the sigmoidal shape of the *TCP* curve as a function of dose, there are two saturation levels, at low and high doses, with *TCP* values close to 0% and 100%, respectively (see Figure 5.16). *IBED*(tumour) as a function of dose can be approximated best by a second order polynomial curve, so that there is no saturation in *IBED* as a function of dose (see Figure 5.17). Based on these considerations, when the *TCP* values are in one of the saturation portions of the curve, the agreement between the *TCP* and *IBED*(tumour) behaviour as a function of dose is not always established.

Different behaviour between the *NTCP* and *IBED*(brain) can be explained best by the fact that the *NTCP* calculations are influenced by volume effects (through the parameter n), i.e., a low value of the parameter n implies that portions of the structure volume receiving high doses have a considerable weight on the calculated *NTCP*, whereas this is not the case for *IBED*(brain) calculations. Thus, depending on the characteristics of the dose distribution, the *NTCP* and *IBED*(brain) will or will not present the same behaviour as a function of dose. This can be observed by comparing Figures 5.5 and 5.7 for the dynamic rotation technique. Particularly for this technique, the dose distribution is altered depending on the number of isocenters used (see Section 5.6), and this difference in dose distribution makes the behaviour of the *NTCP* different from the behaviour of *IBED*(brain) as a function of dose.

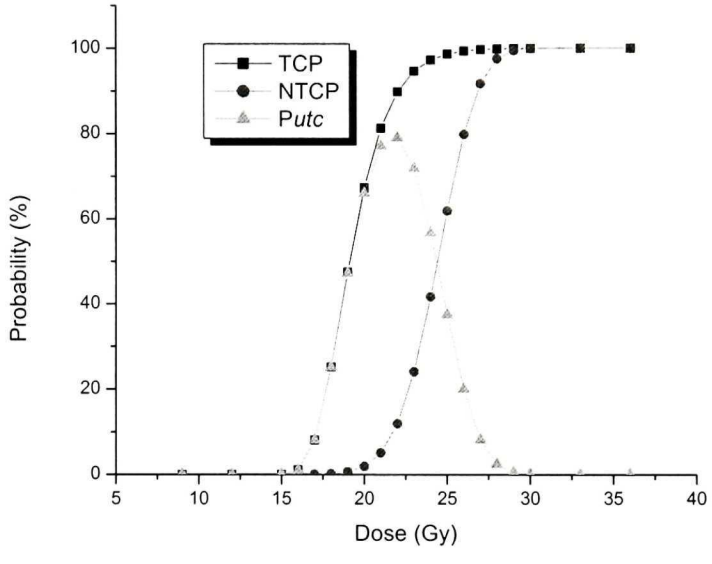

Figure 5.16 - Graphs of the *TCP*, the *NTCP*, and the P_{utc} as a function of dose for a treatment plan obtained for the 3.0 cm diameter hemispherical target and the dynamic rotation technique.

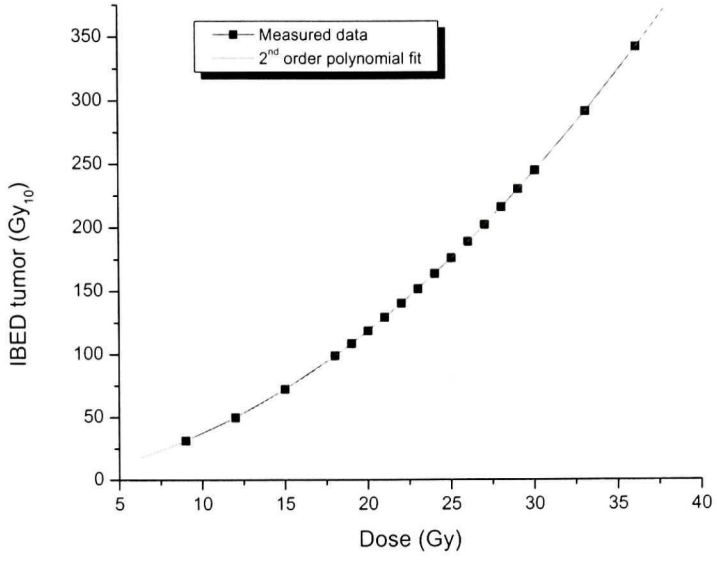

Figure 5.17 - Graph of *IBED*(tumour) as a function of dose for a treatment plan obtained for the 3.0 cm diameter hemispherical target and the dynamic rotation technique.

Results for spherical targets - Results for the 1.5 and 3.0 cm diameter spherical targets are shown in the form of tables in Appendix B.

5.5 RESULTS OF THE CORRELATION BETWEEN PHYSICAL AND BIOLOGICAL PARAMETERS

Correlation between physical and biological parameters was evaluated for all targets and techniques. The pairs of parameters considered for the evaluation of correlation were: *PITV* and *TCP*/*NTCP*; *MDPD* and *TCP*/*NTCP*; *PITV* and *IBED*(tumour)/*IBED*(brain); and *MDPD* and *IBED*(tumour)/*IBED*(brain). The results, presented in the form of graphs, for the 1.5 cm diameter hemispherical target are shown in Figures 5.18 through 5.29. Results for the other targets are presented in the form of tables in Appendix B.

Figures 5.18 (a) and (b) show, respectively, graphs of the *TCP* and the *NTCP* as a function of the *PITV* for the dynamic rotation technique and the 1.5 cm diameter hemispherical target.

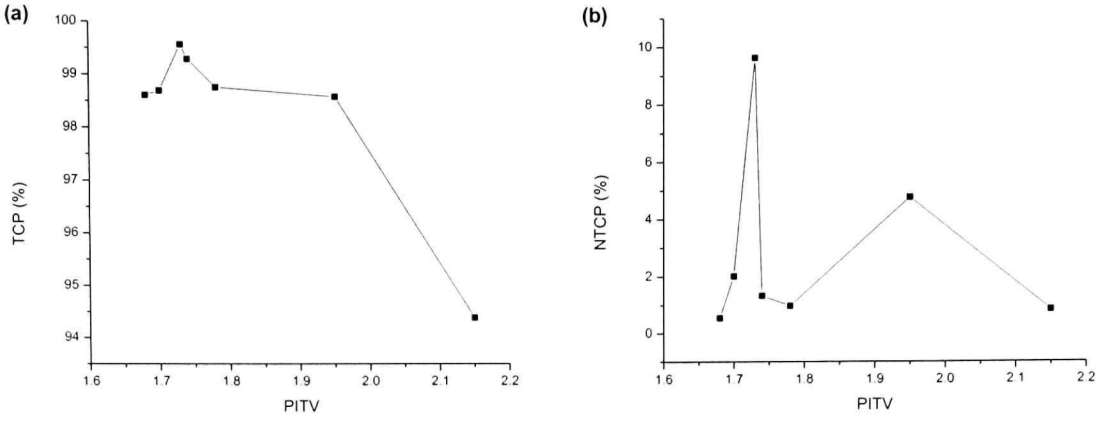

Figures 5.18 (a) and (b) – Graphs of the *TCP* (a) and the *NTCP* (b) as a function of the *PITV* for the dynamic rotation technique and the 1.5 cm diameter hemispherical target.

Figures 5.19 (a) and (b) show, respectively, graphs of the *TCP* and the *NTCP* as a function of the *PITV* for the static conformal beam technique and the 1.5 cm diameter hemispherical target.

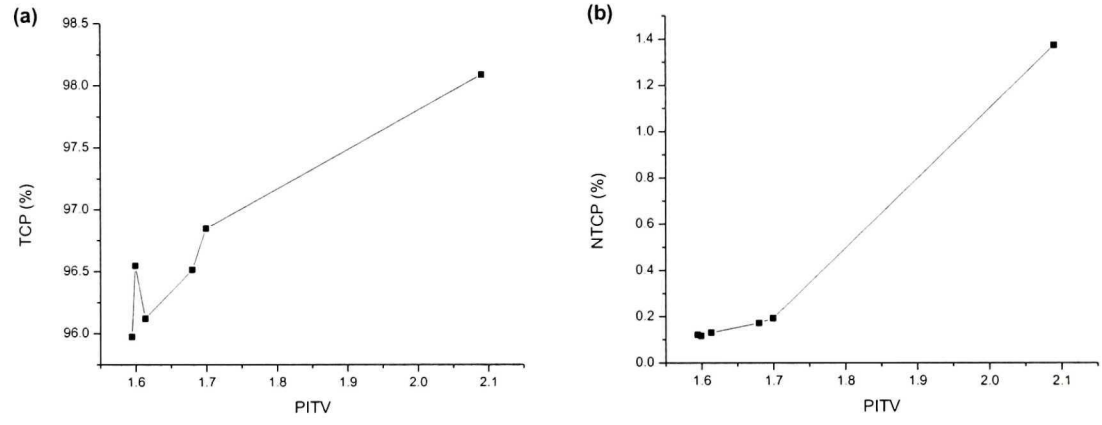

Figures 5.19 (a) and (b) – Graphs of the *TCP* (a) and the *NTCP* (b) as a function of the *PITV* for the static conformal beam technique and the 1.5 cm diameter hemispherical target.

Figures 5.20 (a) and (b) show, respectively, the graphs of the *TCP* and the *NTCP* as a function of the *PITV* for the IMRS technique and the 1.5 cm diameter hemispherical target.

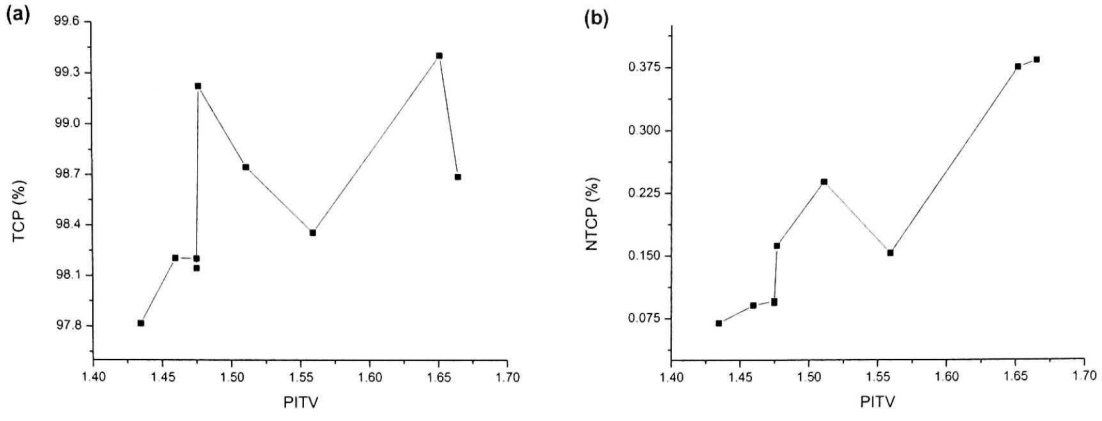

Figures 5.20 (a) and (b) – Graphs of the *TCP* (a) and the *NTCP* (b) as a function of the *PITV* for the IMRS technique and the 1.5 cm diameter hemispherical target.

Figures 5.21 (a) and (b) show, respectively, the graphs of the *TCP* and the *NTCP* as a function of the *MDPD* for the dynamic rotation technique and the 1.5 cm diameter hemispherical target.

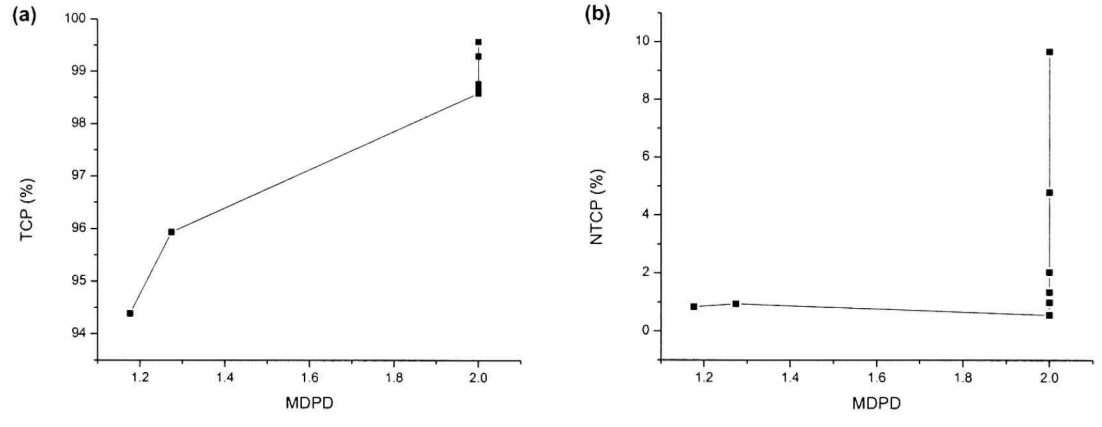

Figures 5.21 (a) and (b) – Graphs of the *TCP* (a) and the *NTCP* (b) as a function of the *MDPD* for the dynamic rotation technique and the 1.5 cm diameter hemispherical target.

Figures 5.22 (a) and (b) show, respectively, the graphs of the *TCP* and the *NTCP* as a function of the *MDPD* for the static conformal beam technique and the 1.5 cm diameter hemispherical target.

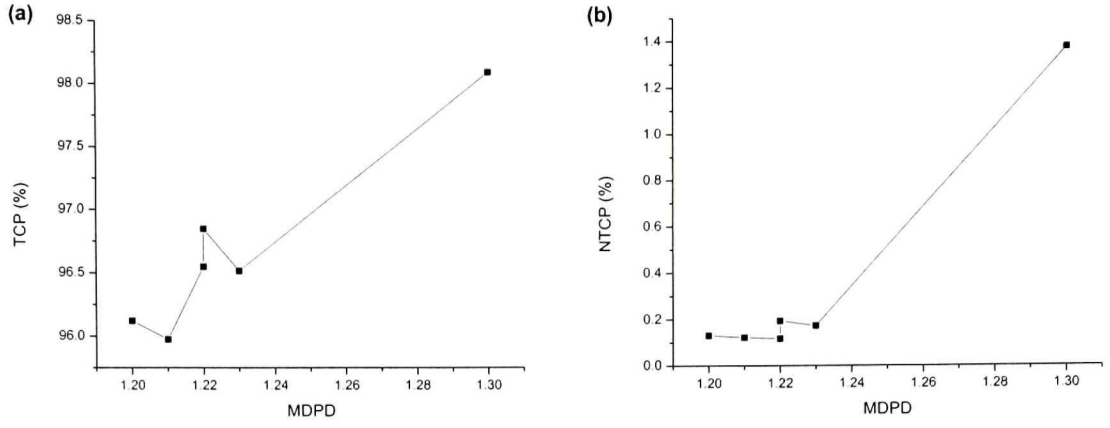

Figures 5.22 (a) and (b) – Graphs of the *TCP* (a) and the *NTCP* (b) as a function of the *MDPD* for the static conformal beam technique and the 1.5 cm diameter hemispherical target.

Figures 5.23 (a) and (b) show, respectively, the graphs of the *TCP* and the *NTCP* as a function of the *MDPD* for the IMRS technique and the 1.5 cm diameter hemispherical target.

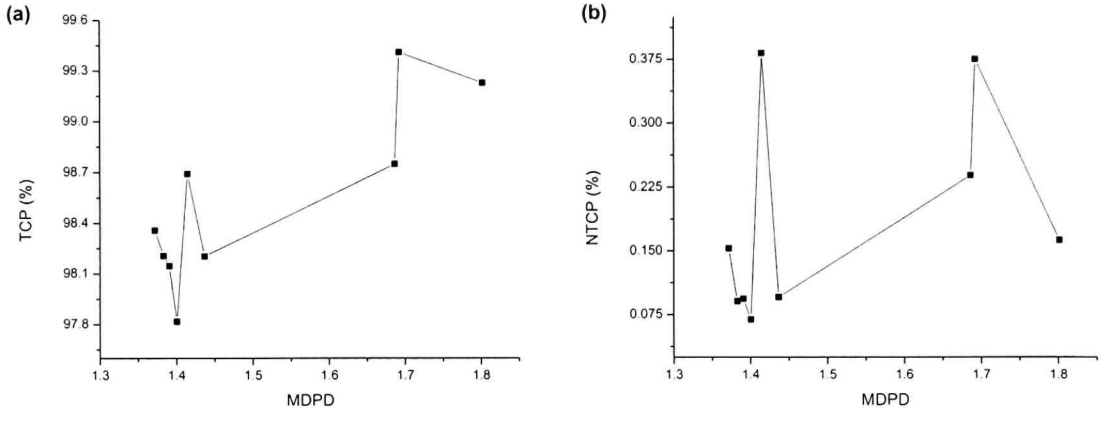

Figures 5.23 (a) and (b) – Graphs of the *TCP* (a) and the *NTCP* (b) as a function of the *MDPD* for the IMRS technique and the 1.5 cm diameter hemispherical target.

Figures 5.24 (a) and (b) show, respectively, the graphs of *IBED*(tumour) and *IBED*(brain) as a function of the *PITV* for the dynamic rotation technique and the 1.5 cm diameter hemispherical target.

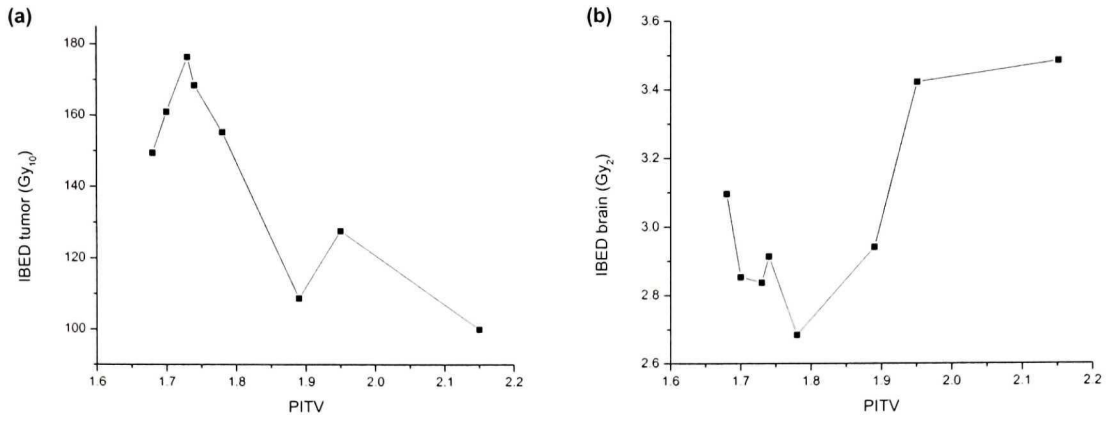

Figures 5.24 (a) and (b) – Graphs of *IBED*(tumour) (a) and *IBED*(brain) (b) as a function of the *PITV* for the dynamic rotation technique and the 1.5 cm diameter hemispherical target.

Figures 5.25 (a) and (b) show, respectively, the graphs of *IBED*(tumour) and *IBED*(brain) as a function of the *PITV* for the static conformal beam technique and the 1.5 cm diameter hemispherical target.

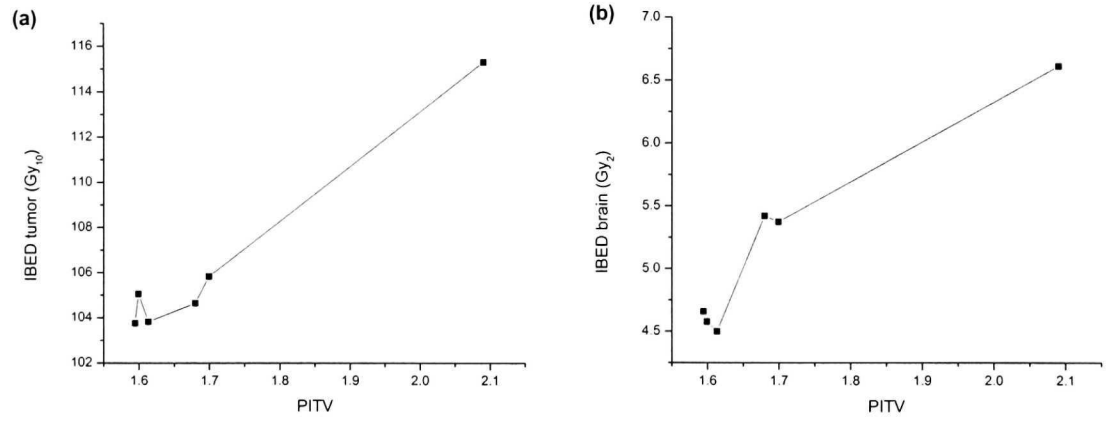

Figures 5.25 (a) and (b) – Graphs of *IBED*(tumour) (a) and *IBED*(brain) (b) as a function of the *PITV* for the static conformal beam technique and the 1.5 cm diameter hemispherical target.

Figures 5.26 (a) and (b) show, respectively, the graphs of *IBED*(tumour) and *IBED*(brain) as a function of the *PITV* for the IMRS technique and the 1.5 cm diameter hemispherical target.

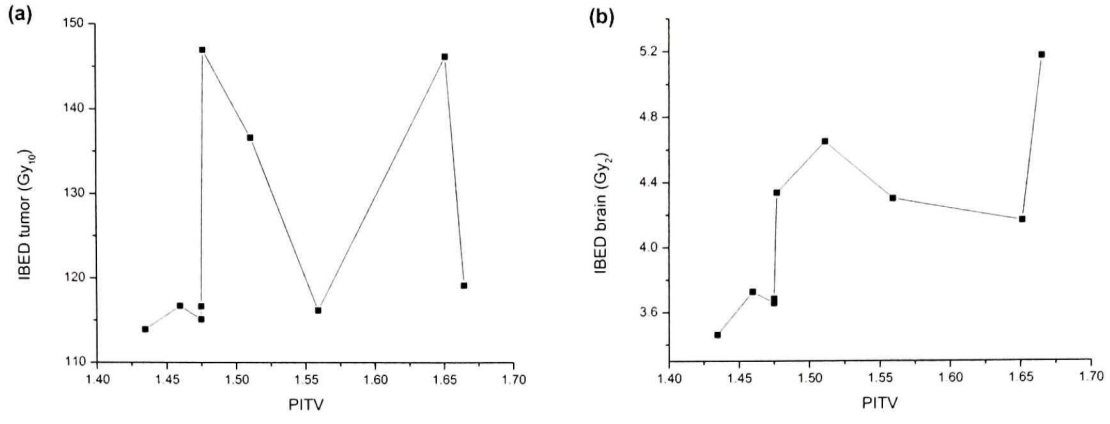

Figures 5.26 (a) and (b) – Graphs of *IBED*(tumour) (a) and *IBED*(brain) (b) as a function of the *PITV* for the IMRS technique and the 1.5 cm diameter hemispherical target.

Figures 5.27 (a) and (b) show, respectively, the graphs of *IBED*(tumour) and *IBED*(brain) as a function of the *MDPD* for the dynamic rotation technique and the 1.5 cm diameter hemispherical target.

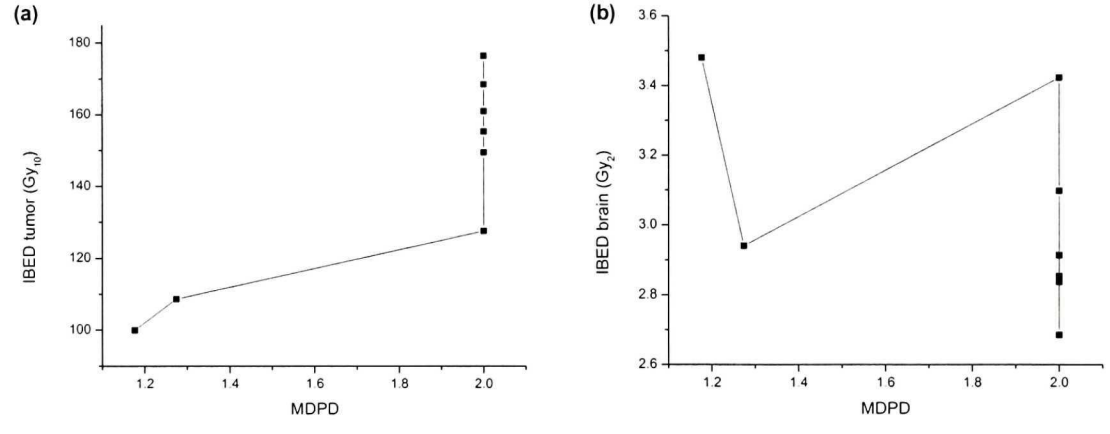

Figures 5.27 (a) and (b) – Graphs of *IBED* (tumour) (a) and *IBED* (brain) (b) as a function of the *MDPD* for the dynamic rotation technique and the 1.5 cm diameter hemispherical target.

Figures 5.28 (a) and (b) show, respectively, the graphs of *IBED*(tumour) and *IBED*(brain) as a function of the *MDPD* for the static conformal beam technique and the 1.5 cm diameter hemispherical target.

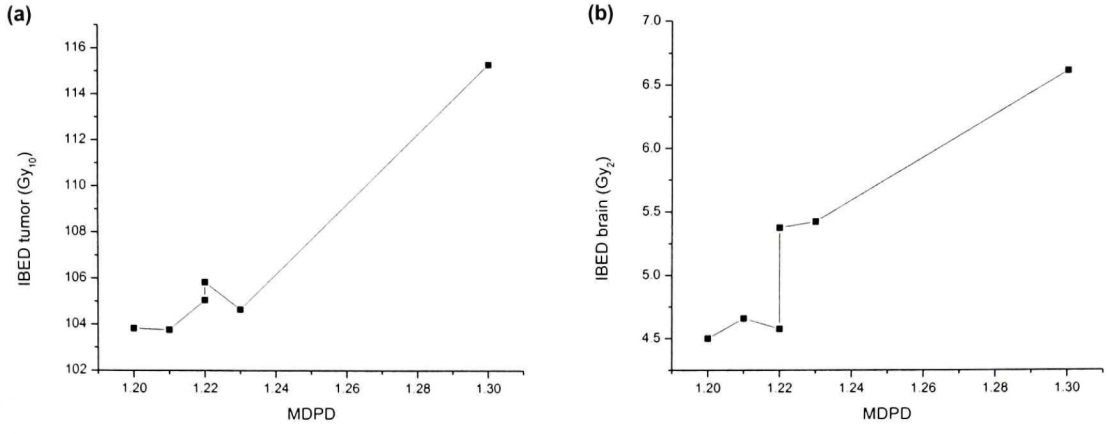

Figures 5.28 (a) and (b) – Graphs of *IBED*(tumour) (a) and *IBED*(brain) (b) as a function of the *MDPD* for the static conformal beam technique and the 1.5 cm diameter hemispherical target.

Figures 5.29 (a) and (b) show, respectively, the graphs of *IBED*(tumour) and *IBED*(brain) as a function of the *MDPD* for the IMRS technique and the 1.5 cm diameter hemispherical target.

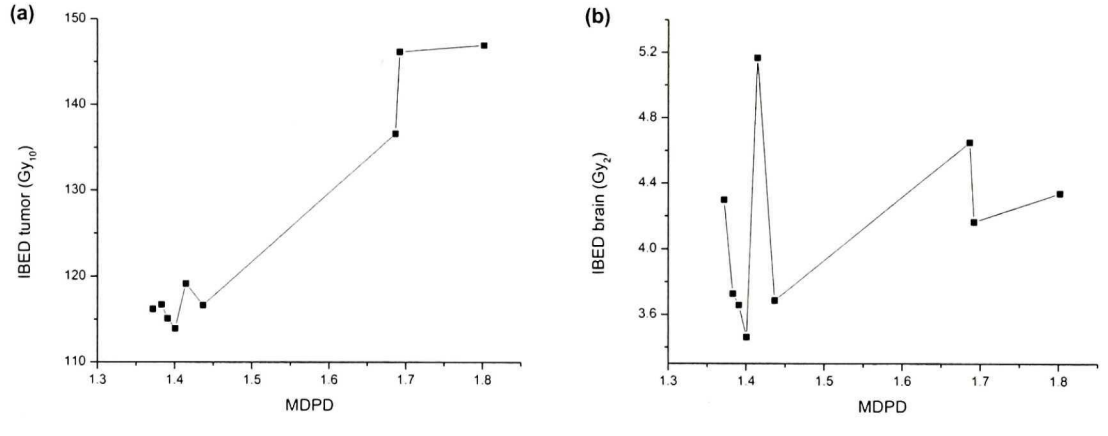

Figures 5.29 (a) and (b) – Graphs of *IBED*(tumour) (a) and *IBED*(brain) (b) as a function of the *MDPD* for the IMRS technique and the 1.5 cm diameter hemispherical target.

From the results shown in Figures 5.18 through 5.29 and in Appendix B, it can be seen that, in general, good correlation between physical and biological parameters was found for the static conformal beam technique, weaker correlation for the IMRS technique, and poor correlation for the dynamic rotation technique. In terms of pairs of parameters, in general, the *MDPD* was better correlated with the *TCP* and *IBED*(tumour), and the *PITV* was better correlated with the *NTCP* and *IBED*(brain). These results suggest that the

TCP/IBED(tumour) is mostly influenced by the *MPDP*, in the sense that higher dose inhomogeneities inside the target increase the *TCP/IBED*(tumour). Although the *NTCP/IBED*(brain) was better correlated with the *PITV*, the analysis of both physical parameters is important for the assessment of tissue damage. This can be observed, for example, in the case of a treatment plan that exhibits a low *PITV*, but a high *MDPD*, such that small fractions of the normal tissue volume (located inside the prescription isodose surface), may be irradiated to higher doses. This overexposed small fraction of the normal tissue may substantially increase the *NTCP*. Conversely, a similar *NTCP* may be obtained with a lower *MDPD* and a higher *PITV*. Consequently, the combination of the *PITV* and the *MDPD* is important when analyzing tissue damage.

Based on these results, some additional experiments were performed with the dynamic rotation technique in an attempt to understand better the particular characteristics of this technique in order to explain the poor correlation found between physical and biological parameters. The description, results and discussion of these experiments are given in the following section.

5.6 EXPERIMENTS PERFORMED WITH THE DYNAMIC ROTATION TECHNIQUE

5.6.1 The *TCP* and the *NTCP* as Related to the Dose Distribution

When multiple isocenters are used in the dynamic rotation technique, the dose distribution is determined by the cone size used for each isocenter as well as the position of each isocenter relative to the others. Given this consideration, two experiments were performed in which the expected dose distributions were known, to see if the behaviour of the *TCP* and the *NTCP* could be explained based on dose distributions.

First, using the 3.0 cm diameter hemispherical target, three isocenters with the same cone size were entered. Keeping the position of the isocenters fixed, five plans were generated with increasing the cone size of the isocenters in steps of 0.25 cm. In this way, the regions of overlap between the dose distributions of the isocenters would always increase with

increasing the cone size [see Figure 5.30 (a)]. In another experiment, the same target and the same configuration of isocenters was used except that, as the cone size was increased, the isocenters were displaced away from each other in such a way that the region of overlap between the dose distribution of the three isocenters (approximately equal to the 80% isodose surface) was the same for all plans [see Figure 5.30 (b)]. Again five plans were generated.

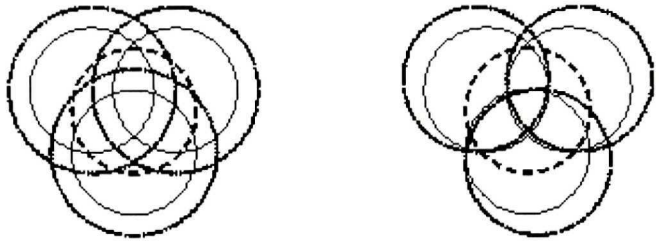

(a) **(b)**

Figure 5.30 – Experiments performed with the dynamic rotation technique to explain, based on dose distributions, the behaviour of the *TCP* and the *NTCP*. In (a) the position of the isocenters was kept fixed, while the cone size of the isocenters was increased. In (b) the isocenters were displaced away from each other as the cone size was increased. In both cases, five plans were generated. Dashed contours in figures (a) and (b) represent the target.

The *TCP* and the *NTCP* were calculated for all these plans, and the results are given in Figures 5.31 and 5.32, which show graphs of the *TCP* as a function of the *PITV* for cases (a) and (b), and the *NTCP* as a function of the *PITV* for cases (a) and (b), respectively.

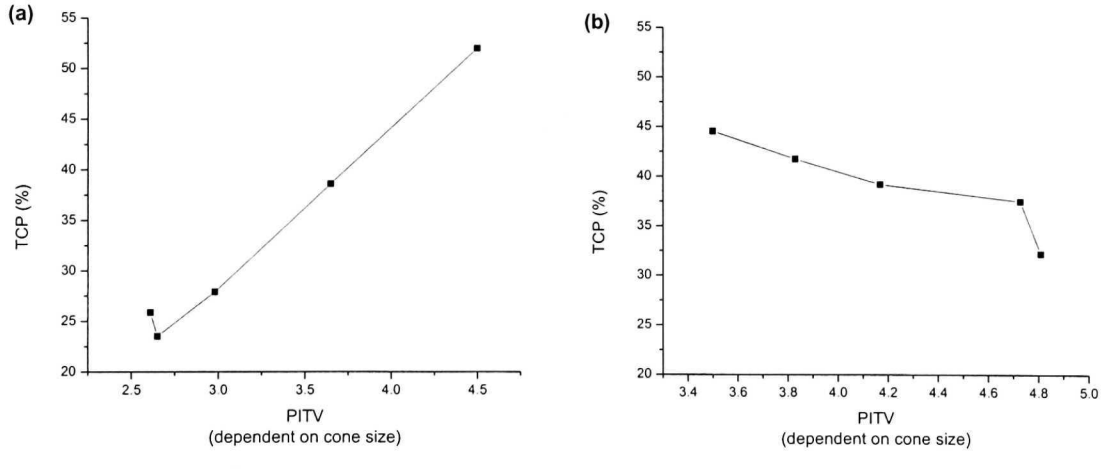

Figures 5.31 (a) and (b) – Graphs of the *TCP* as a function of the *PITV* (directly related to the cone size) for the two experiments [cases (a) and (b), respectively] used to explain, as a function of the dose distribution, the *TCP* and the *NTCP* behaviour in the dynamic rotation technique.

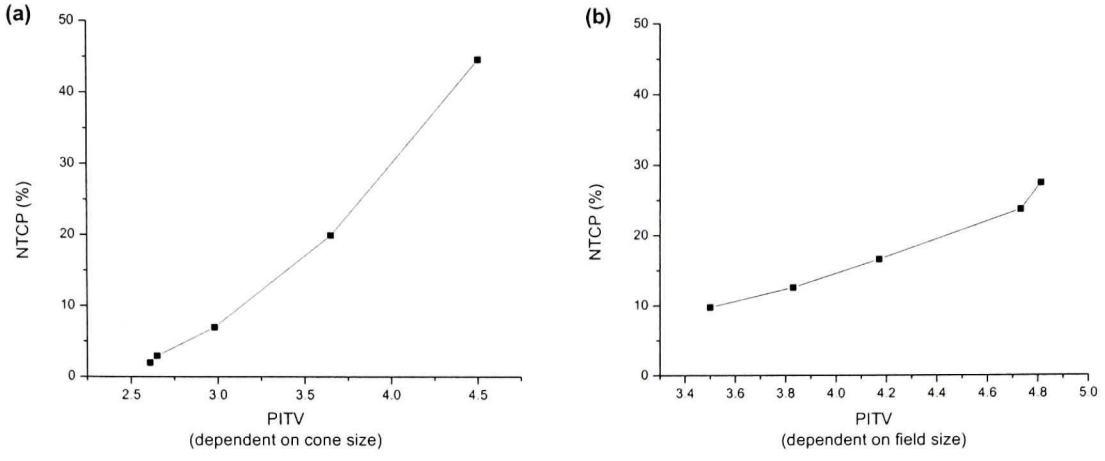

Figures 5.32 (a) and (b) – Graphs of the *NTCP* as a function of the *PITV* (directly related to the cone size) for the two experiments [cases (a) and (b), respectively] used to explain, as a function of the dose distribution, the *TCP* and the *NTCP* behaviour in the dynamic rotation technique.

From Figures 5.31 (a) and (b), the *TCP* increased as a function of the *PITV* in the first case (a) and decreased in the second case (b). This can be explained by the fact that the calculated *TCP* is higher for those plans that exhibit larger portions of the target volume irradiated to higher dose levels (80% and above, when prescribing to the 50% isodose). In these experiments, considering the 80% isodose surface that corresponds approximately to the region of overlap between the dose distributions of the three isocenters in the middle of the target, by comparing the five plans in case (a), it can be seen that the volume of this overlapping region increased with increasing the cone size (see Figure 5.33). The increase in the *TCP* as a function of the *PITV* was then attributed to the increase in this overlapping region with increasing the cone size for case (a). For case (b), in which the volume of the 80% isodose was kept constant, it was observed that, as the cone size was increased, and the isocenters displaced, the volume inside the 50% isodose surface increased, while the volume inside the 90% isodose surface decreased. The decrease in the *TCP* as a function of the *PITV* in case (b), was then attributed to this decrease in portions of the target volume irradiated to higher dose levels (90% isodose surface) with increasing the cone size of the isocenters. Table 5.6 shows the volume inside the 50, 80 and 90% isodose surfaces for the five plans obtained in experiment (b).

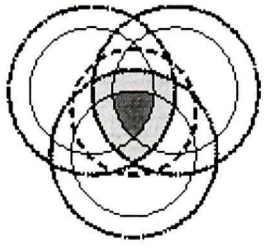

Figure 5.33 – Picture illustrating the increase in the region of overlap between the dose distributions of the three isocenters with increasing the cone size of the isocenters, in case (a). Dashed contour represents the target.

Table 5.6 - Volume inside the 50, 80, and 90% isodose surfaces for the five plans obtained in experiment (b).

Cone size / Isodose Surface	2.75 cm Vol. (cm^3)	3.00 cm Vol. (cm^3)	3.25 cm Vol. (cm^3)	3.50 cm Vol. (cm^3)	3.75 cm Vol. (cm^3)
50 %	34.36	37.64	40.96	46.51	47.22
80 %	3.11	3.11	3.11	3.11	3.11
90 %	0.83	0.63	0.48	0.49	0.45

From Figures 5.32 (a) and (b), the *NTCP* increased as a function of the *PITV* for both cases, however, with a higher relative increase in the first case (a), when compared with the second case (b). This can be explained by the fact that the greatest contribution to the calculated *NTCP* comes from portions of the normal tissue volume irradiated to higher dose levels (especially for tissues that exhibit low volume effects, characterized by a low value of the parameter n). In this case, these portions correspond to fractions of the normal tissue volume located in the intersections of the dose distribution of adjacent isocenters. By comparing these regions in cases (a) and (b) [see Figures 5.34 (a) and (b)], it can be seen that their increase is higher with increasing cone size for case (a), when compared to case (b).

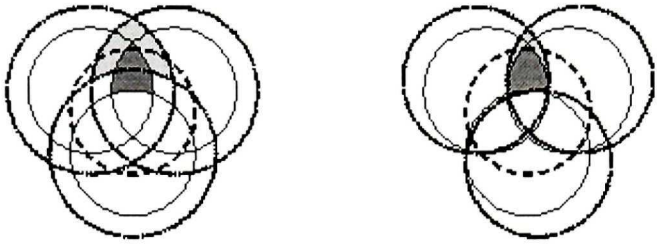

(a) (b)

Figures 5.34 (a) and (b) – Picture illustrating the increase in the region of overlap between the dose distributions of adjacent isocenters with increasing the cone size of the isocenters, in cases (a) and (b), respectively. Dashed contours in figures (a) and (b) represent the target.

Based on the results of these experiments we can speculate that the calculation of the *TCP* and the *NTCP* is highly sensitive to the dose distribution, at least for tissues that exhibit low volume effects (low value of the parameter n), as is the case of normal brain. Given this consideration, the volume of normal tissue enclosed by several isodose levels was obtained for all plans generated for the 3.0 cm diameter hemispherical target (see Table 5.7). These plans were then ranked in terms of tissue damage only by comparing the relative amount of normal tissue inside the highest isodose levels for all plans (see Table 5.8). The plans ranking in terms of tissue damage was exactly the same as the plans ranking in terms of the *NTCP* (see Table 5.9). Therefore, for the dynamic rotation technique, at least for tissues that exhibit low volume effects, tissue damage is more easily correlated with the dose distribution (maximum dose in the histogram) than with physical parameters (particularly the *PITV*).

Table 5.7 – Volume enclosed by several isodose surfaces for the plans generated for the 3.0 cm diameter hemispherical target using the dynamic rotation technique. Bold isodose levels indicate the prescription isodose. Above the prescription, the quantity in parenthesis corresponds to the volume of normal tissue inside the isodose surface. Below this level the volume of normal tissue corresponds to the volume reported in the table, minus the tumour volume of 9.82 cm^3.

1 isocenter		**5 isocenters**		**6 isocenters**		**9 isocenters**		**10 isocenters**	
98%	0.44	90%	0.78	90%	0.92	90%	0.80 *(0.01)*	90%	0.96
85%	18.36	80%	2.22 *(0.01)*	80%	3.20 *(0.02)*	80%	3.51 *(0.22)*	80%	3.43 *(0.01)*
68%	26.42	70%	4.93 *(0.04)*	70%	6.47 *(0.65)*	70%	6.91 *(1.02)*	70%	6.54 *(0.34)*
51%	36.63	60%	9.65 *(1.20)*	60%	10.48 *(2.13)*	60%	10.61 *(2.30)*	60%	10.20 *(1.48)*
34%	61.63	**50%**	16.95	**50%**	16.38	**50%**	16.13	**50%**	15.41
17%	188.87	40%	27.10	40%	26.70	40%	24.64	40%	22.50
		30%	41.41	30%	46.00	30%	39.40	30%	34.39
		20%	76.80	20%	85.81	20%	72.97	20%	66.06
		10%	210.83	10%	235.76	10%	225.86	10%	183.20

Table 5.8 – Plans ranking in terms of dose distribution (from higher to lower probability of tissue damage).

9
6
10
5
1

Table 5.9 – Plans ranking in terms of the calculated *NTCP* (from higher to lower *NTCP*).

# isocenters	***NTCP* (%)**
9	1.29
6	0.58
10	0.42
5	0.20
1	0.09

Overall, this different behaviour of the dynamic rotation technique is due to the fact that when multiple isocenters are used, the overlapping of the dose distributions from all isocenters generates a less uniform final dose distribution, presenting different dose gradients throughout the higher dose region (prescription isodose level and above). This less uniform final dose distribution results in poorer correlation between physical and biological parameters for the dynamic rotation technique. This same argument is also used to explain the good correlation for the static conformal beam technique and intermediate correlation for the IMRS technique. In the former case, the higher

correlation is explained by the use of a single isocenter and uniform intensity for all beams, while in the second case, although a single isocenter is also used, due to the beam intensity modulation, the resulting dose distribution does not present a uniform gradient as for the static conformal beam technique.

5.7 COMPARATIVE STUDY – BIOLOGICAL PARAMETERS

Tables 5.10 through 5.14 below list the biological parameters [*TCP*, *NTCP*, *IBED*(tumour), and *IBED*(brain)] of the best plans, in terms of biological parameters, for the dynamic rotation, the static conformal beam, and the IMRS techniques, for the 1.5 cm diameter spherical, 3.0 cm diameter spherical, 1.5 cm diameter hemispherical, 3.0 cm diameter hemispherical, and C-shaped targets, respectively.

As the primary objective was to adequately treat the tumour, these plans were selected based on providing the highest *TCP*, independent of the *NTCP*. It must be stated that some plans in Tables 5.10 through 5.14 do not correspond to the same best plans in terms of physical parameters (see Tables 5.1 to 5.5), especially for those techniques which presented a weak correlation between the physical and biological parameters.

Table 5.10 – Biological parameters [*TCP*, *NTCP*, *IBED*(tumour), and *IBED*(brain)] of the best plans, in terms of biological parameters, obtained for the 1.5 cm diameter spherical target for the dynamic rotation, the static conformal beam, and the IMRS techniques.

Technique / Parameter	Dynamic Rotation	Static Beams	IMRS
***TCP* (%)**	95.87	97.56	98.69
***NTCP* (%)**	0.41	1.60	0.45
***IBED*(tumour) (Gy_{10})**	106.94	111.85	148.20
***IBED*(brain) (Gy_2)**	3.39	8.94	6.99

Table 5.11 – Biological parameters [*TCP*, *NTCP*, *IBED*(tumour) and *IBED*(brain)] of the best plans, in terms of biological parameters, obtained for the 3.0 cm diameter spherical target for the dynamic rotation, the static conformal beam, and the IMRS techniques.

Technique / Parameter	Dynamic Rotation	Static Beams	IMRS
TCP (%)	2.59E-12	1.15E-6	0.27
NTCP (%)	7.65E-4	4.81E-3	2.04E-3
IBED(tumour) (Gy_{10})	46.04	51.68	70.15
IBED(brain) (Gy_2)	5.35	9.90	8.48

Table 5.12 – Biological parameters [*TCP*, *NTCP*, *IBED*(tumour), and *IBED*(brain)] of the best plans, in terms of biological parameters, obtained for the 1.5 cm diameter hemispherical target for the dynamic rotation, the static conformal beam, and the IMRS techniques.

Technique / Parameter	Dynamic Rotation	Static Beams	IMRS
TCP (%)	99.56	98.09	99.41
NTCP (%)	9.63	1.37	0.37
IBED(tumour) (Gy_{10})	176.44	115.30	146.18
IBED(brain) (Gy_2)	2.84	6.60	4.16

Table 5.13 – Biological parameters [*TCP*, *NTCP*, *IBED*(tumour), and *IBED*(brain)] of the best plans, in terms of biological parameters, obtained for the 3.0 cm diameter hemispherical target for the dynamic rotation, the static conformal beam, and the IMRS techniques.

Technique / Parameter	Dynamic Rotation	Static Beams	IMRS
TCP (%)	33.50	29.40	91.09
NTCP (%)	0.42	0.81	2.64
IBED(tumour) (Gy_{10})	100.79	80.85	129.47
IBED(brain) (Gy_2)	5.88	10.50	10.78

Table 5.14 – Biological parameters [*TCP*, *NTCP*, *IBED*(tumour), and *IBED*(brain)] of the best plans, in terms of biological parameters, obtained for the C-shaped target for the dynamic rotation, the static conformal beam, and the IMRS techniques.

Technique / Parameter	Dynamic Rotation	Static Beams	IMRS
***TCP* (%)**	1.79	0.81	2.34
***NTCP* (%)**	0.38	0.12	8.84E-3
***IBED*(tumour) (Gy_{10})**	73.18	66.24	75.45
***IBED*(brain) (Gy_2)**	6.80	9.09	8.42

From the results listed in Tables 5.10 through 5.14 it can be seen that for the 1.5 cm diameter hemispherical and C-shaped targets the technique that provided the highest *NTCP* and the one that provided the highest *IBED*(brain) were not the same. This can be explained by the same arguments mentioned in Section 5.4, i.e., different behaviour between the *NTCP* and *IBED*(brain) are due to influence of volume effects on the *NTCP* calculations (through the parameter n), whereas volume effects are not included in *IBED*(brain) calculations.

5.8 COMPARATIVE STUDY FOR THE C-SHAPED TARGET – SPARING OF THE CRITICAL STRUCTURE

Biological parameters (*NTCP* and *IBED*) were calculated for the critical structure for all plans generated for the C-shaped target in the dynamic rotation, the static conformal beam, and the IMRS techniques. Table 5.15 lists the results for the best plan, in terms of sparing the critical structure (lowest *NTCP* and *IBED* for the critical structure), obtained for each technique.

Table 5.15 – Biological parameters (*NTCP* and *IBED* calculated for the critical structure) of the best plan, in terms of sparing the critical structure, obtained for the C-shaped target for the dynamic rotation, the static conformal beam, and the IMRS techniques.

Technique / Parameter	Dynamic Rotation	Static Conformal	IMRS
NTCP crit. struc. (%)	82.275	36.720	29.980
IBED(crit. struc.) ($Gy_{2.5}$)	277.022	91.116	78.574

Based on the results presented in Table 5.15, the technique best suited to provide sparing of the critical structure was the IMRS technique, followed by the static conformal beam, and finally the dynamic rotation technique. These best plans for sparing the critical structure were obtained by using 10 isocenter placements, 15 beams, and 7 beams for the dynamic rotation, the static conformal beam, and the IMRS techniques, respectively. In the case of the dynamic rotation and the static conformal beam techniques, these plans correspond to the same best plans in terms of physical parameters (see Table 5.5), whereas for the IMRS technique, the best plan is not the same whether physical parameters or sparing of the critical structure is concerned.

5.9 SOME CONSIDERATIONS AND GENERAL DISCUSSION

5.9.1 Influence of Beam Energy on the Comparisons Performed between the Dynamic Rotation, the Static Conformal Beam, and the IMRS Techniques

In this study different linear accelerators with different beam energies were considered for each technique. For the dynamic rotation technique a 10 MV (Varian, Clinac-18) beam was considered, whereas for the other two techniques 6 MV beams were used. Although the dynamic rotation technique uses a different beam energy as compared to the other two techniques, a study published in the literature[2] comparing several linac-based radiosurgery techniques in terms of beam energy, field size, as well as number of arcs showed that the influence in varying the beam energy is only significant at lower (10%) isodose levels that are not generally clinically significant.

The physical parameters used in our study to compare the three techniques, namely the *PITV* and the *MDPD*, are influenced by the dose distribution at higher isodose levels (prescription and above). Also, concerning the biological parameters, the *TCP* is calculated at the prescription isodose level and above (considering 100% target coverage), and the influence of lower isodose levels on the *NTCP* calculations was verified to be negligible. Based on these arguments, the different beam energies employed by the different techniques did not influence our final results.

5.9.2 Choice of DVH Reduction Method for *NTCP* Calculations

In this study, the effective volume DVH reduction method was used for the calculation of the *NTCP*. This method was selected because studies published in the literature comparing the interpolation and the effective volume methods,[3,4] have shown that the interpolation method is rather insensitive to dose distribution variations in the irradiated volume, as long as the mean dose remains the same, whereas the effective volume method allows a distinction between plans with the same mean dose but a different dose uniformity. In the latter method, the ability to make such a distinction is based on the strength of the volume effects (value of the parameter n). That is, for small values of the parameter n, which means a high dependence of complication probability with dose, the method provides, as it should, that the calculated probability is correlated with the largest dose in the histogram. For large values of the parameter n (close to unity), complication probability is correlated with the mean dose, and for this case both methods provide the same results.

It is important to note that in our study only normal organs with small values of n were considered (brain and brain stem), for which the effective volume method should provide more accurate results.

REFERENCES

1 E. Shaw, R. Kline, M. Gillin, L. Souhami, A. Hirschfeld, R. Dinapoli, and L. Martin, "Radiation Therapy Oncology Group: Radiosurgery Quality Assurance Guidelines," Int. J. Radiat. Oncol., Biol., Phys. **27**, 1231-1239 (1993).

2 C. F. Serago, P. V. Houdek, B. Bauer-Kirpes, A. A. Lewin and A. A. Abitbol, S. Gonzalez-Arias, V. A. Marcial Vega, and J. G. Schwade, "Stereotactic radiosurgery: Dose-volume analysis of linear accelerator techniques," Med. Phys. **19**, 181-195 (1992).

3 G. J. Kutcher, C. Burman, L. Brewster, M. Goitein, and R. Mohan, "Histogram reduction method for calculating complication probabilities for three-dimensional treatment planning evaluations," Int. J. Radiat. Oncol., Biol., Phys. **21**, 137-146 (1991).

4 V. Moiseenko, J. Battista, and J. V. Dyk, "Normal tissue complication probabilities: Dependence on choice of biological model and dose-volume histogram reduction scheme," Int. J. Radiat. Oncol., Biol., Phys. **46**, 983-993 (2000).

CHAPTER 6

CONCLUSIONS

6.1 SUMMARY OF THE THESIS

This thesis presents a comparative study among three linac-based radiosurgery techniques. The techniques compared are the dynamic rotation, static conformal beam, and intensity-modulated radiosurgery (IMRS) techniques. The study was performed using simulated targets placed in the center of the head of a modified anthropomorphic Rando phantom. The targets were spherical, hemispherical, and C-shaped wrapped around a critical structure. The parameters considered for treatment plan evaluation were: (i) the dose distribution, (ii) the physical parameters, the *PITV* (planning isodose volume to the target volume ratio) and the *MPDP* (maximum dose to the prescription dose ratio), and (iii) the biological parameters, the integral biologically effective dose (*IBED*), tumour control probability (*TCP*), and normal tissue complication probability (*NTCP*).

Results of the comparative study showed that for spherical targets, in general, comparable plans can be obtained using the three techniques. For hemispherical targets, comparable plans in terms of the *PITV* can be obtained using the three techniques; however, with higher *MDPD* and higher complexity (several isocenters) for the dynamic rotation technique, and higher *MDPD* for the IMRS technique. For the C-shaped target that exhibits a concave surface, the IMRS technique provided the best plan.

Because treatment outcome may be reflected better by biological instead of physical parameters, correlation between physical and biological parameters was evaluated for the three techniques. The importance of establishing such a correlation is that, as the objective in routine treatment planning is to obtain plans that minimize physical parameters, it is essential to know if the corresponding biological parameters are also minimized. To evaluate this correlation, for each target with each technique several plans

were generated, with varying the *PITV*, and the *MDPD*, and for each plan all the biological parameters were calculated. Correlations were evaluated graphically by observing possible trends in the behaviour of a given biological parameter in relation to an increase or decrease in the *PITV* or the *MDPD*.

Results of the evaluation of correlation between physical and biological parameters have shown that, in general, good correlation is found for the static conformal beam technique, weaker correlation for the IMRS technique, and poor correlation for the dynamic rotation technique. Given the poor correlation found for the dynamic rotation technique, experiments were performed in order to explain, in terms of dose distributions, the lack of correlation found for this technique. These experiments suggest that, for the dynamic rotation technique, treatment plans should be evaluated by analysing the dose distributions in addition to analysing physical parameters.

This different behaviour of the dynamic rotation technique is due to the fact that when multiple isocenters are used, the overlapping of the dose distributions from all isocenters generates a final dose distribution that presents different dose gradients throughout the higher dose regions (prescription isodose level and above). This final dose distribution results in poorer correlation between physical and biological parameters for the dynamic rotation technique. This same argument is used to explain the good correlation for the static conformal beam technique and intermediate correlation for the IMRS technique. In the former case, the better correlation is explained by the use of a single isocenter and uniform intensity for all beams, while in the second case, although a single isocenter is also used, due to the beam intensity modulation the resulting dose distribution does not present a uniform gradient as for the static conformal beam technique.

In terms of pairs of parameters, better correlation was, in general, found between the *MDPD* and the *TCP/IBED*(tumour) and between the *PITV* and the *NTCP/IBED*(brain). These results suggest that the *TCP/IBED*(tumour) is mostly influenced by the *MDPD*, in the sense that higher dose inhomogeneities inside the target increase the *TCP/IBED*(tumour). Although the *NTCP/IBED*(brain) was better correlated with the

PITV, both physical parameters are important in the assessment of tissue damage, because in the case of a treatment plan that exhibits a low *PITV*, but a high *MDPD*, small fractions of the normal tissue volume (located inside the prescription isodose surface) being irradiated to higher doses may increase the *NTCP*. Conversely, a similar *NTCP* may be obtained with a lower *MDPD* and a higher *PITV*. Consequently, the combination of the *PITV* and the *MDPD* is important when analysing tissue damage.

Considering the results of the *TCP* and the *NTCP* calculations, we noticed that for the largest targets, the calculated values for both parameters were, in general, very low, suggesting that the prescribed dose could be increased in an attempt to improve the *TCP*, while still keeping the *NTCP* at an acceptable level. However, as doses were prescribed based on clinical practice, the very low values calculated indicate that the *TCP* and the *NTCP* models used do not necessarily reflect the results obtained in the clinic, and the calculated values cannot be taken in an absolute sense. For these targets, doses higher than those used in clinical practice and located in the linear portion of the *TCP* curve could have been prescribed in this theoretical study. This was not done because our intention was to explore the ranking of clinically relevant treatment plans, and the calculated absolute *TCP* and *NTCP* values were not considered as important. However, one can speculate that a better correlation between physical and biological parameters might have been found, if higher doses had been prescribed for these targets.

Overall, these results reflect the simplicity of the *TCP* and *NTCP* models used as well as the limited amount of input clinical data for these models. In the case of the *NTCP*, although the model input parameters suggested by Emami were the results of the experience of many different groups, they were reported for a conventional 2 Gy per fraction radiotherapy scheme, for a limited number of fractional volumes (1/3 to 1.0) and only for two tolerance levels, 5% and 50%. Extrapolation to other fractional volumes and tolerance levels beyond the ranges reported by Emami substantially decreases the confidence in the calculated values. Moreover, in the case of the *TCP*, a more reliable model should include additional biological variables like for example, cellular radiosensitivity, etc. Yet, given these considerations and limitations, the application of the

TCP and the *NTCP* in the relative sense for the ranking of treatment plans is nonetheless useful in providing a biological basis for plan comparisons.

6.2 FUTURE WORK

This thesis can be seen to represent a starting point in the clinical implementation of the *TCP* and the *NTCP* models not only in radiosurgery applications, but also for other kinds of treatment and other sites. Particularly, it would be helpful to implement other *TCP* and *NTCP* models that include additional variables, in an attempt to obtain more reliable results. However, as the prediction of a percentage incidence (*NTCP* or *TCP*) depends deeply on the values of the input parameters and given that the data now available is still limited, one must wait for further clinical data before being able to agree on the predicted values.

Considering the important aspect of establishing a correlation between physical and biological parameters, it would also be interesting to use the same *TCP* and *NTCP* models and prescribe higher doses, located in the linear portion of the *TCP* curve, for the largest targets, in order to evaluate if better correlation is found between physical and biological parameters.

LIST OF FIGURES

(coordinates, etc), and of a selected beam (table, gantry, and collimator angles, etc). (Courtesy of BrainLAB Inc., AG, Germany).

2.7 Image obtained from the CORVUS treatment planning system, displaying information provided by the system, concerning the treatment plan, such as: (i) cumulative DVHs, (ii) isodose lines superimposed on an axial image, and (iii) dose statistics.

3.1 Dose-volume histograms; (a): differential; (b): integral, in which relative volume is plotted against dose.

3.2 Scheme to illustrate how the *PITV* ratio is determined. The black and grey contours represent, respectively, the target and the prescription isodose line. In this case, 10 cm^3 is the volume enclosed by the prescription isodose and 5 cm^3 is the target volume. The *PITV* ratio is then $\left(\frac{10\ cm^3}{5\ cm^3}\right) = 2.0$.

3.3 Scheme to illustrate how the *MDPD* homogeneity index is calculated. The black and grey contours represent, respectively, the target and the prescription isodose line. In this case, 100% is the maximum dose given to the target and the dose is prescribed to the 50% isodose line, resulting in an *MDPD* of 2.0.

3.4 Graph of a typical cell survival curve, illustrating both the linear and quadratic mechanisms that contribute to cell killing for a low LET radiation, and also, the ratio α/β that represents the dose for which the contribution of both effects is the same. The fraction of surviving cells (capable of dividing) is plotted on a logarithmic scale, against the radiation dose on a linear scale.

3.5 (a) DVH reduction using linear interpolation; (b) DVH reduction using the effective volume method.

3.6 Optimization of the uncomplicated tumour control (P_{utc}). *TCP* and *NTCP* are shown as a function of radiation dose. At dose A tumour control will be improbable, but complications will be negligible. At dose C, tumour control will be highly probable, but the complication rate will be excessive. The optimum dose B will result in the greatest probability of uncomplicated tumour control.

In (b) the isocenters were displaced away from each other as the cone size was increased. In both cases, five plans were generated. Dashed contours in figures (a) and (b) represent the target.

5.31 Graphs of the *TCP* as a function of the *PITV* (directly related to the cone size) for the two experiments [cases (a) and (b), respectively] used to explain, as a function of the dose distribution, the *TCP* and the *NTCP* behaviour in the dynamic rotation technique.

5.32 Graphs of the *NTCP* as a function of the *PITV* (directly related to the cone size) for the two experiments [cases (a) and (b), respectively] used to explain, as a function of the dose distribution, the *TCP* and the *NTCP* behaviour in the dynamic rotation technique.

5.33 Picture illustrating the increase in the region of overlap between the dose distributions of the three isocenters with increasing the cone size of the isocenters, in case (a). Dashed contour represents the target.

5.34 Picture illustrating the increase in the region of overlap between the dose distributions of adjacent isocenters with increasing the cone size of the isocenters, in cases (a) and (b), respectively. Dashed contours in figures (a) and (b) represent the target.

LIST OF TABLES

5.4 Physical parameters (*PITV* and *MDPD*), and complexity (number of isocenters for dynamic rotation, and number of beams for the static conformal and the IMRS techniques, as well as approximate time spent for treatment planning), of the best plans, in terms of physical parameters, obtained for the 3.0 cm diameter hemispherical target for the dynamic rotation, static conformal beam, and IMRS techniques.

5.5 Physical parameters (*PITV* and *MDPD*), and complexity (number of isocenters for dynamic rotation, and number of beams for the static conformal and the IMRS techniques, as well as approximate time spent for treatment planning), of the best plans, in terms of physical parameters, obtained for the C-shaped target for the dynamic rotation, static conformal beam, and IMRS techniques.

5.6 Volume inside the 50, 80 and 90% isodose surfaces for the five plans obtained in experiment (b).

5.7 Volume enclosed by several isodose surfaces for the plans generated for the 3.0 cm diameter hemispherical target using the dynamic rotation technique. Bold isodose levels indicate the prescription isodose. Above the prescription, the quantity in parenthesis corresponds to the volume of normal tissue inside the isodose surface. Below this level the volume of normal tissue corresponds to the volume reported in the table, minus the tumour volume of 9.82 cm^3.

5.8 Plans ranking in terms of dose distribution (from higher to lower probability of tissue damage).

5.9 Plans ranking in terms of the calculated *NTCP* (from higher to lower *NTCP*).

5.10 Biological parameters [*TCP*, *NTCP*, *IBED*(tumour), and *IBED*(brain)] of the best plans, in terms of biological parameters, obtained for the 1.5 cm diameter spherical target for the dynamic rotation, the static conformal beam, and the IMRS techniques.

5.11 Biological parameters [*TCP*, *NTCP*, *IBED*(tumour) and *IBED*(brain)] of the best plans, in terms of biological parameters, obtained for the 3.0 cm diameter

APPENDIX A

Table A.1 - Example of an EXCEL spreadsheet used to calculate the *IBED* for tumour and normal brain for a plan generated for the 1.5 cm diameter hemispherical target using the static conformal beam technique.

Tumour Diff DVH (cc)	Dose interval (%)	Dose interval(Gy)	*ΔBED* (tumour)	Normal Brain Diff DVH (cc)	Dose interval(Gy)	*ΔBED* (normal brain)
0	1	0.24	0	140.6630	0.24	0.0252
0	2	0.48	0	255.7486	0.48	0.1015
0	3	0.72	0	231.5812	0.72	0.1512
0	4	0.96	0	124.4435	0.96	0.1179
0	5	1.2	0	95.7211	1.2	0.1225
0	6	1.44	0	95.9857	1.44	0.1585
0	7	1.68	0	77.4271	1.68	0.1596
0	8	1.92	0	47.6030	1.92	0.1194
0	9	2.16	0	31.5677	2.16	0.0946
0	10	2.4	0	24.4332	2.4	0.0860
...	...	...	...	...	...	...
0	99	23.76	0	0.1461	23.76	0.0298
0.0003	100	24	0.0082	0.1303	24	0.0271
0.0006	101	24.24	0.0166	0.1386	24.24	0.0294
0.0006	102	24.48	0.0169	0.1346	24.48	0.0291
0.0011	103	24.72	0.0343	0.1337	24.72	0.0294
0.0020	104	24.96	0.0611	0.1332	24.96	0.0299
0.0026	105	25.2	0.0798	0.1421	25.2	0.0325
0.0049	106	25.44	0.1533	0.1369	25.44	0.0319
0.0069	107	25.68	0.2199	0.1378	25.68	0.0326
0.0066	108	25.92	0.2141	0.1349	25.92	0.0325
0.0086	109	26.16	0.2838	0.1406	26.16	0.0345
0.0161	110	26.4	0.5381	0.1343	26.4	0.0336
0.0227	111	26.64	0.7711	0.1360	26.64	0.0346
0.0330	112	26.88	1.1400	0.1300	26.88	0.0336
0.0476	113	27.12	1.6711	0.1223	27.12	0.0322
0.0712	114	27.36	2.5350	0.1122	27.36	0.0300
0.0984	115	27.6	3.5595	0.0964	27.6	0.0263
0.1257	116	27.84	4.6142	0.0743	27.84	0.0206
0.1650	117	28.08	6.1484	0.0629	28.08	0.0177
0.2041	118	28.32	7.7159	0.0422	28.32	0.0121
0.2411	119	28.56	9.2507	0.0327	28.56	0.0095
0.2790	120	28.8	10.8615	0.0224	28.8	0.0066
0.3372	121	29.04	13.3212	0.0132	29.04	0.0040
0.3763	122	29.28	15.0781	0.0020	29.28	0.0006
0.4207	123	29.52	17.1028	0.0003	29.52	0.0001
0.3346	124	29.76	13.7968	0	29.76	0
0.0583	125	30	2.4360	0	30	0
0.0052	126	30.24	0.2190	0	30.24	0
0	127	30.48	0	0	30.48	0
0	128	30.72	0	0	30.72	0
0	129	30.96	0	0	30.96	0
0	130	31.2	0	0	31.2	0
0	131	31.44	0	0	31.44	0
	***IBED* tumour**	(Gy *10*)	111.8475	***IBED* normal brain**(Gy**2**)		8.9424

Table A.2 - Example of an EXCEL spreadsheet used to calculate the *TCP* for a plan generated for the 1.5 cm diameter hemispherical target using the static conformal beam technique.

Tumour Diff DVH (cc)	$D_{1\text{-fraction}}$ (Gy)	D_2 (Gy) (2 Gy/fraction)	$P(Di,vi)$
0	0.24	0.2048	1
0	0.48	0.4192	1
0	0.72	0.6432	1
0	0.96	0.8768	1
0	1.20	1.1200	1
0	1.44	1.3728	1
0	1.68	1.6352	1
0	1.92	1.9072	1
...	...	...	...
0	23.52	65.6992	1
0	23.76	66.8448	1
2.87E-04	24.00	68.0000	0.99995
5.74E-04	24.24	69.1648	0.99992
5.74E-04	24.48	70.3392	0.99993
1.15E-03	24.72	71.5232	0.99988
0.0020	24.96	72.7168	0.99982
0.0026	25.20	73.9200	0.99980
0.0049	25.44	75.1328	0.99967
0.0069	25.68	76.3552	0.99961
0.0066	25.92	77.5872	0.99968
0.0086	26.16	78.8288	0.99964
0.0161	26.40	80.0800	0.99942
0.0227	26.64	81.3408	0.99931
0.0330	26.88	82.6112	0.99914
0.0476	27.12	83.8912	0.99894
0.0712	27.36	85.1808	0.99866
0.0984	27.60	86.4800	0.99842
0.1257	27.84	87.7888	0.99829
0.1650	28.08	89.1072	0.99810
0.2041	28.32	90.4352	0.99801
0.2411	28.56	91.7728	0.99801
0.2790	28.80	93.1200	0.99806
0.3372	29.04	94.4768	0.99802
0.3763	29.28	95.8432	0.99814
0.4207	29.52	97.2192	0.99825
0.3346	29.76	98.6048	0.99883
0.0583	30.00	100.0000	0.99983
0.0052	30.24	101.4048	0.99999
0	30.48	102.8192	1
0	30.72	104.2432	1
0	30.96	105.6768	1
0	31.20	107.1200	1
0	31.44	108.5728	1
	$TCP=\prod P(D,v)=$		0.97562

$$D_2 = D_{1\text{-fraction}}*(\alpha/\beta+D_{1\text{-fraction}})/(\alpha/\beta+2)$$

$\alpha/\beta = 10\ Gy$

$\Gamma = 3$

$D50 = 3.7\ ln\ (10E07*V/0.693)$

$V = 2.87\ cm^3$

$D50 = 64.895\ Gy\ (2\ Gy/Fraction)$

$$P(D,v)=2^{-e^{[e\Gamma(1-D/D50)+ln(v)]}}$$

Table A.3 - Example of an EXCEL spreadsheet used to perform the histogram reduction (calculate V_{eff}) and to calculate the parameter t in a plan generated for the 1.5 cm diameter hemispherical target using the static conformal beam technique.

Brain Diff DVH (cc)	$D_{1\text{-fraction}}$ (Gy)	D_2 (Gy) (2Gy/Fraction)	$\Delta Veff_i$
140.663005	0.24	0.1344	0
255.748570	0.48	0.2976	0
231.581161	0.72	0.4896	0
124.443487	0.96	0.7104	0
95.721101	1.20	0.9600	0
95.985715	1.44	1.2384	0.0000001
77.427147	1.68	1.5456	0.0000002
47.602968	1.92	1.8816	0.0000002
...	...	...	...
0.137473	23.28	147.1296	0.0220012
0.146657	23.52	150.0576	0.0253960
0.146083	23.76	153.0144	0.0273501
0.130298	24.00	156.0000	0.0263552
0.138621	24.24	159.0144	0.0302695
0.134603	24.48	162.0576	0.0317075
0.133742	24.72	165.1296	0.0339623
0.133168	24.96	168.2304	0.0364290
0.142065	25.20	171.3600	0.0418364
0.136899	25.44	174.5184	0.0433705
0.137760	25.68	177.7056	0.0469199
0.134890	25.92	180.9216	0.0493595
0.140630	26.16	184.1664	0.0552522
0.134316	26.40	187.4400	0.0566248
0.136038	26.64	190.7424	0.0615005
0.130011	26.88	194.0736	0.0629906
0.122262	27.12	197.4336	0.0634462
0.112217	27.36	200.8224	0.0623357
0.096432	27.60	204.2400	0.0573078
0.074333	27.84	207.6864	0.0472328
0.062853	28.08	211.1616	0.0426791
0.042189	28.32	214.6656	0.0305970
0.032718	28.56	218.1984	0.0253293
0.022386	28.80	221.7600	0.0184901
0.013202	29.04	225.3504	0.0116279
0.002009	29.28	228.9696	0.0018859
0.000287	29.52	232.6176	0.0002870
0	29.76	236.2944	0
0	30.00	240.0000	0
0	30.24	243.7344	0
...	...	...	...
0	31.20	258.9600	0
0	31.44	262.8384	0
	Veff =		1.3348073

$$D_2 = D_{1\text{-fraction}}*(\alpha/\beta+D_{1\text{-fraction}})/(\alpha/\beta+2)$$

α/β (*brain*) = 2 *Gy*

$v = V_{eff}/V_{ref} = 0.00089$

$TD50(v) = D50(1)/v\text{^}n = 347.3917$

$t = (D_{max} - TD50(v))/(m*TD50(v)) = -2.2026$

APPENDIX B

Results from dynamic rotation technique

Table B.1 – 1.5 cm diameter spherical target

# of isocenters / Parameter	1 (cone 2.25 cm)
PITV	1.46
MDPD	1.24
*IBED*tumour (Gy_{10})	106.94
*IBED*brain (Gy_2)	3.39
TCP (%)	95.87
NTCP (%)	0.41

Table B.2 – 3.0 cm diameter spherical target

# of isocenters / Parameter	1 (cone 3.75 cm)
PITV	1.30
MDPD	1.18
*IBED*tumour (Gy_{10})	46.04
*IBED*brain (Gy_2)	5.35
TCP (%)	2.59E-12
NTCP (%)	7.65E-4

Table B.3 – 1.5 cm diameter hemispherical target

# of isocenters / Parameter	1 (cone 2.00 cm)	1 (cone 2.25 cm)	3	4	5	6	9	10
PITV	1.89	2.15	1.95	1.78	1.74	1.73	1.70	1.68
MDPD	1.27	1.18	2.00	2.00	2.00	2.00	2.00	2.00
*IBED*tumour (Gy_{10})	108.68	99.96	127.62	155.30	168.51	176.44	160.99	149.48
*IBED*brain (Gy_2)	2.94	3.48	3.42	2.68	2.91	2.84	2.85	3.10
TCP (%)	95.93	94.39	98.58	98.76	99.29	99.56	98.69	98.61
NTCP (%)	0.93	0.83	4.76	0.98	1.33	9.63	2.01	0.55

Table B.4 – 3.0 cm diameter hemispherical target

# of isocenters / Parameter	1	5	6	9	10
PITV	1.87	1.73	1.67	1.64	1.57
MDPD	1.18	2.00	2.00	2.00	2.00
*IBED*tumour (Gy_{10})	62.20	93.82	98.74	98.47	100.79
*IBED*brain (Gy_2)	6.97	7.00	7.55	6.88	5.88
TCP (%)	0.33	25.22	23.33	23.41	33.50
NTCP (%)	0.09	0.20	0.58	1.29	0.42

Table B.5 – C-shaped target

# of isocenters / Parameter	1	3	6	9	10
PITV	5.10	3.82	2.61	2.57	2.40
MDPD	1.32	2.00	1.96	2.00	2.00
*IBED*tumour (Gy_{10})	56.12	70.80	73.18	71.53	67.80
*IBED*brain (Gy_2)	12.77	12.88	6.80	6.39	6.00
TCP (%)	3.83E-3	0.61	1.79	0.13	0.06
NTCP (%)	0.68	3.91	0.38	0.43	0.20

Results from static conformal beam technique

Table B.6 – 1.5 cm diameter spherical target

# of beams / Parameter	5	5	5	5	5	10	10
PITV	1.82	1.53	1.54	1.53	1.48	1.52	1.43
MDPD	1.26	1.19	1.19	1.19	1.17	1.19	1.17
*IBED*tumour (Gy_{10})	111.85	102.71	102.28	101.57	99.97	100.96	99.32
*IBED*brain (Gy_2)	8.94	6.41	6.52	6.84	6.31	5.41	5.58
TCP (%)	97.56	94.24	93.94	93.45	92.47	93.02	91.94
NTCP (%)	1.60	0.37	0.41	0.39	0.31	0.35	0.23

Table B.7 – 3.0 cm diameter spherical target

# of beams / Parameter	5	5	5	5	5	10	10
PITV	1.58	1.39	1.44	1.48	1.50	1.37	1.44
MDPD	1.27	1.22	1.23	1.26	1.26	1.22	1.25
*IBED*tumour (Gy_{10})	51.68	47.39	48.38	49.81	50.52	47.14	49.48
*IBED*brain (Gy_2)	9.90	6.59	6.95	7.49	7.18	5.76	6.54
TCP (%)	1.15E-6	1.04E-10	1.29E-9	2.81E-8	1.28E-7	5.42E-11	1.44E-8
NTCP (%)	4.81E-3	1.03E-3	1.47E-3	2.04E-3	2.46E-3	8.88E-4	1.52E-3

Table B.8 – 1.5 cm diameter hemispherical target

# of beams / Parameter	5	5	5	7	9	10	10	10	10	15
PITV	2.09	1.70	1.68	1.54	1.49	1.42	1.59	1.61	1.60	1.42
MDPD	1.30	1.22	1.23	1.19	1.20	1.20	1.21	1.20	1.22	1.19
*IBED*tumour (Gy_{10})	115.30	105.84	104.65	99.63	101.25	99.43	103.76	103.82	105.05	99.67
*IBED*brain (Gy_2)	6.60	5.37	5.42	4.79	4.59	4.35	4.66	4.50	4.58	4.31
TCP (%)	98.09	96.85	96.52	94.14	94.92	93.95	95.97	96.12	96.55	94.06
NTCP (%)	1.37	0.19	0.17	0.10	0.08	0.06	0.12	0.13	0.12	0.07

Table B.9 – 3.0 cm diameter hemispherical target

# of beams / Parameter	5	5	5	7	9	10	10	10	15
PITV	1.94	1.60	1.60	1.53	1.50	1.47	1.41	1.47	1.40
MDPD	1.41	1.25	1.24	1.21	1.24	1.19	1.19	1.23	1.21
*IBED*tumour (Gy_{10})	80.85	67.36	67.66	63.91	66.87	64.02	63.28	65.90	63.63
*IBED*brain (Gy_2)	10.50	8.30	8.31	7.27	6.97	6.69	6.66	6.76	6.45
TCP (%)	29.40	3.07	3.45	0.80	2.44	0.81	0.51	1.65	0.65
NTCP (%)	0.81	0.04	0.04	0.02	0.02	0.02	0.01	0.02	0.01

Table B.10 – C-shaped target

# of beams / Parameter	5	7	9	10	15
PITV	2.72	2.63	2.58	2.17	2.14
MDPD	1.72	1.70	1.62	1.51	1.45
*IBED*tumour (Gy_{10})	66.19	67.09	66.24	57.87	54.80
*IBED*brain (Gy_2)	10.61	10.18	9.09	7.47	7.61
TCP (%)	0.04	0.43	0.81	3.52E-3	1.26E-4
NTCP (%)	0.28	0.21	0.12	0.02	0.01

Results from intensity-modulated radiosurgery technique

Table B.11 – 1.5 cm diameter spherical target

# of beams / Parameter	5	5	5	5	5	10	10
PITV	1.34	1.39	1.40	1.48	1.40	1.37	1.39
MDPD	1.81	1.42	1.39	1.42	1.41	1.32	1.35
*IBED*tumour (Gy_{10})	148.20	112.60	114.44	122.73	116.02	109.01	111.45
*IBED*brain (Gy_2)	6.99	5.85	6.58	7.04	5.75	5.23	5.03
TCP (%)	98.69	96.82	97.16	98.38	97.34	96.00	96.57
NTCP (%)	0.45	0.28	0.33	0.74	0.32	0.24	0.27

Table B.12 – 3.0 cm diameter spherical target

# of beams / Parameter	5	5	5	5	5	10	10
PITV	1.35	1.35	1.51	1.46	1.50	1.40	1.41
MDPD	2.04	2.00	1.74	1.67	1.69	1.61	1.74
*IBED*tumour (Gy_{10})	70.15	70.28	65.15	63.24	63.39	58.48	64.03
*IBED*brain (Gy_2)	8.48	8.36	10.10	9.46	8.77	7.85	7.57
TCP (%)	0.27	0.21	0.18	0.05	0.06	1.58E-3	0.05
NTCP (%)	2.04E-3	1.77E-3	6.88E-3	4.44E-3	5.31E-3	2.07E-3	2.45E-3

Table B.13 – 1.5 cm diameter hemispherical target

# of beams / Parameter	5	5	5	7	9	10	10	10	10
PITV	1.48	1.66	1.51	1.56	1.46	1.65	1.43	1.47	1.47
MDPD	1.80	1.41	1.69	1.37	1.38	1.69	1.40	1.39	1.44
*IBED*tumour (Gy_{10})	146.96	119.18	136.62	116.20	116.72	146.18	113.92	115.11	116.66
*IBED*brain (Gy_2)	4.34	5.17	4.65	4.30	3.73	4.16	3.46	3.66	3.68
TCP (%)	99.23	98.69	98.75	98.36	98.21	99.41	97.82	98.15	98.20
NTCP (%)	0.16	0.38	0.24	0.15	0.09	0.37	0.07	0.09	0.10

Table B.14 – 3.0 cm diameter hemispherical target

# of beams / Parameter	5	5	5	7	9	10	10	10	15
PITV	1.76	1.91	2.10	1.68	1.62	1.52	1.59	1.66	1.51
MDPD	2.15	2.08	2.34	1.63	1.62	2.23	2.00	1.63	1.98
*IBED*tumour (Gy_{10})	105.52	103.75	129.47	85.58	87.78	112.41	102.28	86.39	101.10
*IBED*brain (Gy_2)	10.53	11.33	10.78	8.60	8.13	8.14	8.11	8.17	7.95
TCP (%)	69.59	69.53	91.09	44.57	51.62	73.82	69.64	48.45	64.29
NTCP (%)	0.28	0.51	2.64	0.14	0.13	0.10	0.13	0.13	0.06

Table B.15 – C-shaped target

# of beams / Parameter	5	7	9	10
PITV	2.06	1.92	1.76	1.87
MDPD	1.65	1.84	1.89	2.00
*IBED*tumour (Gy_{10})	62.51	67.94	69.73	75.45
*IBED*brain (Gy_2)	9.72	8.02	7.12	8.42
TCP (%)	0.11	0.52	1.05	2.34
NTCP (%)	9.38E-3	5.00E-3	3.63E-3	8.84E-3

BIBLIOGRAPHY

The numbers in square brackets indicate the page in which the reference is quoted.

Adler, J. R. and R.S. Cox, "Preliminary clinical experience with the Cyberknife: Image-guided stereotactic radiosurgery," in *Radiosurgery*, edited by D. Kondziolka (Karger, Pittsburgh, PA, 1995), pp. 317-326. [4]

Aoyama, H., H. Shirato, T. Nishioka, K. Kagi, R. Onimaru, K. Suzuki, S. Ushikoshi, K. Houkin, S. Kuroda, H. Abe, and K. Miyasaka, "Treatment outcome of single or hypofractionated single-isocenter stereotactic irradiation (STI) using a linear accelerator for intracranial arteriovenous malformation," Radiother. Oncol. **59**, 323-328 (2001). [5]

Betti, O. O. and V. E. Derechinsky, "Hyperselective encephalic irradiation with linear accelerator," Acta Neurochir. Suppl. (Wien) **33**, 385-390 (1984). [3]

Black, P. M., "Solitary brain metastases. Radiation, resection, or radiosurgery?" Chest **103**(Supll.4), 367S-369S (1993). [6]

Boyer, A. L. and T. E Schultheiss, "Effects of dosimetric and clinical uncertainty on complication-free local tumor control," Radiother. Oncol. **11**, 65-71 (1988). [51]

Brahme, A., "Dosimetric precision requirements in radiation therapy," Acta Radiol. Oncol. **23**, 379-391 (1984). [48]

BrainLAB, AG, Germany, "BrainSCAN Software Guide Revision 1.0 – Version 5.1," (2001). [29-31]

Brown, P. D., C. A. Brown, B. F. Pollock, D. A. Gorman, and R. L. Foote, "Stereotactic radiosurgery for patients with "radioresistant" brain metastases," Neurosurgery **51**, 656-665 (2002). [6]

Burman, C., G. J. Kutcher, B. Emami, and M. Goitein, "Fitting of normal tissue tolerance data to an analytic function," Int. J. Radiat. Oncol., Biol., Phys. **21**, 123-135 (1991). [54-56, 58, 59]

Cardinale, R. M., S. H. Benedict, Q. Wu, R. D. Zwicker, H. E. Gaballa, and R. Mohan, "A comparison of three stereotactic radiotherapy techniques; arcs vs. noncoplanar fixed fields vs. intensity modulation," Int. J. Radiat. Oncol., Biol., Phys. **42**, 431-436 (1998). [14]

Chang, J. H., J. W. Chang, Y. G. Park, and S. S. Chung, "Factors related to complete occlusion of arteriovenous malformations after gamma knife radiosurgery," J. Neurosurg. **93**, 96-101 (2000). [5]

Clark, B. G., J. L. Robar, and A. M. Nichol, "Analysis of treatment parameters for conformal shaped field stereotactic irradiation: comparison with non-coplanar arcs," Phys. Med. Biol. **46**, 3089-3101 (2001). [14]

Clark, B. G., L. Souhami, and C. Pla, "The integral biologically effective dose to predict brain stem toxicity of hypofractionated stereotactic radiotherapy," Int. J. Radiat. Oncol., Biol., Phys. **40**, 667-675 (1998). [41, 46, 47, 57]

Clarkson, J. R., "A note on depth doses in field of irregular shapes," Br. J. Radiol. **14**, 265 (1941). [26, 30]

Colombo, F., A. Benedetti, F. Pozza, A. Zanardo, R. C. Avanzo, G. Chierego, and C. Machetti, "Stereotactic radiosurgery utilizing a linear accelerator," Appl. Neurophysiol. **48**, 133-145 (1985). [3]

Colombo, F., A. Benedetti, F. Pozza, R. C. Avanzo, C. Marchetti, G. Chierego, and A. Zenerdo, "External stereotactic irradiation by linear accelerator," Neurosur. **16**, 154-159 (1985). [3]

Colombo, F., P. Francescon, S. Cora, A. Testolin, and G. Chierego, "Evaluation of linear accelerator radiosurgical techniques using biophysical parameters (NTCP and TCP)," Int. J. Radiat. Oncol., Biol., Phys. **31**, 617-628 (1995). [14]

Cunningham, J. R., "Scatter-air-ratios," Phys. Med. Biol. **17**, 42-51 (1972). [26, 30]

Deasy, J., "Tumor Control Probability models for non-uniform dose distributions," In: *Volume and kinetics in tumor control and normal tissue complications* (Medical Physics Publishing, Madison, 1998). [48]

Drzymala, R. E., R. Mohan, L. Brewster, J. Chu, M. Goitein, W. Harms, and M. Urie, "Dose-Volume Histograms," Int. J. Radiat. Oncol., Biol., Phys. **21**, 71-78 (1991). [13, 41]

Dunoyer, C., J. Ragheb, T. Resnick, L. Alvarez, P. Jayakar, N. Altman, A. Wolf, and M. Duchowny, "The use of stereotactic radiosurgery to treat intractable childhood partial epilepsy," Epilepsia **43**, 292-300 (2002). [6]

Emami, B., J. Lyman, A. Brown, L. Coia, M. Goitein, J. E. Munzenrida, B. Shank, L. J. Solin, and M. Wesson, "Tolerance of normal tissue to therapeutic irradiation," Int. J. Radiat. Oncol., Biol., Phys. **21**, 109-122 (1991). [54, 55, 58]

Ezzell, G. A., "Genetic and geometric optimization of three-dimensional radiation therapy treatment planning," Med Phys. **23**, 293-305 (1996). [34]

Flickinger, J. C., D. Kondziolka, A. H. Maitz, and L. D. Lunsford, "An analysis of the dose-response for arteriovenous malformation radiosurgery and other factors affecting obliteration," Radiother. Oncol. **63**, 347-354 (2002). [5]

Fowler, J. F., "Intercomparisons of new and old schedules in fractionated radiotherapy," Semin. Radiat. Oncol. **2**, 67-72 (1992). [45]

Fowler, J. F., "The linear quadratic formula and progress in fractionated radiotherapy – Review article," Br. J. Radiol. **62**, 679-694 (1989). [44, 46, 57]

Galloway, R. L. and R. J. Maciunas, "Stereotactic neurosurgery," Biomedical Engineering **18**, 181-205 (1990). [7]

Gamma Knife Surgery: An Emerging Standard of Care. A Report on the Exponential Growth of Gamma knife Surgery in the Last Five Years (Elekta, 2001). [2]

Goitein, M. and T. E. Schultheiss, "Strategies for treating possible tumor extension: Some theoretical considerations," Int. J. Radiat. Oncol., Biol., Phys. **11**, 1519-1528 (1985). [47, 48]

Goitein, M., "The probability of controlling an inhomogeneously irradiated tumor," In: *Evaluation of treatment planning for particle beam radiotherapy* (National Cancer Institute, Bethesda, 1986). [51]

Hall, E. J., *Radiobiology for the Radiologist* (Lippincott Williams & Wilkins Publishers, 2000). [44, 45]

Hamilton, R. J., F. T. Kuchnir, P. Sweeney, S. J. Rubin, M. Dujovny, C. A. Pelizzari, and G. T. Y. Chen, "Comparison of static conformal field with multiple noncoplanar arc techniques for stereotactic radiosurgery or stereotactic radiotherapy," Int. J. Radiat. Oncol., Biol., Phys. **33**, 1221-1228 (1995). [14]

Hartmann, G. H., W. Schlegel, V. Sturm, B. Kober, O. Pastyr, and W. J. Lorenz, "Cerebral radiation surgery using moving field irradiation at a linac facility," Int. J. Radiat. Oncol., Biol., Phys. **11**, 1185-1192 (1985). [3, 11]

Hoban, P. W., L. C. Jones, and B. G. Clark, "Modeling late effects in hypofractionated stereotactic radiotherapy," Int. J. Radiat. Oncol., Biol., Phys. **43**, 199-210 (1999). [46]

ICRU Report 50, *Prescribing, Recording and Reporting Photon Beam Therapy* (ICRU, Bethesda, MD, 1993). [13, 43]

ICRU Report 62, *Prescribing, Recording and Reporting Photon Beam Therapy (Supplement to ICRU Report 50)* (ICRU, Bethesda, MD, 1999). [42]

Källman, P., A. Ågreen, and A. Brahme, "Tumor and normal tissue responses to fractionated non-uniform dose delivery," Int. J. Radiat. Biol. **62**, 249-262 (1992). [47, 49, 52]

Khan, F. M. and R. A. Potish, *Treatment Planning in Radiation Oncology* (Williams & Wilkins, 1998). [47]

Khoo, V. S., M. Oldham, E. J. Adams, J. L. Bedford, S. Webb, and M. Brada, "Comparison of intensity-modulated tomotherapy with stereotactically guided conformal radiotherapy for brain tumors," Int. J. Radiat. Oncol., Biol., Phys. **45**, 415-425 (1999). [14]

Kooy, H. M., L. A. Medzi, J. S. Loefler, E. Alexander, C. W. Cheng, E. G. Mannarino, E. J. Holupka, and R. L. Siddon, "Treatment planning for stereotactic radiosurgery of intracranial lesions," Int. J. Radiat. Oncol., Biol., Phys. **21**, 44-45 (1991). [11]

Kubo, H. D., C. T. E. Pappas, and R. B. Wilder, "A comparison of arc-based and static mini-multileaf collimator-based radiosurgery treatment plans," Radiother. Oncol. **45**, 89-93 (1997). [14]

Kutcher, G. J. and C. Burman, "Calculation of complication probability factors for non-uniform normal tissue irradiation: The effective volume method," Int. J. Radiat. Oncol., Biol., Phys. **16**, 1623-1630 (1989). [47, 52, 53]

Kutcher, G. J. *et al.*, "Three-dimensional photon treatment planning for carcinoma of the nasopharynx," Int. J. Radiat. Oncol., Biol., Phys. **21**, 169-182 (1991). [47, 48]

Kutcher, G. J., "Quantitative plan evaluation: TCP/NTCP models," Front. Radiat. Ther. Oncol. **29**, 67-80 (1996). [41, 47, 52]

Kutcher, G. J., C. Burman, L. Brewster, M. Goitein, and R. Mohan, "Histogram reduction method for calculating complication probabilities for three-dimensional treatment planning evaluations," Int. J. Radiat. Oncol., Biol., Phys. **21**, 137-146 (1991). [58, 112]

Larsson, B., K. Liden, and B. Sorby, "Irradiation of small structures through intact skull," Acta Radiol. Ther. Phys. Biol. **13**, 513-534 (1974). [3]

Leksell, L., "Cerebral radiosurgery I. Gamma thalamotomy in two cases of intractable pain," Acta Chir. Scand. **134**, 585-595 (1968). [2]

Leksell, L., "The stereotaxis method and radiosurgery of the brain," Acta Chir. Scand. **102**, 316-319 (1951). [1]

Levy, R. P., R. W. Schulte, J. D. Slater, D. W. Miller, and J. M. Slater, "Stereotactic radiosurgery – the role of charged particles," Acta Oncol. **38**, 165-169 (1999). [2]

Llacer, J., "Inverse radiation treatment planning using the Dynamically Penalized Likelihood method," Med Phys. **24**, 1751-1764 (1997). [34]

Lo, Y., C.C. Ling, and D. A. Larson, "The effect of setup uncertainties on the radiobiological advantage of fractionation in stereotactic radiotherapy," Int. J. Radiat. Oncol., Biol., Phys. **34**, 1113-1119 (1996). [7]

Lunsford, L. D., *Stereotactic Radiosurgery Update* (Elsevier, New York, 1992). [1]

Lutz, W., K. R. Winston, and N. Maleki, "A system for stereotactic radiosurgery with a linear accelerator," Int. J. Radiat. Oncol., Biol., Phys. **14**, 373-381 (1988). [3]

Lyman, J. T. and A. B. Wolbarst, "Optimization of radiation therapy: 4. A dose volume reduction algorithm," Int. J. Radiat. Oncol., Biol., Phys. **13**, 103-109 (1987). [53]

Lyman, J. T., "Complication probability as assessed from dose-volume histograms," Radiat. Res. **104**, S13-S19 (1985). [47, 52, 54]

Ma, L., P. Xia, L. J. Verhey, and A. L. Boyer, "A dosimetric comparison of fan-beam intensity modulated radiotherapy with gamma knife stereotactic radiosurgery for treating intermediate intracranial lesions," Int. J. Radiat. Oncol., Biol., Phys. **45**, 1325-1330 (1999). [14]

Maciunas, R. J., R. L. Galloway, and J. W. Latimer, "The application accuracy of stereotactic frames," Neurosurgery **35**, 682-694 (1994). [7]

Maciunas, R. J., R. L. Galloway, J. W. Latimer, C. Cobb, E. Zaccharias, A. Moore, and V. R. Mandava, "An independent application accuracy evaluation of stereotactic frame systems," Stereotact. Funct. Neurosurg. **58**, 103-107 (1992). [7]

Mignano, J. E., M. J. Engler, J. Tsai, and D. E. Wazer, "Comparison of radiobiologic modeling for one- and two-isocenter dose distributions applied to ellipsoidal radiosurgery targets," Int. J. Radiat. Oncol., Biol., Phys. **49**, 833-837 (2001). [52]

Mohan, R. and C. C. Ling, "When becometh less more?" Int. J. Radiat. Oncol., Biol., Phys. **33**, 235-237 (1995). [60]

Moiseenko, V., J. Battista, and J. V. Dyk, "Normal tissue complication probabilities: Dependence on choice of biological model and dose-volume histogram reduction scheme," Int. J. Radiat. Oncol., Biol., Phys. **46**, 983-993 (2000). [53, 112]

Morrill, S. M., R. G. Lane, J. A. Wong, and I. I. Rosen, "Dose-volume considerations with linear programming optimization," Med Phys. **18**, 1201-1210 (1991). [34]

Munro, T. R. and C. W. Gilbert, "The relation between tumor lethal doses and the radiosensitivity of tumor cells," Br. J. Radiol. **34**, 246-251 (1961). [47, 48]

Niemierko, A. and M. Goitein, "Calculation of normal tissue complication probability and dose-volume histogram reduction schemes for tissues with a critical element structure," Radiother. Oncol. **20**, 166-176 (1991). [47, 52]

Niemierko, A. and M. Goitein, "Modeling of normal tissue response to radiation: The critical volume model," Int. J. Radiat. Oncol., Biol., Phys. **25**, 135-145 (1993). [47, 52]

Niemierko, A., "A concept of equivalent uniform dose (EUD)," In: *Volume and kinetics in tumor control and normal tissue complications* (Medical Physics Publishing, Madison, 1998). [48]

Niemierko, A., "Reporting and analyzing dose distributions: A concept of equivalent uniform dose," Med. Phys. **24**, 103-110 (1997). [48]

NOMOS Corporation, Sewickley, PA, USA, "CORVUS inverse treatment planning system manual – version 4.0". [34, 35]

Okunieff, P., D. Morgan, A Niemierko, and H. D. Suit, "Radiation dose-response of human tumors," Int. J. Radiat. Oncol., Biol., Phys. **32**, 1227-1237 (1995). [47]

Peters, T. M., J. A. Clark, A. Olivier, E. P. Marchand, G. Mawko, M. Diemeregard, L. W. Muresan, and R. Ethier, "Integrated stereotaxic imaging with CT, MRI and DSA," Radiol. **161**, 821-826 (1986). [10]

Phillips, M. H., *Physical Aspects of Stereotactic Radiosurgery* (Plenum Medical Book Company, New York, 1993). [4, 59]

Pike, B. G., E. B. Podgorsak, T. M. Peters, and C. Pla, "Dose distributions in dynamic stereotactic radiosurgery," Med. Phys. **14**, 780-789 (1987). [11, 26]

Podgorsak, E. B., A. Olivier, M. Pla, P. Y. Lefebvre, and J. Hazle, "Dynamic stereotactic radiosurgery," Int. J. Radiat. Oncol., Biol., Phys. **14**, 115-125 (1988). [3, 23]

Podgorsak, E. B., G. B. Pike, A. Olivier, M. Pla, and L. Souhami, "Radiosurgery with high energy photon beams: a comparison among techniques," Int. J. Radiat. Oncol., Biol., Phys. **16**, 857-865 (1989). [14]

Prott, F. J., U. Haverkamp, H. Eich, A. Resch, O. Micke, A. R. Fischedick, N. Willich, and R. Potter, "Effect of distortions and asymmetry in MR images on radiotherapeutic treatment planning," Int. J. Cancer **90**, 46-50 (2000). [9]

Pugachev, A. B., A. L. Boyer, and L. Xing, "Beam orientation optimization in intensity-modulated radiation treatment planning," Med Phys. **27**, 1238-1245 (2000). [34]

Sanchez-Nieto, B. and A. E. Nahum, "Bioplan: software for the biological evaluation of radiotherapy treatment plans," Med. Dosim. **25**, 71-76 (2000). [50, 52, 57]

Schoeggl, A., K. Kitz, M. Reddy, and C. Zauner, "Stereotactic radiosurgery for brain metastases from colorectal cancer," Int. J. Colorectal Dis. **17**, 150-155 (2002). [6]

Schultheiss, T. E., C. G. Orton, and R. A. Peck, "Models in radiotherapy: Volume effects," Med. Phys. **10**, 410-415 (1983). [47, 52]

Serago, C. F., P. V. Houdek, B. Bauer-Kirpes, A. A. Lewin and A. A. Abitbol, S. Gonzalez-Arias, V. A. Marcial Vega, and J. G. Schwade, "Stereotactic radiosurgery: Dose-volume analysis of linear accelerator techniques," Med. Phys. **19**, 181-195 (1992). [111]

Shaw, E., C. Scott, L. Souhami, R. Dinapoli, J. P. Bahary, R. Kline, M. Wharam, C. Schultz, P. Davey, J. Loeffler, J. D. Rowe, L. Marks, B. Fisher, and K. Shin, "Radiosurgery for the treatment of previously irradiated recurrent primary brain tumors and brain metastases: Initial report of Radiation Therapy Oncology Group protocol 90-05," Int. J. Radiat. Oncol., Biol., Phys. **34**, 647-654 (1996). [42]

Shaw, E., C. Scott, L. Souhami, R. Dinapoli, R. Kline, J. Loeffler, and N. Farnan, "Single dose radiosurgical treatment of recurrent previously irradiated primary brain tumors and brain metastases: Final report of RTOG protocol 90-05," Int. J. Radiat. Oncol., Biol., Phys. **47**, 291-298 (2000). [42]

Shaw, E., R. Kline, M. Gillin, L, Souhami, A. Hirschfeld, R. Dinapoli, and L. Martin, "Radiation Therapy Oncology Group: Radiosurgery Quality Assurance Guidelines," Int. J. Radiat. Oncol., Biol., Phys. **27**, 1231-1239 (1993). [14, 41-43, 71, 92]

Shin, M., S. Kawamoto, H. Kurita, M. Tago, T. Sasaki, A. Morita, K. Ueki, and T. Kirino, "Retrospective analysis of a 10-year experience of stereotactic radiosurgery for arteriovenous malformations in children and adolescents," J. Neurosurg. **97**, 779-784 (2002). [5]

Shiu, A. S., H. M. Kooy, J. R. Ewton, S. S. Tung, J. Wong, K. Antes, and M. H. Maor, "Comparison of miniature multileaf collimation (M-MLC) with circular collimation for stereotactic treatment," Int. J. Radiat. Oncol., Biol., Phys. **37**, 679-688 (1997). [14]

SimuPlan Sociedad Limitada, "SimuPlan treatment planning system manual – version for Apple Macintosh power PC computers," (2000). [26]

Smith, V., L. Verhey, and C. F. Serago, "Comparison of radiosurgery treatment modalities based on complication and control probabilities," Int. J. Radiat. Oncol., Biol., Phys. **40**, 507-513 (1998). [14, 47, 50-52, 57]

Solberg, T. D., K. L. Boedeker, R. Fogg, M. T. Selch, and A. A. F. DeSalles, "Dynamic arc radiosurgery field shaping: a comparison with static field conformal and noncoplanar circular arcs," Int. J. Radiat. Oncol., Biol., Phys. **49**, 1481-1491 (2001). [14]

Verhey, L. J., V. Smith, and C. F. Serago, "Comparison of radiosurgery treatment modalities based on physical dose distributions," Int. J. Radiat. Oncol., Biol., Phys. **40**, 497-505 (1998). [14]

Vernimmen, F. J., J. K. Harris, J. A. Wilson, R. Melvill, B. J. Smit, and J. P. Slabbert, "Stereotactic proton beam therapy of skull base meningiomas," Int. J. Radiat. Oncol., Biol., Phys. **49**, 99-105 (2001). [2]

Villavicencio, A. T., P. M. Black, D. C. Shrieve, M. P. Fallon, E. Alexander, and J. S. Loeffler, "Linac radiosurgery for skull base meningiomas," Acta Neurochir. (Wien) **143**, 1141-1152 (2001). [6]

Webb, S. and A. E. Nahum, "A model for calculating tumor control probability in radiotherapy including the effects of inhomogeneous distributions of dose and clonogenic cell density," Phys. Med. Biol. **38**, 653-666 (1993). [51]

Webb, S., "Optimization by simulated annealing of three-dimensional, conformal treatment planning for radiation fields defined by a multileaf collimator: II. Inclusion of two-dimensional modulation of the X-ray intensity," Phys. Med. Biol. **37**, 1689-1704 (1992). [34]

Wen, P. Y. and J. S. Loeffler, "Brain metastases," Curr. Treat. Options Oncol. **1**, 447-458 (2000). [6]

Withers, H., "The 4 R's of Radiotherapy," in *Advances in radiation biology Vol.15*, edited by J. Lett and H. Adler (Academic Press, New York, 1975), pp. 241-271. [6]

Woo, S. Y., W. H. Grant, D. Bellezza, R. Grossman, P. Gildenberg, S. Carpenter, M. Carol, and E. B. Butler, "A comparison of intensity modulated conformal therapy with a conventional external beam stereotactic radiosurgery system for the treatment of single and multiple intracranial lesions," Int. J. Radiat. Oncol., Biol., Phys. **35**, 593-597 (1996). [14]

Wowra, B., M. Siebels, A. Muacevic, F. W. Kreth, A. Mack, and A. Hofstetler, "Repeated gamma knife surgery for multiple brain metastases from renal cell carcinoma," J. Neurosurg. **97**, 785-793 (2002). [6]

Xing, L. and G. T. Y. Chen, "Iterative methods for inverse treatment planning," Phys. Med. Biol. **41**, 2107-2123 (1996). [34]

Yu, C., G. Luxton, G. Jozsef, M. L. J. Apuzzo, and Z. Petrovich, "Dosimetric comparison of three photon radiosurgery techniques for an elongated ellipsoid target," Int. J. Radiat. Oncol., Biol., Phys. **45**, 817-826 (1999). [14]

Zabel, A., S. Milker-Zabel, C. Thilmann, I. Zuna, B. Rhein, M. Wannenmacher, and J. Debus, "Treatment of brain metastases in patients with non-small cell lung cancer (NSCLC) by stereotactic linac-based radiosurgery: prognostic factors," Lung Cancer **37**, 87-94 (2002). [6]

Zagars, G. K., T. E. Schultheiss, and L. J. Peters, "Inter-tumor heterogeneity and radiation dose-control curves," Radiother. Oncol. **8**, 353-361 (1987). [52]